



**HYDROGEN PHYSISORPTIVE STORAGE**  
**IN**  
**METAL-ORGANIC FRAMEWORKS (MOFs)**

By

**TSHIAMO SEGAKWENG**

Dissertation submitted in partial fulfilment of the requirements for the degree of

**MSc (Applied Science): Chemical Technology**

Department of Chemical Engineering

Faculty of Engineering, the Built Environment and Information Technology

University of Pretoria

Republic of South Africa

**Supervisor: Prof. Philip Crouse**

**Co-Supervisors:**

**Dr Jianwei Ren**

**Dr Henrietta Langmi**

**April 2016**

## DECLARATION

I, Tshiamo Segakweng, student No. 28197322, hereby declare that all the work provided in this dissertation is to the best of my knowledge original (except where cited) and that neither the whole work nor any part of it has been, or is to be, submitted for another degree at University of Pretoria or any other University or tertiary education institution or examining body.

*SIGNATURE*.....*DATE*.....

*TSHIAMO SEGAKWENG*

## TABLE OF CONTENTS

|  |      |
|--|------|
| ABSTRACT .....   | vi   |
| ACKNOWLEDGEMENTS .....   | viii |
| ACHIEVEMENTS DURING MASTERS STUDY .....                                      | ix   |
| LIST OF FIGURES .....  | xi   |
| LIST OF TABLES .....   | xiii |
| LIST OF REACTIONS .....  | xiii |
| NOMENCLATURE .....   | xiv  |
| Chapter 1 .....  | 1    |
| 1.1 Background and motivation .....  | 1    |
| 1.2 Problem statement .....  | 3    |
| 1.3 Project objectives.....  | 4    |
| Chapter 2 .....  | 5    |
| Literature review .....  | 5    |
| 2.1 Chapter outline .....  | 5    |
| 2.2 Structural features, properties and applications of MOFs .....           | 5    |
| 2.2.1 Structure and composition of MOF-5.....                                | 6    |
| 2.2.2 Structure and composition of Zr-MOF.....                               | 7    |
| 2.2.3 Structure and composition of Cr-MOF.....                               | 8    |
| 2.3 Synthesis and activation of MOFs.....                                    | 8    |
| 2.4 Characterisation of MOFs .....   | 12   |
| 2.5 Hydrogen storage in MOFs .....   | 13   |
| 2.6 Definitions of concepts and terms used in hydrogen storage research..... | 13   |
| 2.6.1 Sorption and desorption.....   | 13   |
| 2.6.2 Adsorption and absorption .....  | 13   |
| 2.6.3 Chemisorption and physisorption.....                                   | 14   |
| 2.6.4 Langmuir surface area and BET surface area.....                        | 14   |
| 2.6.5 Excess hydrogen adsorption and total hydrogen adsorption .....         | 15   |
| 2.6.6 Isosteric heat of adsorption.....                                      | 16   |
| 2.7 Cryogenic hydrogen storage in MOFs.....                                  | 16   |
| 2.7.1 Creating open metal sites.....   | 17   |
| 2.7.2 Making use of guest metal ions .....                                   | 17   |
| 2.7.3 Promoting hydrogen “spillover”.....                                    | 19   |
| 2.7.4 Controlling surface area, pore volume and pore size .....              | 20   |
| 2.7.5 Catenation.....  | 21   |

|   |    |
|---|----|
| Chapter 3 .....   | 23 |
| Experimental .....  | 23 |
| 3.1 Chapter outline .....   | 23 |
| 3.2 Synthesis of MOF-5 crystals .....                                   | 24 |
| 3.2.1 Chemicals and materials .....                                     | 24 |
| 3.2.2 Solvothermal synthesis of MOF-5 crystals .....                    | 24 |
| 3.3 Synthesis of Zr-MOF crystals .....                                  | 31 |
| 3.3.1 Chemicals and materials .....                                     | 31 |
| 3.3.2 Modulated solvothermal synthesis of Zr-MOF crystals .....         | 31 |
| 3.3.3 Microwave-assisted synthesis of Zr-MOF crystals .....             | 32 |
| 3.4 Synthesis of Cr-MOF crystals .....                                  | 33 |
| 3.4.1 Chemicals and materials .....                                     | 33 |
| 3.4.2 Modulated synthesis of Cr-MOF crystals .....                      | 33 |
| 3.5 Characterisation techniques .....                                   | 36 |
| 3.5.1 Scanning Electron Microscopy (SEM) .....                          | 36 |
| 3.5.2 Powder X-ray Diffraction (PXRD) .....                             | 37 |
| 3.5.3 Thermo Gravimetric Analysis (TGA) .....                           | 37 |
| 3.5.4 Surface area and pore size determination .....                    | 37 |
| 3.5.5 Hydrogen adsorption measurements .....                            | 38 |
| Chapter 4 .....   | 39 |
| Results and discussion .....  | 39 |
| 4.1 Chapter outline .....   | 39 |
| 4.2 Characterisation of MOF-5 crystals .....                            | 39 |
| 4.2.1 Effect of solvent choice: DEF and DMF .....                       | 39 |
| 4.2.2 Effect of stirring speed on the MOF-5 crystals .....              | 44 |
| 4.2.3 Effect of reaction temperature on the MOF-5 crystals .....        | 45 |
| 4.2.4 Effect of reaction time on the MOF-5 crystals .....               | 46 |
| 4.2.5 MOF-69c conversion to MOF-5 .....                                 | 47 |
| 4.2.6 Optimised MOF-5 synthesis .....                                   | 51 |
| 4.3 Characterisation of Zr-MOF crystals .....                           | 52 |
| 4.3.1 Solvothermal synthesis of Zr-MOF: effect of modulator ratio ..... | 52 |
| 4.3.2 Effect of synthesis time on the crystallisation of Zr-MOF .....   | 57 |
| 4.3.3 TGA analysis .....  | 58 |
| 4.3.4 Microwave-assisted synthesis of Zr-MOF .....                      | 60 |
| 4.3.5 Optimised Zr-MOF synthesis .....                                  | 63 |
| 4.4 Characterisation of Cr-MOF crystals .....                           | 64 |



|             |   |    |
|-------------|---|----|
| 4.4.1       | Solvothermal synthesis of Cr-MOF: Effect of modulator ratio.....      | 64 |
| 4.4.2       | Effect of synthesis time on the crystallisation of Cr-MOF.....        | 69 |
| 4.4.3       | TGA analysis.....   | 71 |
| 4.4.4       | Optimised Cr-MOF synthesis.....                                       | 73 |
| 4.5         | Hydrogen storage studies .....  | 73 |
| 4.5.1       | Hydrogen adsorption isotherms of MOF-5 .....                          | 73 |
| 4.5.2       | Hydrogen adsorption isotherms of MOF-69c and transitioned MOF-5 ..... | 75 |
| 4.5.3       | Hydrogen adsorption isotherms of Zr-MOF.....                          | 76 |
| 4.5.4       | Hydrogen adsorption isotherms of microwave-assisted Zr-MOF .....      | 77 |
| 4.5.5       | Hydrogen adsorption isotherms of solvothermal Cr-MOF.....             | 78 |
| Chapter 5   | .....   | 80 |
| Conclusions | .....   | 80 |
| References  | .....   | 82 |

## ABSTRACT

Generation of power from fossil fuels produces large amounts of carbon dioxide which is a major contributor to global warming and many other environmental problems. Alternative sources of energy are available but fossil fuels remain the main source of energy for on-board energy generation. One alternative source that has gained great popularity in recent years has been hydrogen. The characteristics which it possesses make it an ideal alternative to fossil fuels for on-board energy generation and also for stationary (portable) power applications. Widespread use of hydrogen as an energy carrier can only be realised once a reliable storage method which is safe and affordable becomes available. Such a storage medium should have sufficient hydrogen storage capacity, fast kinetics, and be capable of delivering hydrogen gas to a fuel cell at ambient or near-ambient conditions.

This study investigated the storage of hydrogen using metal-organic frameworks (MOFs). MOFs are a class of porous inorganic-organic crystalline materials that store hydrogen by adsorption. What makes MOFs such an attractive option for hydrogen storage is that they have exceptionally high surface areas and porosity, as well as tunable pore sizes and internal surfaces. MOFs have provided successful hydrogen storage at cryogenic temperatures (77 K) and a major challenge is to reach high storage capacities at ambient temperatures and acceptable pressures. The HySA Infrastructure Centre of Competence (CoC), one of three centres of competence established by the Department of Science and Technology (DST) to implement the National Hydrogen and Fuel Cells Strategy, is tasked with R&D on hydrogen generation, storage and distribution. A major part of the hydrogen storage R&D is the development of MOFs for hydrogen storage with the ultimate aim of using the developed MOFs for practical applications, including fuel cell vehicles and portable power applications, using metals that promote the beneficiation of South African mineral resources.

The MOFs that were investigated in this study are zinc-based MOF (Zn-MOF, MOF-5), zirconium-based MOF (Zr-MOF, UiO-66) and chromium-based MOF (Cr-MOF, MIL-101). These MOFs were chosen because they were envisaged as potential hydrogen

storage options. MOF-5 in particular was seen as an ideal starting point for this study as it has been reported to have high surface area, permanent porosity, good thermal stability and a high synthetic yield. In addition, MOF-5 is amongst the most widely investigated MOFs for hydrogen storage. In this study, MOF-5 with high crystallinity and good morphology was synthesised using either N,N-diethylformamide (DEF) or dimethylformamide (DMF) as solvent. As DMF is a cheaper solvent than DEF the synthesis conditions were optimised for the DMF-synthesised MOF-5 and detailed analyses performed. It was discovered at some point that MOF-69c was produced as a product instead of MOF-5. Successful transition from MOF-69c to MOF-5 was achieved by employing a simple heat treatment. Due to the moisture sensitivity of MOF-5 which results from the weak interaction of Zn metal with O atoms in the framework, MOF-5 and other MOFs with different metal centres were synthesised in an attempt to overcome the moisture sensitivity problem.

This led to the investigation of Zr-MOF (UiO-66) as it had the best results and had been reported to be moisture stable. Zr-MOF was synthesised using a solvothermal synthesis procedure and a microwave-assisted synthesis approach. The solvothermal synthesis was optimised using formic acid as a modulator and the microwave-assisted synthesis provided a rapid synthesis technique. The optimised synthesis produced octahedral-shaped Zr-MOF crystals of high crystallinity, with excellent moisture and thermal stability. As the synthesis of MOF-5 and Zr-MOF employed DMF, an environmentally harsh solvent, the need to pursue a greener MOF synthesis led to the investigation of Cr-MOF (MIL-101). A successful modulated synthesis of Cr-MOF using formic acid instead of HF as modulator, and water as the reaction solvent was achieved.

The synthesised MOFs were characterised and their hydrogen adsorption capacity measured at 77 K and at pressures up to 1 bar. It was found that MOF-5 had a maximum hydrogen uptake of 1.60 wt% (DEF-synthesised MOF-5) and 1.40 wt% (DMF-synthesised MOF-5) whilst MOF-69c had a maximum uptake of 1.90 wt%. Zr-MOF had a maximum hydrogen uptake of 1.50 wt% and a maximum hydrogen uptake of 1.92 wt% was achieved for the Cr-MOF. Hydrogen uptake was found to be related to the quality of the MOF crystals and also directly related to the surface area, pore volume and/or pore size of the particular MOF.

## ACKNOWLEDGEMENTS

First and foremost, I would like to thank the Lord Almighty for blessing me with this great opportunity and to have seen me through all the struggles I have faced and giving me strength to complete my master's degree.

My CSIR supervisors, Dr Jianwei Ren and Dr Henrietta Langmi, for their guidance and support and seeing the potential within me. Many thanks for this great opportunity.

My Tuks supervisor, Prof Philip Crouse; for his guidance and continued support. I could have not done it without you.

Mr Joel Lekitima for his continued support and wise words in times of need.

The love of my life and mother to my baby, Miss Elsie Mpye. Thank you for your undying love and pushing me to be the best I can be.

Many thanks to my CSIR HySA family for the fun times at the CSIR, the laughter and support.

The candidate would like to thank the DST for its financial support through the HySA Infrastructure programme.

To my extended family and close friends for their support and encouragement.

## ACHIEVEMENTS DURING MASTERS STUDY

The subject of this work has been published in several peer reviewed journals:

1. Ren, J., Musyoka, N.M., Langmi, H.W., Segakweng, T., North, B.C., Mathe, M. and Kang, X. (2014) "Modulated synthesis of chromium-based metal-organic framework (MIL-101) with enhanced hydrogen uptake", *International Journal of Hydrogen Energy*, 39 (23), 12018-12023.
2. Ren, J., Rogers, D.E., Segakweng, T., Langmi, H.W., North, B.C., Mathe, M. and Bessarabov, D. (2014) "Thermal treatment induced transition from  $Zn_3(OH)_2(BDC)_2$  (MOF-69c) to  $Zn_4O(BDC)_3$  (MOF-5)", *International Journal of Materials Research*, 105(1), 89-93.
3. Ren, J., Segakweng, T., Langmi, H.W., Musyoka, N.M., North, B.C., Mathe, M. and Bessarabov, D. (2014) "Microwave-assisted modulated synthesis of zirconium-based metal-organic framework (Zr-MOF) for hydrogen storage applications" *International Journal of Materials Research*, 105(5), 516-519.
4. Ren, J., Segakweng, T., Langmi, H.W., North, B.C. and Mathe, M. (2015), "Ni foam-immobilized MIL-101 (Cr) nanocrystals toward system integration for hydrogen storage", *Journal of Alloys and Compounds*, 645(1), 170 – 173.
5. Segakweng, T., Musyoka, N.M., Ren, J., Crouse, P., Langmi, H.W., (2015) "Comparison of MOF-5 and MIL-101 derived carbons for hydrogen storage" *Progress in Natural Science: Materials International*, submitted.

The work has been presented at several conference proceedings, namely:

1. Modulated synthesis of Cr-MOF (MIL 101) for hydrogen storage applications.  
T Segakweng, J Ren, HW Langmi, BC North.  
In SACI Green Chemistry Conference, 2014, Durban South Africa, Southern Sun Hotel and Conference Centre, 17-21 August 2014.
2. Zirconium-based metal organic framework (Zr-MOF) material with high hydrostability for hydrogen storage applications  
J Ren, NM Musyoka, HW Langmi, T Segakweng, BC North, M Mathe.  
In The 5th World Hydrogen Technologies Convention (WHTC2013), Shanghai Everbright Convention & Exhibition Centre, 25-28 September 2013.

The candidate was nominated for the best master's candidate at the CSIR-MSM Awards in 2014.

He was also awarded the Gordon Research Conferences' GRC Carl Storm International Diversity (CSID) Award to attend the 2015 Hydrogen-Metal Systems Gordon Research Conference (GRC) and Gordon Research Seminar (GRS) in the United States from the 11<sup>th</sup> July to the 17<sup>th</sup> July, 2015.

## LIST OF FIGURES

|  |    |
|--|----|
| Figure 1: Metal-organic framework structures (1D, 2D, and 3D) reported in the Cambridge Structural Database (CSD) from 1971 to 2011. (Furukawa et al. 2013)..... | 6  |
| Figure 2: Simulated structure of MOF-5 (Yaghi et al. 2003).....  | 7  |
| Figure 3: Simulated structure of Zr-MOF (UiO-66) (Valenzano et al. 2011).....  | 7  |
| Figure 4: Simulated structure of Cr-MOF (MIL-101) showing the supertetrahedra (Lebedev et al. 2005).....   | 8  |
| Figure 5: Simplified flow diagram of the industrial synthesis of MOFs.....   | 10 |
| Figure 6: Synthesis conditions commonly used for MOF preparation (Dey et al. 2013).....  | 12 |
| Figure 7: Hydrogen uptake of PdNPs@[SNU-3] and pristine SNU-3 (Cheon & Suh 2009).....  | 20 |
| Figure 8: Different forms of catenation (Rowsell & Yaghi 2005).....  | 21 |
| Figure 9: a) Catenated PCN-6 and b) Non-catenated PCN-6' (Ma & Zhou 2010). ....  | 22 |
| Figure 10: Synthesis route for MOF-5.....  | 26 |
| Figure 11: Stability of MOFs to steam. (Canivet et al. 2014).....  | 30 |
| Figure 12: Structure of Cr-MOF (MIL-101) showing how F and O are directly attached to the Cr metal centres (Maksimchuk et al. 2012). ....                        | 34 |
| Figure 13: PXRD patterns of MOF-5 synthesised in DEF.....  | 40 |
| Figure 14: SEM images of MOF-5 synthesised in DEF.....   | 41 |
| Figure 15: PXRD patterns of MOF-5 synthesised in DMF.....  | 41 |
| Figure 16: SEM images of MOF-5 synthesised in DMF.....   | 42 |
| Figure 17: PXRD of MOF-5 obtained by a) Panella et al. using DEF (2006) and b) simulated PXRD obtained by Huang et al. (2003).....                               | 42 |
| Figure 18: Nitrogen adsorption isotherm for MOF-5 synthesised using DMF at 77 K.....   | 43 |
| Figure 19 : Nitrogen adsorption isotherm for MOF-5 synthesised using DEF at 77 K.....  | 44 |
| Figure 20: SEM images showing the effect of different stirring speeds.....   | 45 |
| Figure 21: SEM images of MOF-5 samples synthesised at a) 130 °C and b) 140 °C.....   | 46 |
| Figure 22: SEM images of MOF-5 synthesised in a) 3 h and b) 4 h.....   | 47 |
| Figure 23: (a) PXRD patterns and (b) SEM images of MOF-69c samples A and sample B after activation. ....   | 48 |
| Figure 24: Thermal treatment induced transition from MOF-69c to MOF-5 structure.....   | 49 |
| Figure 25: Nitrogen adsorption isotherms (insert, Horvath-Kawazoe differential pore volume plot) of the obtained MOF samples.....                                | 50 |
| Figure 26: PXRD patterns of Zr-MOF from differing modulator ratios. ....   | 54 |
| Figure 27: Nitrogen adsorption isotherms of the 0, 10 and 100 eq Zr-MOF samples.....   | 56 |
| Figure 28: PXRD patterns of Zr-MOF from differing reaction times. ....   | 58 |
| Figure 29: TGA curves of modulated and non-modulated Zr-MOF.....   | 59 |

Figure 30: SEM and PXRD patterns of Zr-MOF, respectively obtained using an oil bath after 24 h for temperature control, and microwave heating after 5 min ..... 60

Figure 31: Nitrogen adsorption isotherms of the Zr-MOF obtained using an oil bath for temperature control and microwave conditions..... 62

Figure 32: TGA curves of the oil bath and microwave Zr-MOF samples..... 63

Figure 33: PXRD patterns of Cr-MOF from differing modulator ratios. .... 66

Figure 34: SEM images of Cr-MOF obtained using different modulator equivalents ..... 67

Figure 35: Nitrogen sorption isotherms of 0, 50 and 100 eq Cr-MOF ..... 68

Figure 36: PXRD patterns of Cr-MOF samples obtained in different synthesis times using 100 eq of formic acid..... 70

Figure 37: SEM images of Cr-MOF samples obtained in different synthesis times using 100 eq of formic acid..... 71

Figure 38 : TGA mass loss analysis of 0, 50, and 100 eq Cr-MOF..... 72

Figure 39: Hydrogen adsorption of MOF-5 synthesised in DEF obtained at 77 K and up to 1 bar ..... 74

Figure 40: Hydrogen adsorption of MOF-5 synthesised in DMF obtained at 77 K and up to 1 bar ..... 75

Figure 41: Hydrogen uptake isotherms for MOF-5 and MOF-69c samples ..... 76

Figure 42: Hydrogen uptake isotherms for Zr-MOF (UiO-66) obtained at 77 K and up to 1 bar..... 77

Figure 43: Hydrogen uptake isotherms for Zr-MOF from the microwave and oil bath synthesis. .... 78

Figure 44: Hydrogen uptake isotherms for Cr-MOF (MIL-101) samples..... 79

## LIST OF TABLES

|  |    |
|--|----|
| Table 1: Classification of porous materials .....  | 15 |
| Table 2: Variables for optimisation of MOF-5 synthesis .....   | 28 |
| Table 3: MOF-69c Samples with different heat treatments .....  | 29 |
| Table 4: MOFs with different metal centers.....  | 30 |
| Table 5: Variables investigated for Zr-MOF optimisation .....  | 32 |
| Table 6 : Properties of F compared to Cl and S.....  | 35 |
| Table 7: Variables investigated for Cr-MOF optimization .....  | 36 |
| Table 8: Pore characteristics of prepared MOF samples .....  | 51 |
| Table 9: Optimised variables for the synthesis of MOF-5 .....  | 52 |
| Table 10: Comparison of physical properties of the Zr-MOF samples from this work with those reported in the literature ..... | 57 |
| Table 11: Optimised variables for the synthesis of Zr-MOF.....   | 64 |
| Table 12: Physical properties of the desolvated Cr-MOF (MIL-101) samples .....   | 68 |

## LIST OF REACTIONS

|  |    |
|--|----|
| Reaction 1: Preparation of MOF-5 .....       | 9  |
| Reaction 2: Reaction of DMF with water ..... | 55 |

## NOMENCLATURE

|                    |  |
|--------------------|--|
| ASAP               | Accelerated Surface Area and Porosity          |
| bdc                | 1,4-Benzene-dicarboxylate                      |
| BET                | Brunauer–Emmett–Teller                         |
| bpdc               | 4,4' -Biphenyldicarboxylate                    |
| BTB                | 4,4',4''-Benzene-1,3,5-triyl-tribenzoate       |
| BTC                | Benzene-1,3,5-carboxylate                      |
| COF                | Covalent Organic Framework                     |
| DEF                | Diethylformamide                               |
| DMA                | N,N-Dimethylacetamide                          |
| DMA                | Dimethylammonium                               |
| H <sub>2</sub> BDC | 1,4 benzenedicarboxylic acid                   |
| H-K                | Horvath-Kawazoe                                |
| HKUST              | Hong Kong University of Science and Technology |
| Me                 | Methyl   |
| MIL                | Matériel Institute Lavoisier                   |
| MOFs               | Metal-Organic Frameworks                       |
| mtb                | Methanetetra-benzoate                          |
| MW                 | Microwave                                      |
| NDC                | 2,6-naphthalenedicarboxylate                   |
| NOTT               | Nottingham                                     |
| Ntb                | 4,4',4''-nitrilotrisbenzoate                   |
| NU                 | North-western University                       |
| PCN                | Porous Coordination Network                    |
| PXRD               | Powder X-ray Powder Diffraction                |
| R&D                | Research and Development                       |
| SEM                | Scanning Electron Microscopy                   |
| SNU                | Seoul National University;                     |
| TEM                | Transmission Electron Microscopy               |
| TGA                | Thermos Gravimetric Analysis                   |
| THF                | Tetrahydrofuran                                |
| UiO                | University of Oslo                             |

|         |  |
|---------|--|
| US DOE  | United States Department of Energy                   |
| wt%     | Weight percent                                       |
| ZIF     | Zeolite A Imidazolate Framework                      |
| Zn-EZIF | Electrochemically made Zeolite Imidazolate Framework |

## Chapter 1

### Introduction

#### 1.1 Background and motivation

Generation of power from fossil fuels produces large amounts of carbon dioxide which is a major contributor to climate change and many other environmental problems (Murray, Dincă & Long 2009, Sandrock 1999). Although alternative sources of energy are available, fossil fuels remain the main source of energy. Therefore finding alternative energy sources with no greenhouse gas emissions has become a major focus of energy research. The leading contenders for alternative energy sources are nuclear, solar, wind and hydrogen. Whilst nuclear, wind and solar energy are excellent contenders for stationary power applications; they have little potential for on-board applications due to a number of reasons including safety, efficiency and practicality. Hydrogen on the other hand, is relatively safe to use, has high energy per unit mass, is very abundant (being the most abundant element in the universe although not readily available in its free form as molecular hydrogen), and its use excludes greenhouse gas emissions (Sandrock 1999, Grochala & Edwards 2004). These characteristics which hydrogen possesses make it an ideal alternative to fossil fuels for on-board energy generation.

Electrical cars can be powered by fuel cells which combine hydrogen and oxygen to produce electricity with relatively high efficiency (50 – 60 %); their only waste products are water and heat. Widespread use of hydrogen as a fuel can only be realised once a storage method which is reliable, safe, affordable and efficient is found. Some of the desirable characteristics of such a storage method are high volumetric and gravimetric hydrogen storage capacities, fast kinetics, and the capability of delivering hydrogen gas to a fuel cell at ambient or near-ambient conditions.

At first glance, one would assume that hydrogen can simply be used as compressed gas in cylinders, but it is not that simple. The reason for this is that modern cars which use fossil fuels require an average volume of 30 – 40 litres of fuel to travel a distance of ~500 km and a full tank of fuel weighs about ~80 kg. If an electric vehicle were to be fitted with a hydrogen fuel cell, it would need about 5 kg of hydrogen to travel the same distance. Whilst 5 kg may

seem low in comparison to the 80 kg of fuel for a modern car, the very low density of hydrogen ( $0.0899 \text{ kg}\cdot\text{m}^{-3}$ ) at ambient conditions implies that 5 kg of hydrogen occupies a volume of nearly 55,000 litres, which is equivalent to a sphere with a diameter of about 5 m. This would be very impractical for on-board use (Schlapbach 2009). Therefore it is necessary to store hydrogen in forms that will require fuel tanks with dimensions comparable to those of fuel tanks in modern cars. Hydrogen may also be applied in stationary (portable) power applications, in which case the weight and volume requirements are less stringent.

Hydrogen can be stored in three ways: as a liquid, as compressed gas, and in a solid material. The large amount of energy consumed during liquefaction, and the continuous boil-off of hydrogen, limit the possible use of liquid-hydrogen storage technology. Compressing hydrogen is an energy consuming process and requires a very high pressure to obtain enough hydrogen for reasonable usage cycles. This in turn leads to safety issues such as storage tank ruptures. Therefore, current attention is focused on solid storage materials. The storage of hydrogen in solid materials can be achieved by one of two processes:

- Chemical reactions in which hydrogen reacts with the solid material to form a new compound; and
- Adsorption in which hydrogen is adsorbed on the surface of the solid material.

Materials for hydrogen storage through chemical reactions include for example, metal hydrides, complex hydrides, and nitrides. These materials with relatively high hydrogen storage capacities usually have hydrogen release temperatures above 473 K as a consequence of the high energy required to break the chemical bonds between the hydrogen and other atoms. Such a high release temperature is a technical challenge to applications for on-board hydrogen storage. The United States Department of Energy (US DOE) has set 2017 targets for hydrogen storage capacities at 5.5 wt% and  $40 \text{ g H}_2\cdot\text{L}^{-1}$ , and operational temperatures at between 313 K and 353 K and the targeted costs are 67 \$ per kW·h net (United States Department of Energy 2009).

Porous materials with high surface areas such as activated carbons, carbon nanotubes and zeolites have been widely investigated for hydrogen storage by adsorption. The temperature of

hydrogen release is usually low. However, they have relatively low hydrogen storage capacities. Metal-organic frameworks (MOFs) have attracted much attention because of their structure and properties as well as their potential applications (Li et al. 1999). They offer exceptionally high surface areas and porosity as well as tunable pore sizes and internal surfaces. They have potential applications as gas storage materials particularly hydrogen. Since Yaghi and coworkers began exploring MOFs as hydrogen storage materials in 2003 (Yaghi et al. 2003) MOFs have provided successful hydrogen storage at cryogenic temperatures (77 K/ -195 °C) and a key challenge is to reach high storage capacities at ambient and/or near ambient temperatures and acceptable pressures.

The South African Department of Science and Technology (DST) launched a national hydrogen and fuel cells programme, known as Hydrogen South Africa (HySA) in 2008. Three HySA Centres of Competence (CoCs) were established to conduct research and development (R&D) to meet the objectives of the programme. HySA Infrastructure Centre of Competence is tasked with R&D on hydrogen generation, storage and distribution. A major part of the hydrogen storage R&D is the development of MOFs for hydrogen storage with the ultimate aim of using MOFs for practical applications including fuel cell vehicles and/or portable power applications, using metals that promote the beneficiation of South African mineral resources. The aim is to deliver technologies for hydrogen storage that meet the set cost targets and provide the best balance of safety, reliability, robustness, quality and functionality. The development of such storage technologies encompasses the following:

- Hydrogen storage materials development and measurements;
- Evaluation of hydrogen storage system level performance; and
- Exploration of the fundamental science.

The development of hydrogen storage materials with relatively high hydrogen adsorption capacities and fast hydrogen charge/discharge kinetics is the first goal.

## **1.2 Problem statement**

MOFs have demonstrated attractive storage capacities at cryogenic conditions. However, the synthesis of many of the current MOFs requires environmentally harmful materials and is inefficient. It is necessary to optimise their synthesis procedures for cost reduction and to make the synthesis as environmentally friendly as possible. Achieving this goal will result in

high quality materials being obtained reproducibly. Optimisation of synthesis procedures can increase the hydrogen uptake of MOFs whilst maintaining reasonable costs.

### 1.3 Project objectives

The overall aim of this study was to evaluate the potential offered by MOFs for hydrogen storage. The study was broken down into several segments, each with its own objectives.

The compounds that formed the focus of the study were three specific MOFs: the Zn-based MOF (MOF-5); Zr-based MOF (UiO-66); and Cr-based MOF (MIL-101). The study investigated the optimisation of the three different MOFs for hydrogen storage by gaining an understanding of their optimal synthesis conditions.

The following specific objectives were set:

- To synthesise MOF-5 using two different solvents and optimise the synthesis conditions.
- To synthesise Zr-MOF using a solvothermal method and a microwave-assisted approach, and optimise the synthesis conditions.
- To synthesise Cr-MOF using more environmentally friendly solvents/reagents, and optimise the synthesis conditions.
- To characterise the synthesised MOFs in terms of phase purity, crystallinity, morphology, crystal size, surface area, porosity and thermal stability.
- To evaluate the low-pressure hydrogen adsorption capacity of the developed MOFs at cryogenic temperatures.

The results from this study will be used to design and synthesise MOFs with optimised hydrogen storage capabilities and at reasonable costs with potential to approach the 2017 targets set by the US DOE.

## Chapter 2

### Literature review

#### 2.1 Chapter outline

MOFs have been researched as a potential hydrogen storage option because of their structural diversity, low weight, high surface area, and pore size that can be tailored to suit hydrogen storage. In this chapter, hydrogen storage in MOFs will be reviewed. The chapter begins with a general introduction to MOFs wherein the structure and composition of the three types of MOFs investigated in this study are described. It then provides information on the synthesis methods, activation and characterisation of MOFs. This is followed by a definition of the terms associated with hydrogen storage research. The chapter ends with a review of the factors that can be varied or utilised to increase the storage capacities of MOFs at cryogenic temperatures.

#### 2.2 Structural features, properties and applications of MOFs

MOFs are crystalline porous materials that have been researched for, amongst others, gas storage, gas separation and heterogeneous catalysis. (Mines et al. 2002, Czaja, Trukhanb & Ulrich 2009, Halder et al. 2002). MOFs consist of organic molecules that are bound to metals or metal clusters through coordination bonds. The vast variety of metal ions that can be used with different organic linkers allows researchers to design an almost infinite number of MOFs tailoring the desired property. Figure 1 shows a number of MOF structures reported in the Cambridge Structural Database (CSD) from 1971 to 2011. The number of structures reported has increased significantly year on year with the increase in the number of 3D structure types doubling in the same period (Furukawa et al. 2013). MOFs with three-dimensional structures have near constant pores which can be occupied by guest molecules via adsorption. MOFs have exceptionally high specific surface areas because they are open structures with pores without walls. The topology of the MOF is determined by the building blocks used. They typically have small pores which are less than 20 Å. This results in MOFs having strong interactions with adsorbed molecules (Langmi et al. 2014).

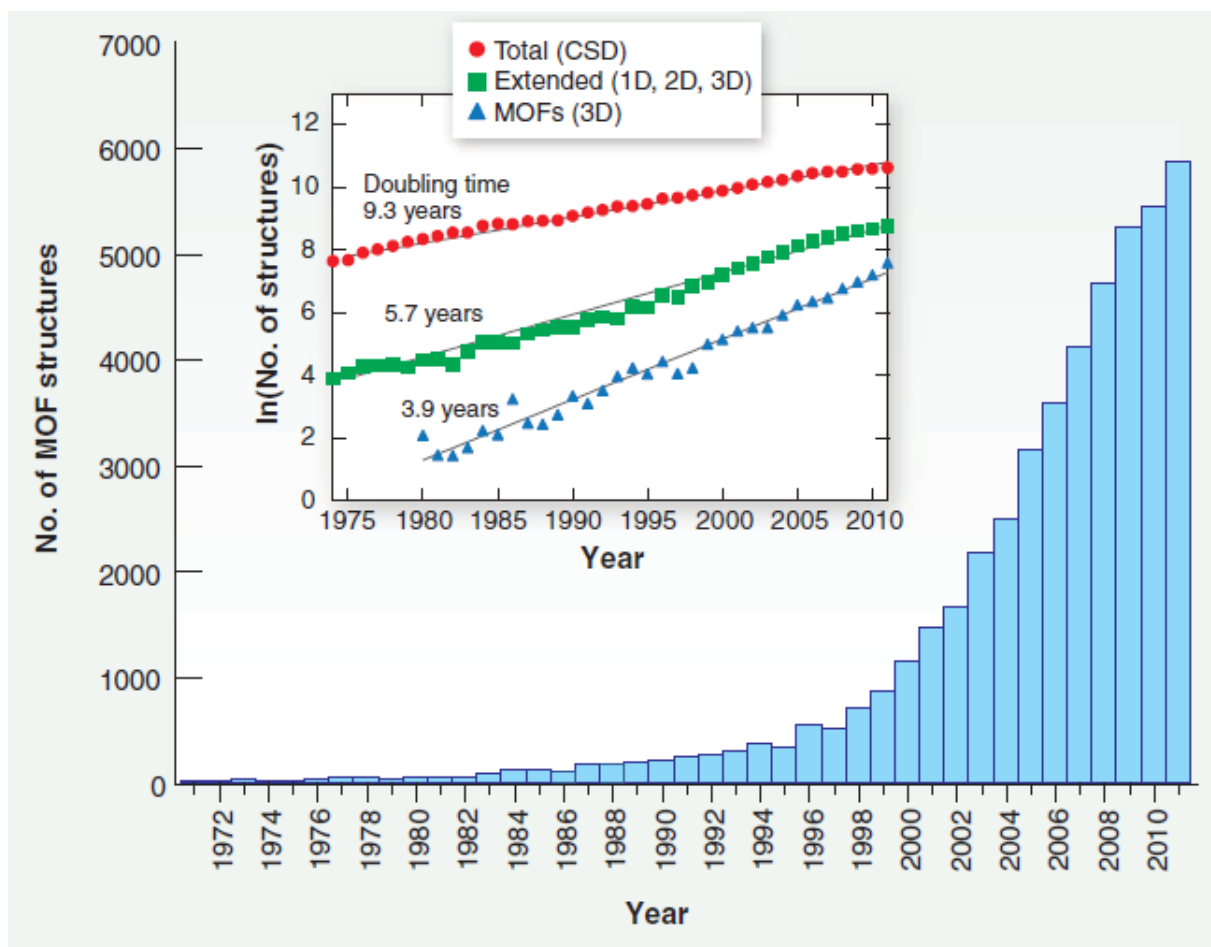


Figure 1: Metal-organic framework structures (1D, 2D, and 3D) reported in the Cambridge Structural Database (CSD) from 1971 to 2011. (Furukawa et al. 2013)

### 2.2.1 Structure and composition of MOF-5

Metal-organic framework-5 (MOF-5) of composition  $Zn_4O(BDC)_3$  (BDC = 1,4-benzenedicarboxylate) has a cubic three-dimensional extended porous structure. MOF-5 consists of inorganic  $[ZnO_4]^{6+}$  groups which are joined to an octahedral arrangement of  $[O_2C-C_6H_4-CO_2]^{2-}$  (1,4- BDC) groups to form a strong and highly porous cubic framework (Yaghi et al. 2003, Rosi et al. 2005). The MOF-5 structure is ideal for adsorbing gas molecules because the linkers are isolated from each other and accessible from all sides to the gas. The empty skeleton nature of MOF-5 and its derivatives has led to high apparent surface areas in the range of 2500 to 3000  $m^2 \cdot g^{-1}$ . The structure of MOF-5 is shown in Figure 2 with the available space for guest molecules shown by the yellow sphere in the centre of the MOF.

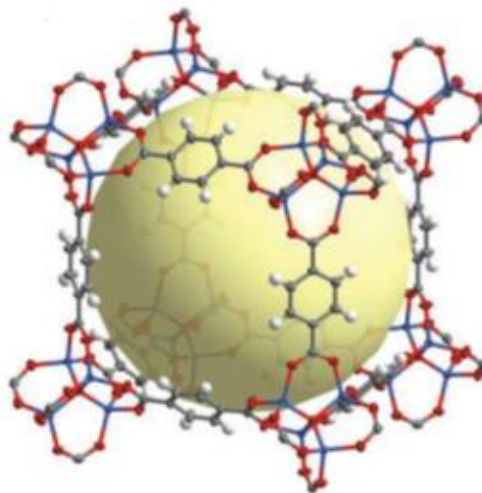


Figure 2: Simulated structure of MOF-5 (Yaghi et al. 2003).

### 2.2.2 Structure and composition of Zr-MOF

Zr-MOF using the terephthalate ion (BDC) as a linker is commonly known as UiO-66 (UiO = University of Oslo) (Valenzano et al. 2011). This MOF is based on a  $Zr_6O_4(OH)_4$  octahedron, forming lattices by 12-fold connection through a 1,4-benzene-dicarboxylate (BDC) linker as shown in Figure 3 with the available space for guest molecules shown by the yellow sphere in the centre of the MOF. The UiO series of MOFs is characterized by high surface areas and by high stability which is linker independent. They owe their high stability to the fact that each Zr ion is 12-fold connected to adjacent octahedra. Zr-MOF is thermally stable up to 375 °C and also stable in various solvents such as water, DMF, acetone and ethanol (Hafizovic et al. 2014).

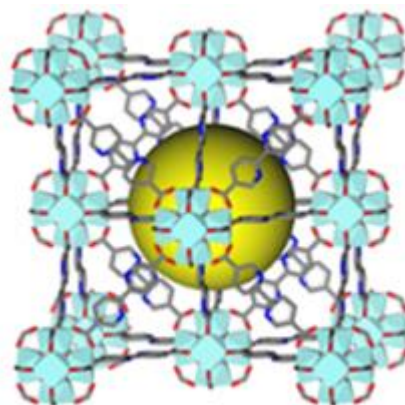


Figure 3: Simulated structure of Zr-MOF (UiO-66) (Valenzano et al. 2011)

### 2.2.3 Structure and composition of Cr-MOF

Cr-MOF, also called MIL-101 (MIL = Matériel Institute Lavoisier), is composed of  $\text{Cr}^{3+}$  ions with the 1,4-benzene-dicarboxylate (BDC) linker, forming the so called supertetrahedra (ST). The corners of the supertetrahedra are formed by four  $\text{Cr}^{3+}$  ions whilst the organic linkers are located at the six edges of the supertetrahedra as shown in Figure 4 (Lebedev et al. 2005). The connection of the supertetrahedra ensures a three-dimensional network of corner-sharing supertetrahedra with an augmented MTN zeotype. The structure contains two kinds of extra-large cages with cavity, as well as pentagonal and hexagonal cage windows (Latroche et al. 2006).

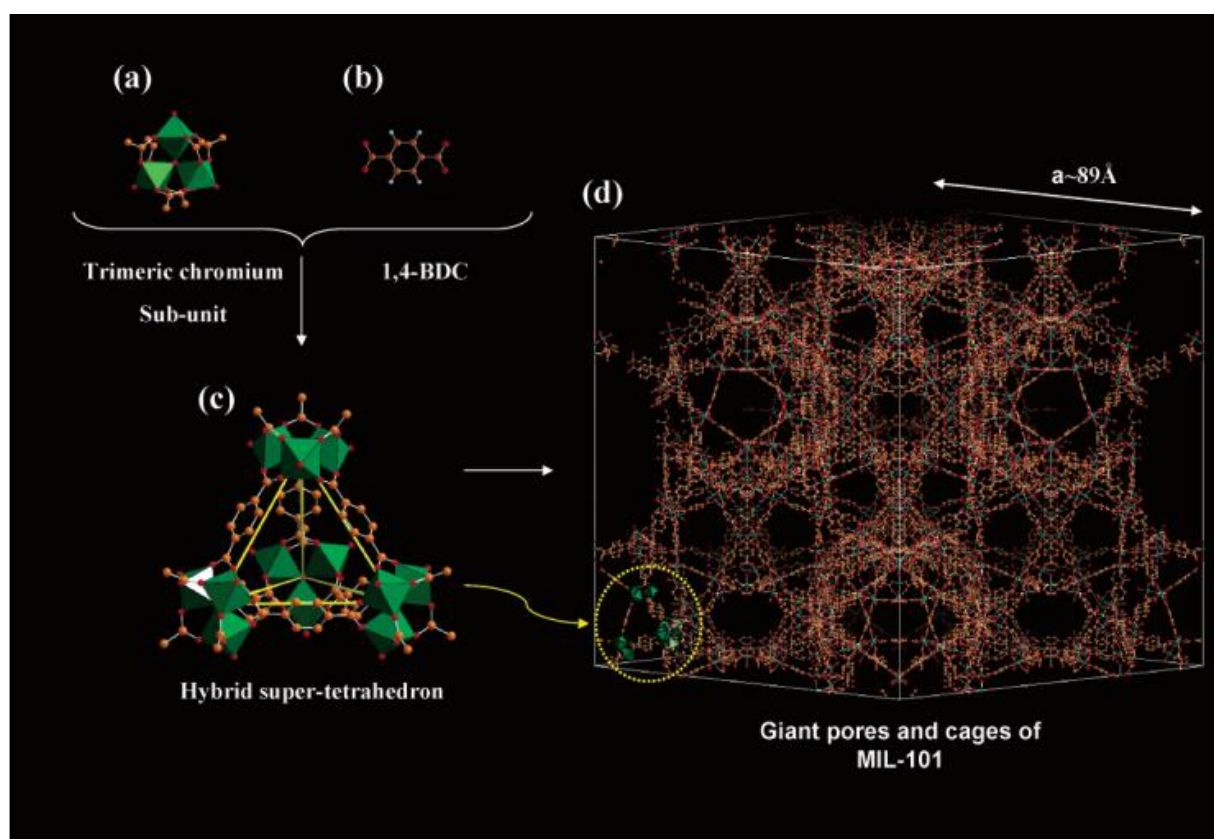


Figure 4: Simulated structure of Cr-MOF (MIL-101) showing the supertetrahedra (Lebedev et al. 2005).

### 2.3 Synthesis and activation of MOFs

The solvothermal synthesis of MOFs generally includes the following components:

- A easily soluble salt as the source for the metal component;
- Organic compounds to form the bridging ligands, mostly mono-, di-, tri- and tetracarboxylic acids; and

- A polar solvent such as dimethylformamide (DMF).

After combination of these inorganic and organic components, the metal–organic structures are formed within a few hours by self-assembly at temperatures starting at room temperature and generally up to 200 °C. A simplified flow diagram of the industrial synthesis of MOFs is shown as an example in Figure 5. The scheme indicates not only the different steps of preparation but also the solvent recycle streams. After the sample is dried, it is further processed into shaped material for system integration. The preparation of, for example MOF-5, is stoichiometrically expressed as:



Reaction 1: Preparation of MOF-5

Here H<sub>2</sub>BDC is terephthalic acid and Zn<sub>4</sub>O(BDC)<sub>3</sub> is the MOF-5 unit composition. It is clearly seen that the equilibrium can be shifted to the right by applying the Le Châtelier's principle (LTP) by decreasing the concentrations of the released water and nitrate. Taking these equilibrium conditions into consideration makes it possible to control the quality of the MOFs, thereby altering the surface area (M. Schubert, U. Müller and H. Mattenheimer, 2007). An important factor to take note of in large scale production of MOFs is the space–time yield (STY) (kg of MOF per m<sup>3</sup> of reaction mixture per day), which should be as high as possible.

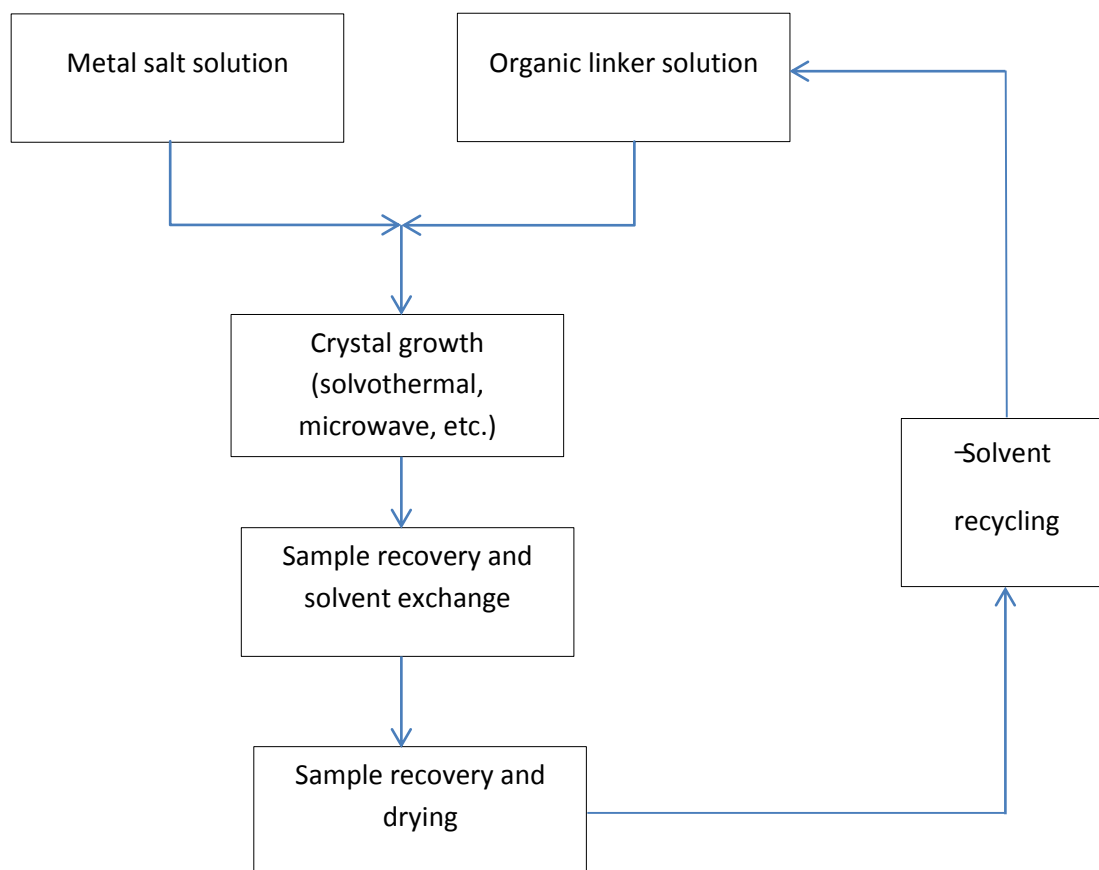


Figure 5: Simplified flow diagram of the industrial synthesis of MOFs

Among the solvents used during the synthesis of MOFs, formamides are popular because they not only dissolve the reactants but also deprotonate the carboxylic acids. In addition, important variables in the reaction conditions including reagent concentration, time, stirring speed, temperature and fractional volume filling of the vessel. Due to the disadvantages of the solvothermal method, such as long reaction time, high temperature, and high cost of solvents, alternative synthetic methods for the synthesis of MOFs have been developed. They include solvent-free syntheses, microwave heating, electrochemical methods, sonochemical and mechanochemical reactions (Son et al. 2008, Pichon, Lazuen-Garay & James 2006). The slow evaporation method is a method using very little, or no external, energy at all. The reaction is done at room temperature, although its main disadvantage is the long reaction times which may take several days to reach completion. In a typical reaction setting, the reagents are concentrated by slowly evaporating the solvent at a fixed temperature. The use of a mixture of solvents may increase the solubility of the reagents and thus speed up the reaction (Dey et al. 2013). In microwave-assisted synthesis, the thermal energy is supplied by the microwave field

coupling directly with the reactants. The reaction is usually fast needing only several minutes to an hour to complete to yields nanosized crystals. Electrochemical syntheses offer the ability to synthesise large MOF crystals under mild conditions by simply adjusting the pH of the solvent at room temperature. The electrochemical synthesis method does not require metal salts, as the metal ion is provided by anodic dissolution into the synthesis mixture which will contain the organic linkers and electrolytes. This method provides a continuous flow reaction that is advantageous to industrial production of MOFs (Dey et al. 2013). Mechanochemical synthesis is a solvent-free synthesis method that uses mechanical force to synthesise the MOFs. Mechanochemical synthesis has been modified to include a small amount of solvent in the solid mixture, called liquid-assisted grinding (LAG), where a small amount of solvent is added into a solid reaction mixture (Dey et al. 2013). Sonochemical synthesis involves the use of intensive ultrasonic radiation (20 kHz–10MHz) to initiate a chemical change in the molecules. The ultrasound radiation induces chemical or physical changes by inducing cavities/ bubbles in a liquid, which then collapse creating local hot spots with a short lifetime and high local temperatures and pressures. These extreme conditions promote chemical reactions by immediate formation of a surplus of crystallization nuclei (Dharmarathna et al. 2012). Figure 6 shows a summary of the different methods for synthesising MOFs.

In hydrogen uptake studies of MOFs, sample activation has been recognized as a key factor towards obtaining reproducible and reliable hydrogen uptake data. In more traditional activation methods, MOF samples are soaked in low boiling solvents, such as dichloromethane, chloroform, ethanol, etc., to exchange and remove the solvents used during the synthesis, which often have high boiling temperatures. The lower boiling point solvents are removed by evacuation or by mild heating. However, this process may lead to poor porosity or even collapse of a MOF structure because of the surface tension. An alternative to solvent exchange is activation via supercritical drying and freeze-drying which has resulted in a significant improvement in pore quality and structural integrity, especially for single crystal synthesis. Both techniques have provided a route towards MOFs that were previously inaccessible.

When using one of these activation methods, the solvent is replaced under mild conditions and the problem of surface tension is eliminated. Mondloch reported on several methods to activate MOFs, including the use of supercritical carbon dioxide (sc-CO<sub>2</sub>) drying procedure which resulted in improved gas permeability in the MOFs (Mondloch et al. 2013). Ma and co-

workers reported that by applying a freeze-drying activation procedure, the Langmuir surface area of a Cu-based MOF, comprised of methanetetra (p-benzoate), was triple that of the sample activated by conventional solvent exchange techniques, moreover, the hydrogen uptake capacity at 77 K and 1 bar was improved by 82 % (Nelson et al. 2008, Ma, Abney & Lin 2009).

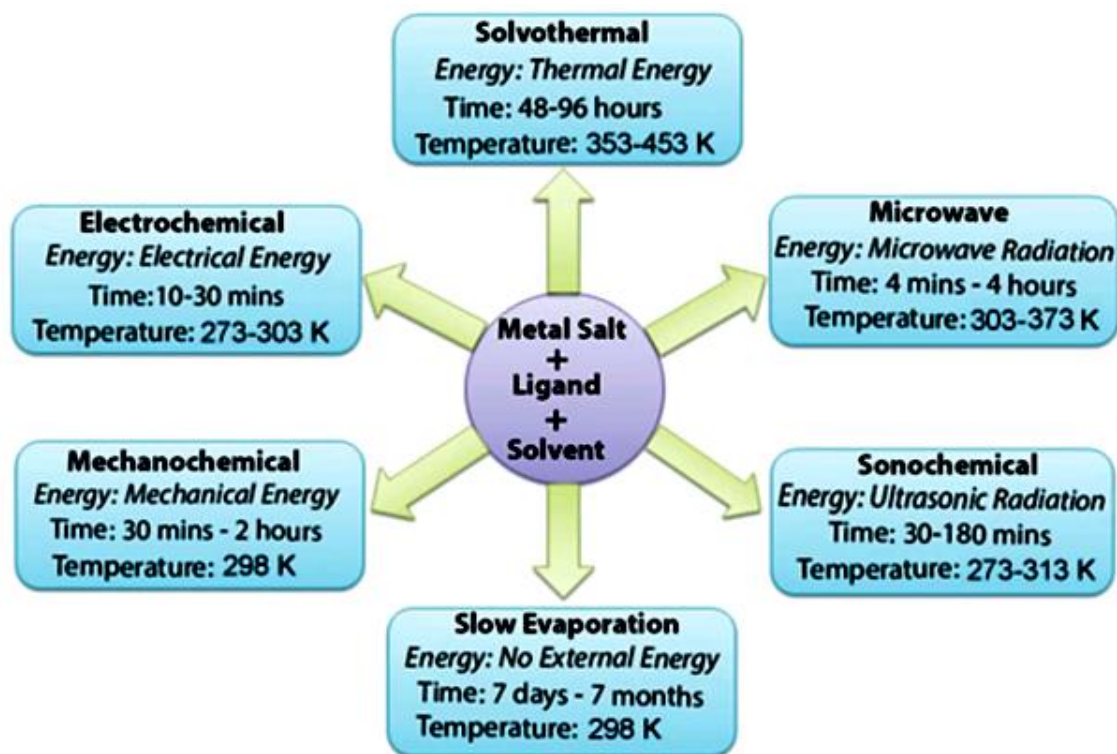


Figure 6: Synthesis conditions commonly used for MOF preparation (Dey et al. 2013)

## 2.4 Characterisation of MOFs

As MOFs are both crystalline and highly porous materials, powder X-ray diffraction (PXRD) is frequently used to characterise the crystallinity and phase purity. Adsorption measurements are performed to evaluate the porosity, and neutron scattering may be used to determine adsorption sites (Rosi et al. 2003, Gedrich et al. 2010). Commercially available equipment using nitrogen uptake at 77 K or argon uptake at 87 K is employed and equivalent surface areas are calculated using the Langmuir or BET equation. However, it should be considered that the underlying model of independent, equivalent and non-infringing sorption sites might be different on a molecular level. Many reports have described localised, rather than bulk, volume adsorption phenomena on metal–organic materials, with some even clearly differentiating between various crystallographic sites and adsorption strengths (Kubota et al.

2005, Yildirim, Hartman 2005).

As the metal content reaches concentrations between 20–40 wt%, it is also desirable to check the local metal cluster arrangements and environments using more sophisticated methods such as extended X-ray Adsorption Fine Structure (EXAFS), X-ray Adsorption Near-Edge Structure (XANES) or X-ray Photoelectron Spectroscopy (XPS). The adsorbates in the pores of MOFs can be investigated by UltraViolet–VISible (UV-VIS), Infra-Red (IR) and Raman spectroscopy (Chae et al. 2004).

## **2.5 Hydrogen storage in MOFs**

Gas adsorption in MOFs was first reported in 1997 by Kondo et al. (Kondo et al. 1997), and then in 2003, Yaghi et al. (Yaghi et al. 2003) began exploring hydrogen storage in MOFs (Rosi et al. 2003, Férey et al. 2003). From then on, MOFs have been successfully used to store hydrogen at cryogenic temperatures (77 K). MOF-5 for example, has shown an excess hydrogen uptake of 7.1 wt% at 77 K and 40 bar (Saha & Deng 2010). At 100 bar, a total uptake of 10.0 wt% could be achieved. MOF-177 gives a total gravimetric uptake of 11.2 wt% at 77 K (Saha, Deng 2010). Moreover, the reproducibility of these MOFs demonstrates that 100% hydrogen uptake and release can be achieved in several minutes without compromising the MOF structure. Although results so far seem to indicate that MOFs are serious candidates for future hydrogen storage, achieving on-board hydrogen storage for automotive applications is still a big challenge. Issues such as moisture sensitivity and the ability to store hydrogen at near ambient temperatures need to be resolved prior to exploring commercial applications. The main challenge now is to reach high storage capacities at ambient temperatures and acceptable pressures (Langmi et al. 2014).

## **2.6 Definitions of concepts and terms used in hydrogen storage research**

### **2.6.1 Sorption and desorption**

The term sorption describes both adsorption and absorption when it is difficult, or impossible, to distinguish between adsorption and absorption, or when they occur at the same time. Desorption is the opposite process of sorption (Suh et al. 2011).

### **2.6.2 Adsorption and absorption**

Adsorption is the reversible binding of hydrogen onto the surface of a storage material. It

differs from absorption in that during absorption, the hydrogen occupies the pores of the storage material and not only the surface. In adsorption, the structure and chemical nature of the absorbing material and that of the adsorbed compound may be modified. Adsorption and absorption refer to the location of the hydrogen relative to the sorbent, i.e. whether it is on the surface or in the bulk of the material respectively (Suh et al. 2011).

### **2.6.3 Chemisorption and physisorption**

Chemisorption occurs on the surface of the storage medium. It is when the interaction force between the surface of the medium and the adsorbate is similar to the chemical bonding in bulk compounds. Physisorption is restricted to adsorption and occurs when the forces involved are weak intermolecular forces (van der Waals forces). Physisorption does not involve a significant change in the electronic structure of the species involved. For a molecular adsorbate where no bond dissociation occurs, it is often difficult to draw a boundary between strong physisorption and weak chemisorption. A notable difference between the two processes is that in molecular physisorption, the H-H bond in the gas phase is preserved during adsorption, and in chemisorption the H-H bond is broken. Chemisorption may occur only in a monolayer on a surface, whereas physisorption is usually accompanied by multilayer adsorption depending on the temperature (Suh et al. 2011).

### **2.6.4 Langmuir surface area and BET surface area**

Porous materials are classified as macroporous, mesoporous, microporous, supermicroporous and ultramicroporous, according to the IUPAC system which utilizes the size of the pores to make the classification. Table 1 below shows the classification of porous materials. Most MOFs reported so far are regarded as microporous. Small pores of the ultramicroporous range are filled at very low relative pressures i.e.  $P/P_0$  and the pore filling mechanism is directed mainly by the gas-solid interactions, and the adsorption rate depends on temperature. Pores in the supermicroporous region exhibit cooperation effects in addition to the gas-solid interactions. This cooperation effect causes pore filling to occur at relatively lower relative pressures (Marsh 1987, Lowell et al. 2010).

**Table 1:** Classification of porous materials

| Classification   | Pore size Å |
|------------------|-------------|
| Macroporous      | >500        |
| Mesoporous       | 20-500      |
| Microporous      | < 20        |
| Supermicroporous | 7-20        |
| Ultramicroporous | <7          |

The specific surface area of porous materials is generally determined using N<sub>2</sub> adsorption isotherms at 77 K. The Langmuir equation and the Brunauer–Emmett–Teller (BET) equation are then used to calculate the surface area. The Langmuir equation is mainly used when working with materials that possess uniform surfaces with the adsorbed compounds forming a monolayer. Most MOFs have different atomic surfaces which interact differently with the adsorbed gas. During the adsorption process, the initial adsorption is at the strong adsorption sites and moves to the weaker adsorption sites as the pressure increases. As with the different adsorption sites, if the MOF contains different sized pores, the narrower pores are filled first before the wider pores are filled. When the Langmuir equation is used to calculate the surface area, accurate results may not be obtained due to the fact that there are many pore filling mechanisms at work in the MOF, especially at low temperatures. BET theory on the other hand, takes into account the different pore filling mechanisms. Because of its simplicity, BET is used worldwide for reporting surface area data for MOFs. Some molecular simulation results that use grand canonical Monte Carlo simulation have also been reported to predict BET surface areas that are very similar to experimental results (Walton & Snurr 2007). Caution needs to be exercised when using the BET surface area equation, as the calculated surface area of the MOF depends on the pressure range used (Dueren et al. 2007). Despite the draw backs of both equations, both are still being used for calculating the surface area of MOFs although, in almost all cases, the surface area calculated using the Langmuir equation is higher than that obtained using the BET equation. An example of this is the surface area reported for MOF-210: the Langmuir surface area is 10400 m<sup>2</sup>·g<sup>-1</sup>, and BET surface area is 4530 m<sup>2</sup>·g<sup>-1</sup> (Furukawa et al. 2010, Rowsell & Yaghi 2005).

### 2.6.5 Excess hydrogen adsorption and total hydrogen adsorption

Excess adsorption is described as the amount of hydrogen adsorbed in a material above that

which can be contained, under identical temperature and pressure conditions, in a free volume which is equivalent to the total pore volume of the sample. It therefore gives an approximation of the quantity of hydrogen adsorbed on the surface of the material. The excess adsorption is the quantity that is measured in experiments. Because of the limits of packing and compressing gas molecules within the pores of a porous solid, the excess adsorption will reach a maximum at a certain pressure and then decrease. Although the excess adsorption will decrease beyond a certain pressure, measurements obtained from excess adsorption are used to assess the compressibility of the gas in the pores of the material as well as the total uptake (Rosi et al. 2003, Rowsell & Yaghi 2005).

The total uptake describes the amount of hydrogen contained in the space occupied by the MOF crystals. It takes into account the hydrogen adsorbed both on the surface of the MOF and in the pores of the MOF. When calculating the total adsorption from the excess adsorption, one needs to know the skeletal density of the MOF which can be obtained from a gas pycnometer using helium gas. The high pressure hydrogen uptakes are generally represented as excess and total adsorption amount. Meanwhile the excess and total adsorption amounts are generally almost identical for hydrogen uptake up to 1 bar. Generally, hydrogen adsorption capacities in MOFs are expressed in wt%, which is the percentage of the total mass (MOF + hydrogen) ascribed to hydrogen (Murray, Dincă & Long 2009).

#### **2.6.6 Isosteric heat of adsorption**

The isosteric heat of adsorption between a MOF and hydrogen molecule is the interaction energy between the MOF and the adsorbed hydrogen. Increasing this heat of adsorption increases the amount of hydrogen adsorbed. There are various ways of doing so including modification of the pore size. It is calculated using the hydrogen adsorption isotherms at two different temperatures, usually 77 K using liquid nitrogen and 87 K using liquid argon. The data is fitted to the virial equation or the Langmuir-Freundlich equation. The equation gives isosteric heat of adsorption which is dependent on the amount of hydrogen adsorbed at each temperature. It does not, however, give information about position of and the number of hydrogen adsorption sites in the MOF (Suh et al. 2011).

### **2.7 Cryogenic hydrogen storage in MOFs**

As stated, MOFs can store large amounts of hydrogen at cryogenic temperatures. Hydrogen adsorption in MOFs occurs by physisorption at low temperatures. This involves weak Van der

Waals forces, and the adsorption isotherms are typically Type I in nature. Hydrogen storage studies are usually performed at cryogenic temperatures as a start before investigating the storage at ambient temperatures. As the highest storage capacities at ambient pressures have been reported at cryogenic temperatures, it is useful to understand the factors that affect the hydrogen storage capacity of MOFs under these conditions before moving to ambient temperatures. Optimisation of these factors as described below can lead to improved hydrogen storage properties.

### **2.7.1 Creating open metal sites**

Open metal sites in MOFs are potentially important for hydrogen storage; these are sites in the MOF crystals that are previously occupied by solvent molecules which are coordinated to the metal centre (Dinca & Long 2005, Liu et al. 2007). These solvent molecules can be removed from the framework by simple desolvation at higher temperatures with the MOF maintaining its structural integrity and, as a result, increase the MOF's hydrogen storage ability (Latroche et al. 2006, Liu et al. 2007). Saturated metal ions in MOFs have little to no effect on the hydrogen storage properties of MOFs (Song et al. 2011). Reported experimental and computational studies have shown that through the interaction that hydrogen has with the exposed or open metal site, the heat of adsorption of hydrogen in a MOF is increased. These interactions have been successfully confirmed using Neutron Powder Diffraction (NPD) experiments and Inelastic Neutron Scattering (INS) spectroscopy (Chae et al. 2004). The isosteric heat of adsorption can be used to assess the effect of the open metal sites. Cheon et al. (2009) prepared the MOF, SNU-15' (SNU refers to the Seoul National University) by removing the terminal water ligands of the MOF SNU-15 at 220 °C under vacuum and in that way making each  $\text{Co}^{2+}$  ion contain a vacant coordination site. SNU-15' absorbed just 0.74 wt% hydrogen at 77 K and 15 bar but its isosteric heat of hydrogen adsorption at zero coverage was  $15.1 \text{ kJ}\cdot\text{mol}^{-1}$  which is considerably high. This high heat of adsorption has been attributed to the open metal site created on each Co(II) ion (Cheon & Suh 2009). The alignment of the open sites relative to the hydrogen can also be tailored to maximise hydrogen adsorption (Gedrich et al. 2010).

### **2.7.2 Making use of guest metal ions**

Guest metal ions can be defined in two different ways: they can be ions that are introduced into the MOF structure to replace metal ions that are already found in the MOF structure, or they can be ions that are added to the pores of the MOFs in order to counterbalance the

negative charges of the ligands or the MOF itself. The addition of such guest metal ions may provide open metal sites, change the electrostatic field of the MOF, or be used to modify the surface area and pore volume of the MOF. These changes result in modification of hydrogen adsorption of the MOF. Wang and co-workers replaced Zn in MOF-5 with Co (Wang et al. 2008). Two Co-doped MOF samples were prepared, namely Co8-MOF-5 and Co21-MOF-5. The amount of Zn that was substituted was limited to 25 wt% of the total metal content. The hydrogen uptake at 77 K and 10 bar for Co21-MOF-5 increased by 7.4% compared to that of the pure MOF-5. At pressures up to 1 bar, the difference in hydrogen adsorption between MOF-5 and Co-MOF-5 materials was very small. However, at higher pressures, the hydrogen adsorption capacity for the Co-MOF-5 material exceeded that of the parent MOF-5. This behaviour suggested that Co incorporation into the framework diminished the high degree of crystallinity in some way, and crystallinity gives rise to robustness and rigidity of the MOF-5 framework. By fitting the experimental isotherms to a theoretical model of adsorption, further deviations for the isotherm of the Co-richer sample were observed. This indicated that there was an additional contribution to the hydrogen adsorption, which might have come from a breakdown of crystal symmetry as a result of Co incorporation, which could initiate framework flexibility at higher pressures.

The effect on a MOFs hydrogen uptake when alkali metals were added to the MOF (Li, Na, and K) has also been investigated. Tan and co-workers studied the variation in hydrogen uptake of MOF-5 when doped with various concentrations of  $\text{Li}^+$ ,  $\text{Na}^+$  and  $\text{K}^+$ . Hydrogen uptake increased significantly when compared to the pristine MOFs (Tan et al. 2011). With the same amount of alkali metal added to the MOF-5, at 77 K and 1 bar, hydrogen uptake increased in the order  $\text{Li}^+ < \text{Na}^+ < \text{K}^+$ . This was in accordance with the increase in size of the alkali cation. Although the hydrogen uptake increased in this manner, the hydrogen binding strength followed a reverse trend, with the strongest hydrogen binding observed for the MOF-5 doped with Li. These changes in hydrogen uptake and hydrogen binding were attributed to structural changes which were as a result of the framework reduction. Other effects such as ligand polarizability and framework displacement also contributed. It was observed as well that there seemed to exist a limit to the amount of dopant that could be added, whilst remaining beneficial to the MOFs hydrogen uptake ability. Beyond a certain point, the hydrogen uptake decreased, eventually falling below the amount adsorbed by the pure MOF. This was because the mechanism of hydrogen uptake enhancement was not through the creation of open metal sites, but involved favourable displacement of interwoven frameworks.

The lack of large special site effects, particularly for the Li-based MOF, indicated that ions might lodge themselves between frameworks, thereby making it difficult for hydrogen to gain access. The heat of adsorption did not differ much for the different levels of metal loading (Mulfort & Hupp 2008).

### 2.7.3 Promoting hydrogen “spillover”

A debatable strategy that has been put forward for possibly increasing hydrogen storage in MOFs, is through the possible contribution from “hydrogen spillover.” The hydrogen spillover is believed to be brought about by the catalytic formation of elemental hydrogen by supported metal catalysts. The monoatomic hydrogen atoms formed, migrate to a support material and then spill over to the MOF, improving hydrogen storage of the MOF. The spillover effect has been studied in MOFs which have had metal nanoparticles incorporated to increase their hydrogen storage capacity (Cheon & Suh 2009, Nouar et al. 2009, Sabo et al. 2007). However, the exact mechanism involved in hydrogen storage enhancement due to spillover effect is not well understood, but it is believed to have a higher significance at room temperature than at cryogenic temperatures. In several publications, hydrogen spillover has been reported for MOFs with Pd nanoparticles incorporated directly onto them. Cheon et al. added Pd nanoparticles of 3.0 nm and 3 wt% Pd in the MOF, SNU-3 (Cheon & Suh 2009). The pristine MOF with no Pd was desolvated to form  $[Zn_3(ntb)_2]_n$  and adsorbed 1.03 wt% hydrogen at 77 K and 1 bar. The hydrogen uptake isotherms are shown in Figure 7. The MOF with the Pd nanoparticles, PdNPs@[SNU-3], had a hydrogen adsorption of 1.48 wt%, but had a reduced surface area. The Langmuir surface area from CO<sub>2</sub> adsorption was 242 m<sup>2</sup>·g<sup>-1</sup> and 559 m<sup>2</sup>·g<sup>-1</sup> for the PdNPs@ [SNU-3] and pristine SNU-3 respectively. The pore volumes were 0.206 and 0.442 cm<sup>3</sup>·g<sup>-1</sup> for the PdNPs@ [SNU-3] and pristine SNU-3 respectively. The ntb organic building block in SNU-3 is redox active and could easily be oxidized by the Pd nanoparticles to the nitrogen radical species which acted as a counterion in the positively charged MOF. The reduced surface area and pore volumes for the Pd-containing MOF were attributed to the presence of the nitrate in the pores of the positively charged framework. The spillover effect was thought to be the cause of the increased hydrogen uptake of the Pd-containing MOF as the pristine MOF had a higher isosteric heat of adsorption of 8.11 kJ·mol<sup>-1</sup>, whilst the PdNPs@[SNU-3] had a lower isosteric heat of adsorption of 6.62 kJ·mol<sup>-1</sup>. Cheon suggested that hydrogen spillover was responsible for the increased hydrogen adsorption in the Pd-containing MOF (Cheon & Suh 2009).

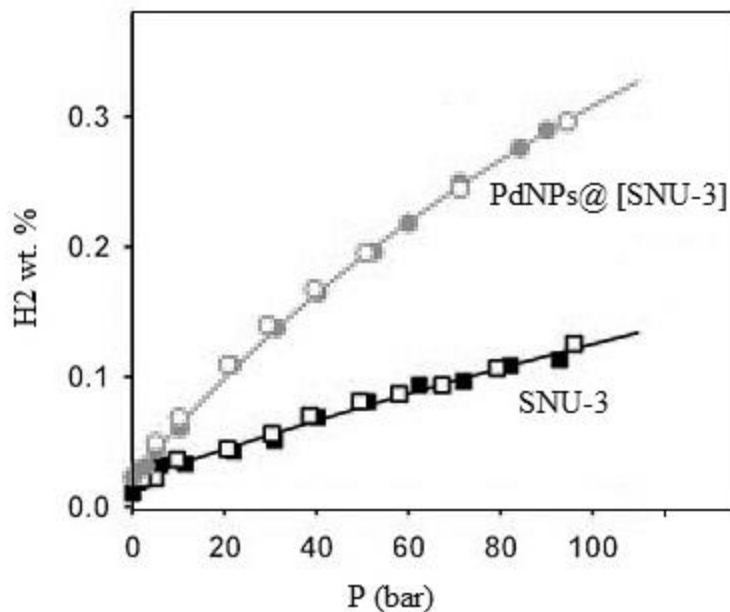


Figure 7: Hydrogen uptake of PdNPs@[SNU-3] and pristine SNU-3 (Cheon & Suh 2009).

#### 2.7.4 Controlling surface area, pore volume and pore size

Although the interaction energy of hydrogen with the MOF surfaces is low, it can be increased by tailoring the pores of the adsorbent to be small enough, such that the potential fields from opposite walls overlap (Zhao et al. 2004). This results in pore sizes that are close to the kinetic diameter of the hydrogen molecule, which leads to a higher interaction with hydrogen (Perles et al. 2005). Yang and co-workers reported a good correlation between hydrogen adsorption and the surface area, as well as effective pore volume for  $\text{Cu}_3(\text{BTC})_2$  (Yang, Orefuwa & Goudy 2011). At low pressure, hydrogen adsorption is influenced by pore size, but, as the pressure increases, it depends on the pore volume (Lin et al. 2009). Hydrogen adsorption on the MOF,  $\text{Mg}_3(\text{NDC})_3$  was investigated at 77 K and 1.2 bar (Dinca & Long 2005). It had a hydrogen adsorption of 0.46 wt%. The Langmuir-Freundlich equation predicted a maximum hydrogen adsorption of 0.6 wt%. The steep slope of the adsorption isotherm suggested that the isotheric heat of adsorption was relatively strong and estimated to be  $7.0\text{--}9.5 \text{ kJ}\cdot\text{mol}^{-1}$ . The higher interaction was suggested to be due to increased Van der Waals forces as a result of a very small pore size ( $3.46\text{--}3.64 \text{ \AA}$ ), which was quite close to the kinetic diameter of hydrogen.

A correlation between hydrogen uptake and surface area (and pore volume) was confirmed for

a series of NbO-type MOFs (NOTT-101, PCN-46 and NOTT-102) (Lin et al. 2009, Zhao et al. 2010). The longer the ligand, the higher the specific surface area, pore volume and high pressure hydrogen uptake. However, the isosteric heat of hydrogen adsorption did not follow this trend. Among these three MOFs, NOTT-101 had the shortest ligand (5.77 Å), lowest surface area (2316 m<sup>2</sup>·g<sup>-1</sup>), pore volume (0.886 cm<sup>3</sup>·g<sup>-1</sup>) and total hydrogen uptake at 77 K and 60 bar (66 mg·g<sup>-1</sup> or 6.2 wt%) while NOTT-102 had the highest values of 10.098 Å, 2942 m<sup>2</sup>·g<sup>-1</sup>, 1.138 cm<sup>3</sup>·g<sup>-1</sup> and 72.0 mg·g<sup>-1</sup> (6.7 wt%), respectively.

### 2.7.5 Catenation

Catenation is the intergrowth of two or more identical frameworks. It can occur as interpenetration or interweaving. Interpenetration involves maximum displacement of frameworks from each other, whilst interweaving involves minimum displacement between the frameworks (Rowsell & Yaghi 2005, Chen et al. 2001). A noticeable consequence of catenation is a reduction of the free diameter of the pores, which can improve the hydrogen adsorption. The different forms of catenation are shown in Figure 8 a – d.

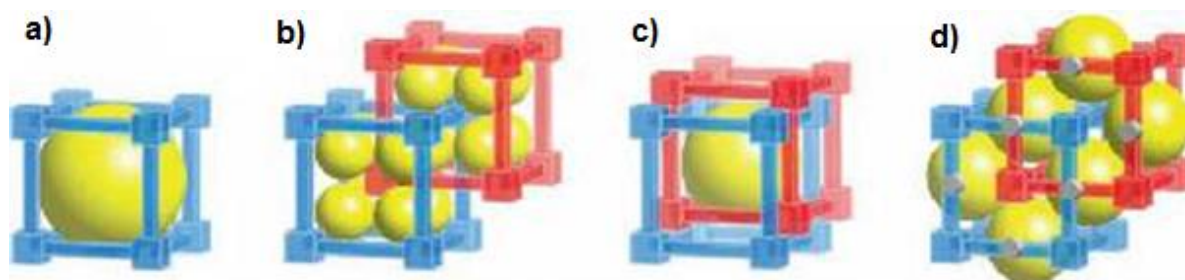


Figure 8: Different forms of catenation (Rowsell & Yaghi 2005)

Figure 8 a. is a schematic representation of a unit cube of a MOF. Secondary building units (SBUs) are shown as cubes and linkers as rods. The yellow sphere represents the large pore to be occupied with hydrogen gas. Catenation of two identical frameworks can be used to restrict the dimensions of the pore considerably by interpenetration shown in b., or to a lesser extent by interweaving as in c. Interweaving can improve the material's rigidity by mutual reinforcement, shown in d. An alternative catenation mode achieved by reducing the close contacts between the frameworks to only the midpoints of a proportion of the linkers (grey discs).

Interpenetration is desired over interweaving as it maximises the exposed surfaces of the MOF. The reason for this is that even though interweaving can strengthen the individual frames by increasing stiffness and stability after desolvation, due to effective wall thickening, the number of adsorptive sites of each atom, which is exposed to the pores, is reduced. In contrast, with interpenetration, the pore size is reduced with the adsorptive site remaining well exposed. The ability of catenation to increase hydrogen adsorption has been demonstrated for a pair of PCN MOFs; PCN-6' (noncatenated) and PCN-6 (catenated) (see Figure 9). The reported hydrogen adsorption at 1 bar and 77 K for the MOFs after having been activated at 50 °C were 1.35 wt% for PCN-6' and 1.74 wt% for PCN-6. This increase in hydrogen adsorption showed that catenation can improve the hydrogen adsorption in MOFs (Ma & Zhou 2010). Catenation can be achieved by tailoring the synthesis conditions to best suit interpenetration or interweaving. Usually, by running the synthesis under static conditions (no stirring), catenation will occur as the crystals will aggregate and grow together.

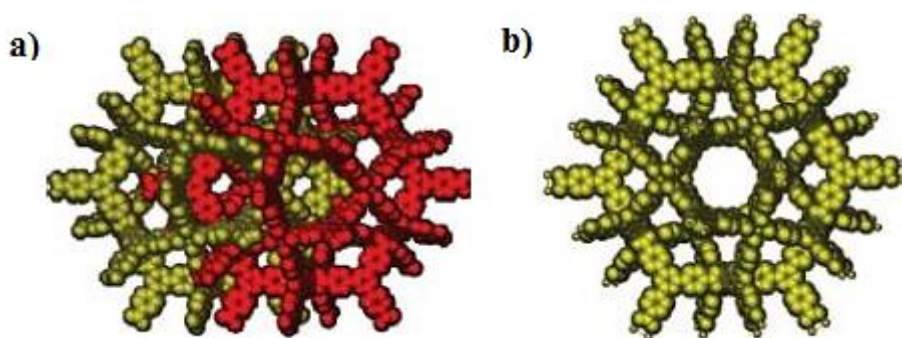


Figure 9: a) Catenated PCN-6 and b) Non-catenated PCN-6' (Ma & Zhou 2010).

## Chapter 3

### Experimental

#### 3.1 Chapter outline

In this chapter, the synthesis of Zn-MOF (MOF-5), Zr-MOF (UiO-66) and Cr-MOF (MIL-101) is discussed. MOF-5 is an attractive hydrogen storage material due to its high surface area, permanent porosity, thermal stability and high synthetic yield. Of the many MOFs available, MOF-5 is amongst the most widely investigated MOF for hydrogen storage. This, together with its properties, made it an ideal starting point for the project. It offers a base from which firm understanding of the typical MOF synthesis can be gained as well as an understanding of the various factors that can affect the hydrogen capacities of MOFs. It also helped in gauging our ability to reproducibly prepare MOFs that were comparable to those reported in the literature. During this work, it was discovered that at some point, MOF-69c was produced as a product instead of MOF-5. Methods of converting MOF-69c to MOF-5 were then investigated.

It must be mentioned, however that MOF-5 has a drawback in that it is moisture sensitive and that led to the investigation of other MOFs that are more moisture tolerant. In addition, MOF-5 was synthesised with different metal centres to overcome the moisture sensitivity problem. The synthesised MOFs were characterised and the one that gave the best results was chosen to be investigated further. Zr-MOF (UiO-66) was chosen as the most promising, and because it had been reported to be moisture stable. In addition, South Africa is amongst the leaders in the world in zircon mineral resources, keeping in line with HySA's mandate of promoting the beneficiation of South African mineral resources. Zr-MOF has also been reported to possess good hydrogen storage abilities. Two synthesis methods were employed in the synthesis of Zr-MOF, namely solvothermal synthesis and microwave-assisted synthesis. Solvothermal synthesis was optimised using formic acid as a modulator. Microwave-assisted synthesis provided a rapid synthesis method for Zr-MOF.

The next part of the chapter discusses the synthesis of Cr-MOF. Whilst MOF-5 provided a firm understanding for the synthesis method and hydrogen storage capacity of MOFs, Zr-MOF provided a moisture stable MOF which could be utilised for practical applications. They both use DMF as solvent which has become undesirable due to environmental concerns. Therefore a greener synthesis route was also investigated, where water was chosen as solvent. This is in

line with the HySA mandate to produce MOFs that utilise metals which have economic value to South Africa, and to pursue more environmentally friendly chemistries. Although the synthesis of Cr-MOF had been reported as requiring hydrofluoric acid (HF) as a modulator (Jhung et al. 2007, Henschel et al. 2008, Maksimchuk et al. 2012), formic acid was used as a modulator in this work.

## 3.2 Synthesis of MOF-5 crystals

### 3.2.1 Chemicals and materials

The following chemicals were purchased and used without any further modifications: zinc nitrate hexahydrate (Sigma-Aldrich, 98%), terephthalic acid (Sigma-Aldrich, 98%), N,N-dimethylformamide (DMF) (Sigma-Aldrich, 99.8%), N,N-diethylformamide (DEF) (Sigma-Aldrich, 99.8%), dried acetone (Sigma-Aldrich, 99.8+%), anhydrous chloroform (Sigma-Aldrich, 99+%) and N<sub>2</sub> ultra-high purity gas (Air Products, South Africa, 99.9995%).

### 3.2.2 Solvothermal synthesis of MOF-5 crystals

As mentioned in Section 3.1, MOF-5 continues to be an attractive hydrogen storage material due to its high surface area, permanent porosity, thermal stability and high synthetic yield. The synthesis of MOF-5 could be up-scaled following a better understanding of the synthetic conditions.

The initial synthesis was a repeat of the BASF process (Mueller et al. 2006) with the only modification being the metal salt. In this work, zinc nitrate hexahydrate was used instead of zinc nitrate tetrahydrate as the metal source due to the availability of zinc nitrate hexahydrate and the fact that these metal salts were both sources of Zn(NO<sub>3</sub>). The solvent used in this synthesis was DEF. A schematic of the synthesis route is shown in Figure 10. The less costly solvent DMF was used instead of DEF by virtue of their similar properties and because DMF has been reported to be a suitable alternative solvent to DEF.

A common known and accepted fact is that MOF-5 materials synthesised in DEF offer better properties compared to those synthesised in DMF. The DEF synthesised MOF-5 materials offer better crystallinity, higher Langmuir surface areas (2500-4000 m<sup>2</sup>.g<sup>-1</sup>) and the PXRD patterns from the DEF synthesised MOF-5 are identical to that of theoretically perfect MOF-5 (simulated PXRD). The MOF-5 materials synthesised from DMF have lower crystallinity, lower Langmuir surface areas (500-1200 m<sup>2</sup>.g<sup>-1</sup>) and the PXRD peak intensities differ

significantly from theoretically perfect MOF-5. The advantage of using DMF over DEF is the reduction in cost and synthesis time.

In a typical synthesis procedure, the experiment was conducted in a 250 mL round-bottom flask. An oil bath was used to provide constant reaction temperature. The apparatus was dried in a thermostatic oven at 120 °C overnight and cooled to around 40 °C before being assembled and connected with a high-purity N<sub>2</sub> gas source. The flask was equipped with a reflux condenser and an elliptical Teflon-lined stirrer (10×19 mm). In the flask, 0.665 g (4 mmol) of terephthalic acid and 3.13 g (10.52 mmol) of zinc nitrate hexahydrate were dissolved in 100 mL of solvent. The flask was under a continuous flow of N<sub>2</sub> gas while being heated to 130 °C and maintained at that temperature for 4 h with stirring at 1000 rpm. In addition, the samples were activated at 120 °C for 24 h under vacuum of less than 50 mbar.

In this work, MOF-5 was synthesised using both DEF and DMF with characteristics similar to those reported in literature. Optimisation of the synthesis of MOF-5 in DMF to closely match the MOF-5 obtained from DEF, was carried out. The effects of several key factors in the synthesis of MOF-5 using DMF as a solvent were investigated. The factors investigated are listed below:

- temperature,
- synthesis time, and
- stirring.

A summary of the complete reaction variables that were optimised for MOF-5 are listed in Table 2. In each instance, the recovered crystals were characterised by SEM and PXRD. The surface area and porosity measurements were done using the ASAP 2020. The results of all the optimisation experiments were used to formulate an optimised synthesis procedure for MOF-5 crystals using DMF as a solvent, instead of DEF.

### **3.2.2.1 Effect of temperature**

During the investigation into the effect of temperature on the MOF-5 crystals, several temperatures, namely 100, 120, 130, 140 °C, were investigated. All the other reaction conditions were kept constant. In the case of the reaction at 100 °C, the growth of the crystals was too slow to produce desired crystals in the allocated time, therefore no crystals could be recovered after the reaction.

### 3.2.2.2 Effect of synthesis time

The effect of reaction time on the morphology of the MOF-5 crystals was investigated. The effects of 1, 2, 3 and 4 h reaction time were studied. In the case of the reaction time of 1 h, no crystals were recovered.

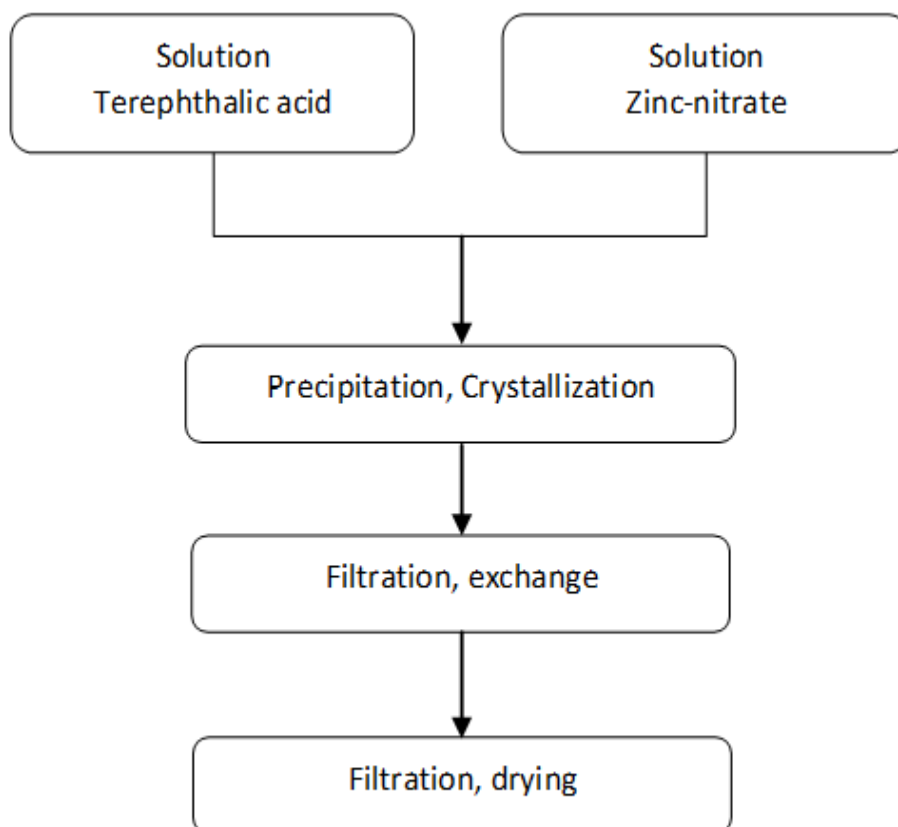


Figure 10: Synthesis route for MOF-5

### 3.2.2.3 Effect of stirring

The effect of the stirring speed on the morphology of the MOF-5 crystals was studied. Four reactions were run in which one was done under static conditions and the other three with different stirring speeds of 250, 1000 and 1400 rpm.

#### **3.2.2.4 Phase transition from MOF 69c to MOF-5**

In the course of synthesising MOF-5, there were instances where MOF-69c was produced instead of MOF-5. In these instances, the products collected after the reaction were given different treatments in an attempt to convert the MOF-69c into MOF-5 as presented below in Table 3. The thermal treatments were conducted in a Büchi TO-50 drying oven with good heat distribution.

#### **3.2.2.5 MOF-5 moisture sensitivity**

Zinc-based MOFs have been shown to be moisture-sensitive as the relatively weak Zn-O coordination bonds allow for attack by water molecules, resulting in the phase transformation and structure collapse (Wu et al. 2010). The stabilities of several MOFs to moisture are compared in Figure 11. Structural decomposition always leads to poor reproducibility and decreased hydrogen sorption capacity in MOF-5 material. This limits their practical implementation as there is a further need to shape them into application-specific configurations (Wu et al. 2013). During the application-specific shaping, they will be exposed to atmospheric moisture which will lead to poor functionality and will greatly reduce their life cycle. Any moisture contamination in the pipe line or in hydrogen gas will result in the same undesirable ending.

**Table 2:** Variables for optimisation of MOF-5 synthesis

| Variables               | Sample ID       | Zn(NO) <sub>3</sub><br>(mmol) | H <sub>2</sub> BDC<br>(mmol) | Zn(NO) <sub>3</sub> /H <sub>2</sub> BDC<br>(mol) | Solvent<br>(mL) | Stirring<br>(rpm) | Temp.<br>(°C) | Time<br>(h) |
|-------------------------|-----------------|-------------------------------|------------------------------|--|-----------------|-------------------|---------------|-------------|
| Solvent                 | MOF-5-<br>DMF   | 10.52                         | 4                            | 2.63   | DMF-100         | Yes               | 130           | 4           |
|                         | MOF-5-<br>DEF   | 10.52                         | 4                            | 2.63   | DEF-100         | Yes               | 130           | 4           |
| Stirring                | MOF-5-<br>Still | 10.52                         | 4                            | 2.63   | DMF-100         | No<br>0           | 130           | 4           |
|                         | MOF-5-<br>Stir  | 10.52                         | 4                            | 2.63   | DMF-100         | Yes<br>250        | 130           | 4           |
|                         | MOF-5-<br>Stir  | 10.52                         | 4                            | 2.63   | DMF-100         | Yes<br>1000       | 130           | 4           |
|                         | MOF-5-<br>Stir  | 10.52                         | 4                            | 2.63   | DMF-100         | yes<br>1400       | 130           | 4           |
| Reaction<br>temperature | MOF-5-<br>100°C | 10.52                         | 4                            | 2.63   | DMF-100         | Yes               | 100           | 4           |
|                         | MOF-5-<br>120°C | 10.52                         | 4                            | 2.63   | DMF-100         | Yes               | 120           | 4           |
|                         | MOF-5-<br>130°C | 10.52                         | 4                            | 2.63   | DMF-100         | Yes               | 130           | 4           |
|                         | MOF-5-<br>140°C | 10.52                         | 4                            | 2.63   | DMF-100         | Yes               | 140           | 4           |
|                         | MOF-5-<br>140°C | 10.52                         | 4                            | 2.63   | DMF-100         | Yes               | 140           | 4           |
| Reaction time           | MOF-5-<br>1H    | 10.52                         | 4                            | 2.63   | DMF-100         | Yes               | 130           | 1           |
|                         | MOF-5-<br>2H    | 10.52                         | 4                            | 2.63   | DMF-100         | Yes               | 130           | 2           |
|                         | MOF-5-<br>3H    | 10.52                         | 4                            | 2.63   | DMF-100         | Yes               | 130           | 3           |
|                         | MOF-5-<br>4H    | 10.52                         | 4                            | 2.63   | DMF-100         | Yes               | 130           | 4           |
|                         | MOF-5-<br>4H    | 10.52                         | 4                            | 2.63   | DMF-100         | Yes               | 130           | 4           |

**Table 3:** MOF-69c Samples with different heat treatments

| Sample ID | Treatment method   |
|-----------|--|
| Sample A  | MOF-69c ultrasonically washed with acetone and dried at 120 °C for 24 h under vacuum                                   |
| Sample B  | MOF-69c exchanged with 50 mL anhydrous chloroform for 24 h, and dried at 120 °C for 24 h under vacuum                  |
| Sample C  | sample A further dried at 200 °C for 24 h under vacuum   |
| Sample D  | sample A further dried at 200 °C for 24 h in open air  |
| Sample E  | sample A further dried at 200 °C for 48 h in open air  |
| Sample F  | sample A further dried at 200 °C for 48 h in open air after contacting with DMF solution containing H <sub>2</sub> BDC |

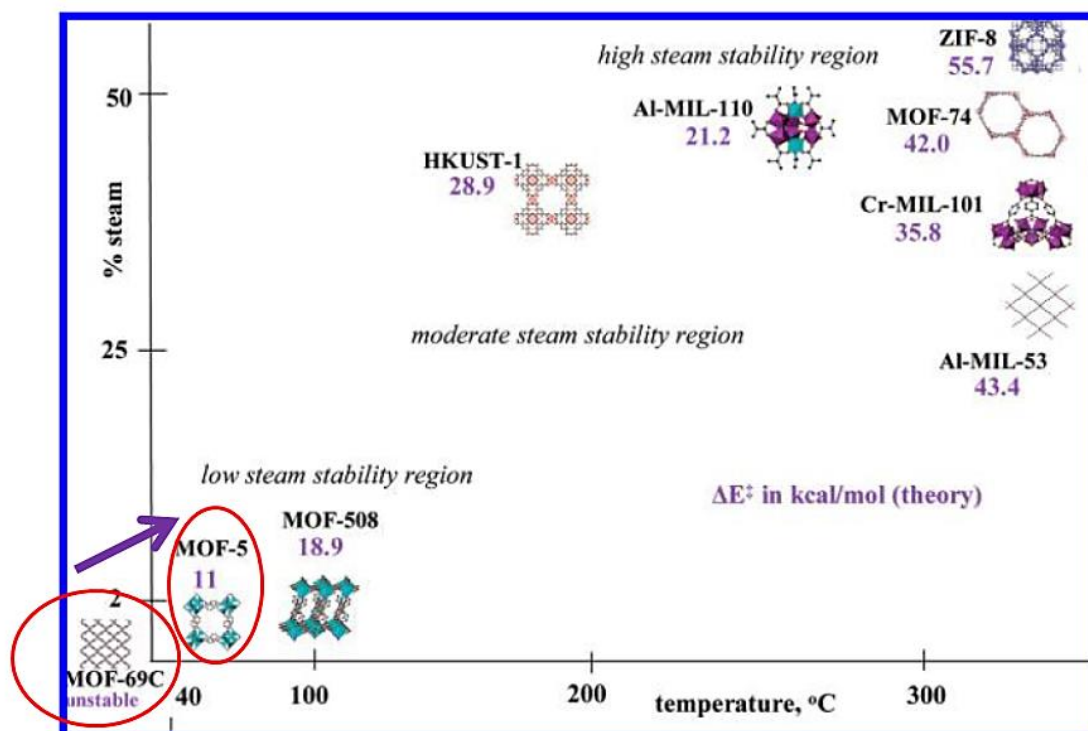


Figure 11: Stability of MOFs to steam. (Canivet et al. 2014)

Possible industrial solutions include using a nitrogen tent around the production and shaping plants and constantly using high purity hydrogen gas. Both these solutions will result in added cost and are impractical for industrial applications. Another possible solution will be to strengthen the Zn-O bond which can be achieved by either replacing the organic mixers or using different metal centers to provide a stronger Metal-O bond. Since the metal center contributes more to the strength of the bond, the effect of different metal centers on the hydrostability of the MOF were studied. Table 4 reports the different metals chosen in accordance with the minerals beneficiation policy of South Africa. Each of the metals chosen is one in which South Africa is amongst the leading producers in the world. All the reactions were performed with stirring and at 140 °C and held at that temperature for 4 hours.

**Table 4:** MOFs with different metal centers

| Metal source  | Sample ID | (mmol)<br>(g)        | H <sub>2</sub> BDC<br>(mmol)<br>(g) | M <sup>2+</sup> /H <sub>2</sub> BD<br>C | DMF (mL) |
|---|-----------|----------------------|-------------------------------------|---|----------|
| C <sub>4</sub> H <sub>6</sub> MnO <sub>4</sub> .4H <sub>2</sub> O | MOF-5-Mn  | 10.515mmol<br>(2.6)  | 4mmol<br>(0.665)                    | 2.63                                    | 100      |
| C <sub>4</sub> H <sub>6</sub> CoO <sub>4</sub> .4H <sub>2</sub> O | MOF-5-Co  | 10.515mmol<br>(2.6)  | 4mmol<br>(0.665)                    | 2.63                                    | 100      |
| MgN <sub>2</sub> O <sub>6</sub> .6H <sub>2</sub> O                | MOF-5-Mg  | 10.515mmol<br>(2.7)  | 4mmol<br>(0.665)                    | 2.63                                    | 100      |
| C <sub>4</sub> H <sub>6</sub> NiO <sub>4</sub> .4H <sub>2</sub> O | MOF-5-Ni  | 10.515mmol<br>(2.6)  | 4mmol<br>(0.665)                    | 2.63                                    | 100      |
| ZrCl <sub>4</sub>   | MOF-Zr    | 10.515mmol<br>(2.45) | 4mmol<br>(0.665)                    | 2.63                                    | 100      |

Based on their hydrogen adsorption, the Zr-based MOF proved to be the most promising and a decision was taken to investigate Zr-MOF further.

### 3.3 Synthesis of Zr-MOF crystals

Having experienced the drawback of MOF-5 in terms of moisture sensitivity, other moisture insensitive MOFs were investigated. Compared to Zn-based MOFs, for example MOF-5, Zr-MOFs have stronger Zr-O bonds than the weak Zn-O bonds in MOF-5. This attribute improves the hydro-stability of Zr-MOFs. However, it is difficult to generate Zr-MOF with a regular crystalline morphology without the use of a modulator. Zr-MOF also requires equimolar amounts of the metal and organic ligand. In this work, Zr-MOF was first synthesised without the use of a modulator, as well as using formic acid as the modulator.

#### 3.3.1 Chemicals and materials

Zirconium tetrachloride ( $\text{ZrCl}_4$ , Sigma Aldrich, 99.5 %), terephthalic acid (Sigma Aldrich, 98%), N, N-dimethylformamide (DMF, Sigma Aldrich, 99.8%), formic acid ( $\text{HCOOH}$ , Sigma Aldrich, 95%) and dried acetone ( $(\text{CH}_3)_2\text{CO}$ , Sigma Aldrich, 99.8%) were purchased and used without further purification.

#### 3.3.2 Modulated solvothermal synthesis of Zr-MOF crystals

Zr-MOF synthesis was conducted using a 250 mL round-bottom flask and an oil bath to provide constant reaction temperature. In the synthesis procedure, 1.82 g (0.011 mol) of terephthalic acid and 2.66 g (0.011 mol) zirconium tetrachloride were dissolved in 100 ml of DMF. To gain a better understanding of the influence of the modulator, different equivalents of formic acid with respect to  $\text{ZrCl}_4$  were added. The round-bottom flask was capped with a Teflon filter paper which was secured in place using cable ties before being placed into the oil bath, pre-heated up to 120 °C and maintained at that temperature for 6 h under static conditions. After the reaction, the flask was cooled to room temperature and the product was collected by filtration. The white product obtained was washed with anhydrous chloroform for 30 min. The solid was re-collected and dried under vacuum at room temperature.

##### 3.3.2.1 Effect of modulator ratio

During the investigations to optimise the synthesis of Zr-MOF, the effect of the modulator ratio was investigated. In this section and henceforth, the term equivalent (eq) refers to the molar ratio between the modulator, formic acid and the MOF sample in a synthesis batch. For example, in a synthesis designated as “100 eq”, the molar ratio of formic acid :  $\text{ZrCl}_4$  is 100:1. Synthesis was carried out using 0, 10, 50 and 100 eq of formic acid. All the other reaction conditions were kept constant.

### 3.3.2.2 Effect of synthesis time

To get a better understanding of the Zr-MOF synthesis, the nucleation rate was studied using the 100 eq Zr-MOF crystals. The effect of reaction time on the morphology of the Zr-MOF crystals was studied. The synthesis times employed were 1, 2, 4, 8, 16 and 24 h while all other reaction conditions were kept constant. Table 5 below summarises the variables investigated for the optimisation of Zr-MOF.

**Table 5:** Variables investigated for Zr-MOF optimisation

| Variables       | Sample ID    | Time (h) |
|-----------------|--------------|----------|
| Modulator ratio | Zr-MOF 0eq   | 24       |
|                 | Zr-MOF 50eq  | 24       |
|                 | Zr-MOF 100eq | 24       |
| Reaction time   | Zr-MOF 1hr   | 1        |
|                 | Zr-MOF 2hr   | 2        |
|                 | Zr-MOF 4hr   | 4        |
|                 | Zr-MOF 8hr   | 8        |
|                 | Zr-MOF 16hr  | 16       |
|                 | Zr-MOF 24hr  | 24       |

### 3.3.3 Microwave-assisted synthesis of Zr-MOF crystals

The same chemical reagents as used in the solvothermal synthesis were used with no further purification. The microwave-assisted synthesis was conducted in an Anton Paar Synthos 3000 microwave. For the microwave synthesis of Zr-MOF, 0.75 g (4.5 mmol) of terephthalic acid and 1.05 g (4.5 mmol) zirconium tetrachloride were dissolved in 40 mL of DMF. 17 mL (450 mmol) of formic acid was then added to the reaction solution. The initial solution was split into four portions into the four glass microwave vessels. The microwave was set to run the

reaction at 120 °C for 5 min under static conditions. After the reaction, the microwave reaction vessels were allowed to cool to room temperature. The Zr-MOF powder was then collected by filtration and washed in anhydrous chloroform with the help of an ultrasonic bath for 30 min. The washed powder was then filtered and dried under vacuum at room temperature.

### 3.4 Synthesis of Cr-MOF crystals

#### 3.4.1 Chemicals and materials

Chromium trichloride hexahydrate ( $\text{CrCl}_3 \cdot 6\text{H}_2\text{O}$ , Sigma Aldrich, 99.5 %), terephthalic acid (Sigma Aldrich, 98%), formic acid ( $\text{HCOOH}$ , Sigma Aldrich, 95 %), de-ionized water and N, N-dimethylformamide (DMF, Sigma Aldrich, 99.8%) were purchased and used without further purification.

#### 3.4.2 Modulated synthesis of Cr-MOF crystals

As mentioned in Section 3.1, the synthesis of Cr-MOF uses water as a solvent but also has been reported to use HF as a modulator. To replace the HF in the synthesis of Cr-MOF, a firm understanding of the role it played together with the other chemicals used in the synthesis was needed. A typical synthesis of Cr-MOF involves the use of  $\text{Cr}(\text{NO}_3)_3 \cdot 9\text{H}_2\text{O}$  as a metal source,  $\text{H}_2\text{BDC}$  as the organic linker, water as the solvent and HF as the modulator. In this case, the HF donates fluorine with the fluorine attaching to the  $\text{Cr}^{3+}$  ion in the structure of the MOF (Figure 12). HF acts as a modulator by directing crystal growth and reducing crystal aggregation leading to anisotropic growth. The best solution to avoid the use of HF was to find a replacement modulator with similar properties to fluorine. Possible candidates were oxygen, sulphur and chlorine (noble gases excluded). Oxygen is already well present as  $\text{H}_2\text{O}$  in the hydrothermal reaction and is attached to Cr in the MOF structure therefore it was excluded as a candidate ion. This left only chlorine and sulphur as possible replacements. Table 6 lists all the similarities between F, Cl and S, and from this comparison, Cl was chosen as the best candidate. The next issue was to find a way of introducing the Cl without the use of any strong or toxic acids such as HCl. The best solution was to combine the metal addition and Cl addition by using a salt that contains both the metal (Cr) and the Cl ions. The salt chosen was  $\text{CrCl}_3 \cdot 6\text{H}_2\text{O}$ . With this in mind, a new synthesis procedure was formulated not employing HF, but instead using formic acid as a modulator.

Experiments were conducted using a 250 mL Teflon-lined Berghof high-pressure reactor (Heizung, Germany). It has been reported that during the synthesis of MIL-101, there is a

potential for the MIL-101 to undergo phase transformation to MIL-53 ( $\text{CrO}_8\text{C}_{14}\text{H}_{11}$ ) during extended reaction times (Khan et al. 2000). Therefore, to avoid this phase change, the molar ratio of  $\text{CrCl}_3 \cdot 6\text{H}_2\text{O} : \text{H}_2\text{BDC} : \text{H}_2\text{O} = 1 : 1 : 550$  for the reaction constituents was maintained. The reaction was conducted within a relatively short synthesis time. The initial synthesis was done without the modulator. For this reaction, 0.83 g (5 mmol) of terephthalic acid and 1.33 g (5 mmol) of chromium chloride were dissolved in 50 mL (2.78 mol) of de-ionized water with the help of an ultrasonic bath. The reaction mixture was then transferred to an autoclave and heated to 210 °C and held at that temperature for 8 h. When the reaction was complete, the autoclave was cooled to room temperature and the products were collected by centrifugation. The products were a mixture of a green powder and colourless needle-like crystals which was identified to be recrystallized terephthalic acid. The latter was removed by washing the products in hot DMF at 80 °C for 1 h. The remaining green powder was then collected and dried under vacuum at room temperature. To study the effect of the modulator, different equivalents of the modulator were added to the reaction mixture.

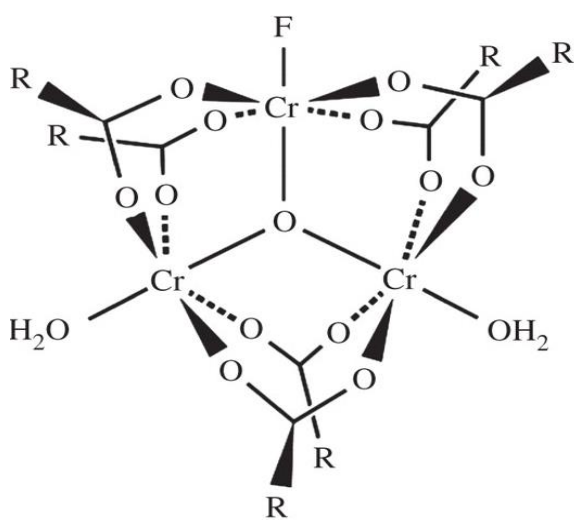


Figure 12: Structure of Cr-MOF (MIL-101) showing how F and O are directly attached to the Cr metal centres (Maksimchuk et al. 2012).

**Table 6** : Properties of F compared to Cl and S

| Property           | Fluorine                             | Sulphur                                | Chlorine                             |
|--------------------|--------------------------------------|--|--------------------------------------|
| Atomic no.         | 9                                    | 16                                     | 17                                   |
| Std. Atomic weight | 18.99                                | 32.06                                  | 35.45                                |
| Electron config.   | [He] 2s <sup>2</sup> 2p <sup>5</sup> | [Ne] 3s <sup>2</sup> 3p                | [Ne] 3s <sup>2</sup> 3p <sup>5</sup> |
| Electronegativity  | 3.98                                 | 2.58                                   | 3.16                                 |
| Oxidation state    | -1 (F <sup>-</sup> ion)              | +6 (in HSO <sub>4</sub> <sup>+</sup> ) | -1 (Cl <sup>-</sup> ion)             |

#### 3.4.2.1 Effect of modulator ratio

During the investigations to optimise the synthesis of Cr-MOF, the effect of the modulator ratio was investigated. 0, 10, 20, 50, 80 and 100 eq of formic acid were used as the modulator. All the other reaction conditions were kept constant.

#### 3.4.2.2 Effect of synthesis time

Cr-MOF suffers from a tendency to undergo a phase change from MIL-101 to MIL-53 for extended reaction times. The phase-transition from MIL-101 to MIL-53 occurs via the reorganisation of the decomposed MIL-101. In this work, the optimum synthesis time was sought that would allow maximum growth of MIL-101 without the phase transformation to MIL-53. To find that optimum time, several Cr-MOF samples using 100 eq modulator were synthesised at different reaction times between 2 and 24 h. PXRD, together with corresponding SEM images, were used to evaluate the nucleation rate and morphological changes.

Table 7 presents the variables for optimisation of Cr-MOF synthesis.

**Table 7:** Variables investigated for Cr-MOF optimization

| Variables       | Sample ID    | Time (h) | Modulator ratio used (equivalents) |
|-----------------|--------------|----------|------------------------------------|
| Modulator ratio | Cr-MOF 0eq   | 8        | 0                                  |
|                 | Cr-MOF 10eq  | 8        | 10                                 |
|                 | Cr-MOF 20eq  | 8        | 20                                 |
|                 | Cr-MOF 50eq  | 8        | 50                                 |
|                 | Cr-MOF 80eq  | 8        | 80                                 |
|                 | Cr-MOF 100eq | 8        | 100                                |
| Reaction time   | Cr-MOF 2h    | 2        | 100                                |
|                 | Cr-MOF 4h    | 4        | 100                                |
|                 | Cr-MOF 6h    | 6        | 100                                |
|                 | Cr-MOF 8h    | 8        | 100                                |
|                 | Cr-MOF 14h   | 14       | 100                                |
|                 | Cr-MOF 16h   | 16       | 100                                |
|                 | Cr-MOF 24h   | 24       | 100                                |

### 3.5 Characterisation techniques

#### 3.5.1 Scanning Electron Microscopy (SEM)

The morphology of the synthesised MOF samples was examined using an Auriga Cobra Focused-Ion Beam Scanning Electron Microscope (FIB-SEM) and a JEOL-JSM 7500F Scanning Electron Microscope. All the samples were mounted on a carbon tape and coated with gold prior to analysis.

### 3.5.2 Powder X-ray Diffraction (PXRD)

PXRD patterns were obtained at room temperature by PANalytical X'Pert Pro powder diffractometer with Pixcel detector using Ni-filtered Cu K-alpha radiation (0.154 nm) in the range of  $2\theta = 1 - 90^\circ$ , and scanning rate of  $0.1^\circ \cdot s^{-1}$ . The exposure time of sample to the environment was about 20 min including the sample preparation and testing procedure. The phase identification was performed by matching obtained patterns with those reported in literature for single crystal synthesis and simulated data. The relative intensities of certain peaks were used to obtain information about the quality of the crystals.

### 3.5.3 Thermo Gravimetric Analysis (TGA)

Thermal stability analysis of the synthesised MOF samples was performed by TGA using a Mettler Toledo TGA, Model TGA/SDTA 851<sup>c</sup>, with an autosampler, Model TSO801RO. The temperature ramp was set from room temperature to 1000 °C at 5 °C per min with the nitrogen gas flow set to 10 mL·min and the flow of the reactive gas at 30 mL·min.

### 3.5.4 Surface area and pore size determination

Surface area and pore characteristics measurements were carried out on an ASAP 2020 HD analyser (Micromeritics), and the  $P/P_0$  range was chosen as 0.05–0.3 for BET determination. All gas sorption isotherms were obtained using ultra-high purity grade Nitrogen gas (99.999 %). The samples to be analysed were outgassed at a temperature that was enough to remove all the solvent molecules without compromising the MOF structure. A different temperature was chosen for each MOF type based on its thermal stability. MOF-5 was degassed at 200 °C, Zr-MOF at 300 °C and Cr-MOF at 200 °C. All MOF samples were degassed to less than  $10^{-5}$  mbar pressure. Both BET and Langmuir methods were used for determining the surface area. The pore volumes were calculated using the Horvath-Kawazoe (H-K) method (Marsh 1987, Lowell et al. 2010, Suh et al. 2011). The methods used are all built into the ASAP 2020 software.

In order to conduct the surface area and porosity measurement on the ASAP 2020, it was necessary to calculate the density of each sample. For this purpose, the Micromeritics Pycnometer AccuPyc II 1340 was used with helium as the analysis gas.

### **3.5.5 Hydrogen adsorption measurements**

Hydrogen adsorption was performed on the Micromeritics ASAP 2020 HD analyser at 77 K by a volumetric method with a liquid nitrogen dewar used to maintain constant temperature. The analysis was performed from maximum vacuum up to 1 bar.

## Chapter 4

### Results and discussion

#### 4.1 Chapter outline

In this chapter the results, based on the chemical, textural, morphological and thermal stability analyses are discussed. The synthesised MOF samples were characterised using SEM, PXRD, TEM and their porosity and surface area were analysed using the ASAP 2020 instrument.

#### 4.2 Characterisation of MOF-5 crystals

##### 4.2.1 Effect of solvent choice: DEF and DMF

###### 4.2.1.1 Morphology and phase studies with SEM and PXRD

Figures 13-17 show the SEM images with their corresponding PXRD patterns of the MOF-5 samples synthesised using DEF and DMF as solvents. The PXRD pattern of the sample synthesised using DEF as the solvent showed an excellent agreement with the experimental and simulated patterns published in the literature (Huang et al. 2003, Panella et al. 2006). The SEM images revealed the cube-like shaped crystals of MOF-5 (Figures 13, 14 and 17) (Huang et al. 2003, Panella et al. 2006). The PXRD patterns of the MOF-5 sample synthesised using DMF as the solvent showed an agreement, in terms of the peak positions, with the experimental single crystal pattern and simulated pattern reported in literature, and the SEM images revealed the cubic shaped crystals of MOF-5 (Figures 15, 16 and 17) (Huang et al. 2003, Panella et al. 2006). However, the first two peaks at  $2\theta = 6.9$  and  $9.8^\circ$  of the PXRD pattern had interchanged intensities whilst all the other peak relative intensities were similar to those of the sample synthesised in DEF. In other words, in the PXRD pattern of the sample synthesised in DEF and in the simulated pattern, the peak at  $6.9^\circ$  has the highest intensity followed by the peak at  $9.8^\circ$ , whereas in the DMF synthesised MOF-5 the peak at  $9.8^\circ$  has the highest intensity followed by the peak at  $6.9^\circ$ . This difference in the intensities at low  $2\theta$  angles was explained by Hafzovic and co-workers as being the result of the residual solvent in the pores of the MOF structure (Hafzovic et al. 2007). For highly porous materials it has been observed that the PXRD peaks at low  $2\theta$  angles are dependent on the amount and scattering power of the guest molecules (Hafzovic et al. 2007). The presence of the DMF in the pores will result in the peak at  $9.8^\circ$  having an increased intensity relative to the  $6.9^\circ$  peak in the DMF synthesised MOF-5 (Hafzovic et al. 2007). In the DEF synthesised sample, the activation process was more efficient in removing all the DEF, hence the peak at  $9.8^\circ$  had a

lower intensity relative to the  $6.9^\circ$  peak. . The PXRD patterns of all samples showed nine signals at  $2\theta = 6.9, 9.8, 13.8, 15, 15.4, 19.5, 20.4, 20.7$  and  $22.6^\circ$ , typical of MOF-5. As mentioned above, when compared to the single-crystal XRD and the simulated data, the PXRD patterns of the MOF-5 synthesised were well-matched (Figure 17) (Huang et al. 2003, Panella et al. 2006). The residual peak positioned at  $2\theta = 8.9^\circ$  (indicated by the star) is attributed to the exposure of the sample to moisture from the atmosphere during XRD measurement, which took about 20 min to complete. Kaye and co-workers (Kaye et al. 2007) reported that 10 min exposure of desolvated MOF-5 sample to humid air would result in the appearance of the peak at  $2\theta = 8.9^\circ$ . Although the PXRD patterns obtained from the MOF-5 synthesised in DEF were identical to theoretically perfect MOF-5, the high cost of DEF makes continued or large scale synthesis impractical. Hence DMF was the solvent of choice for which the synthesis of MOF-5 was optimised by studying the effect of various synthesis parameters.

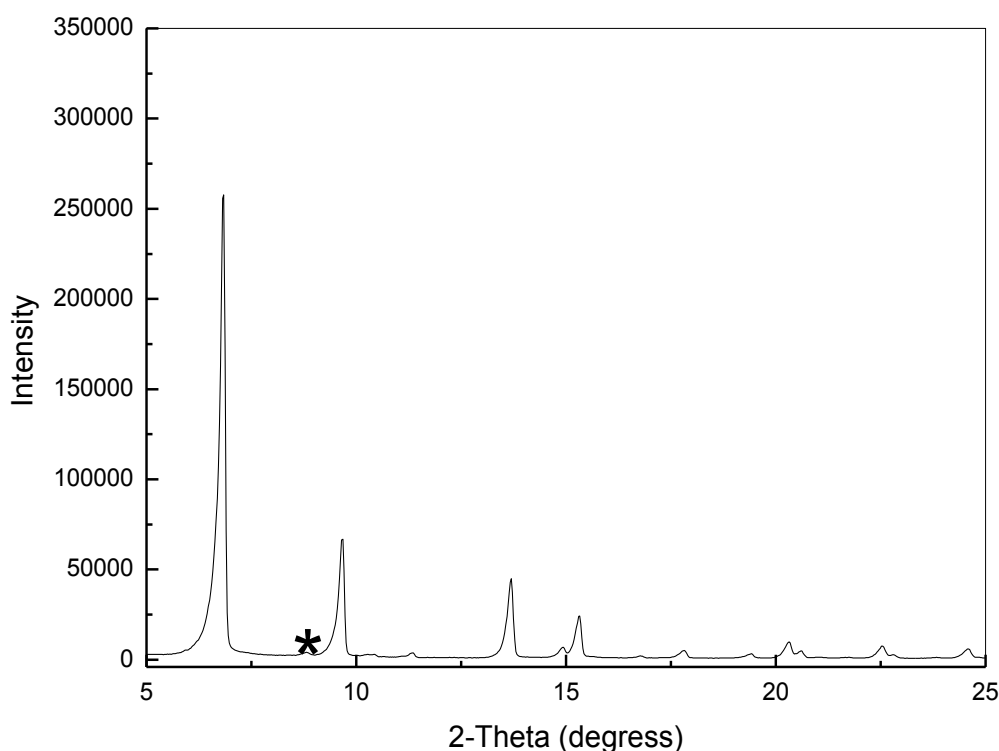


Figure 13: PXRD patterns of MOF-5 synthesised in DEF.

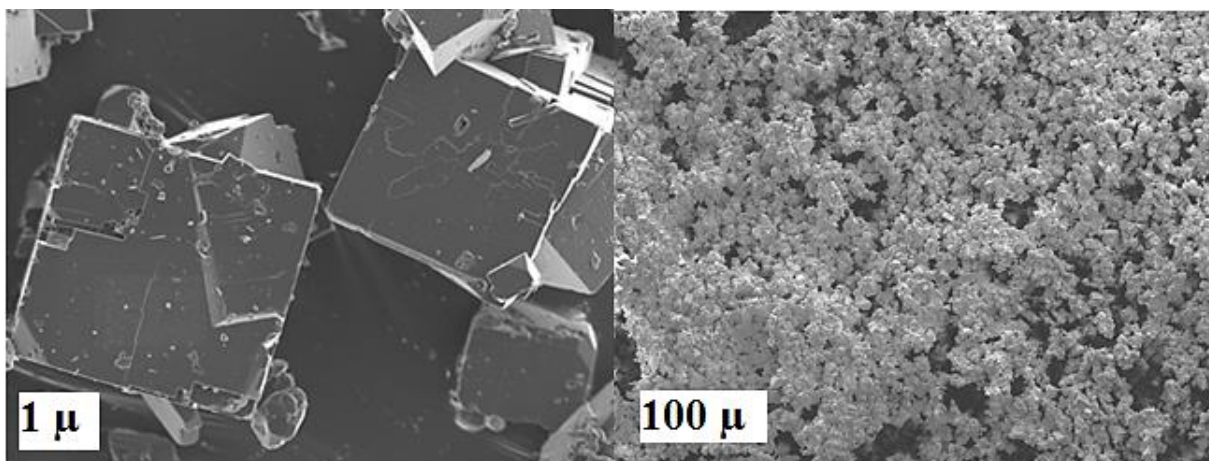


Figure 14: SEM images of MOF-5 synthesised in DEF

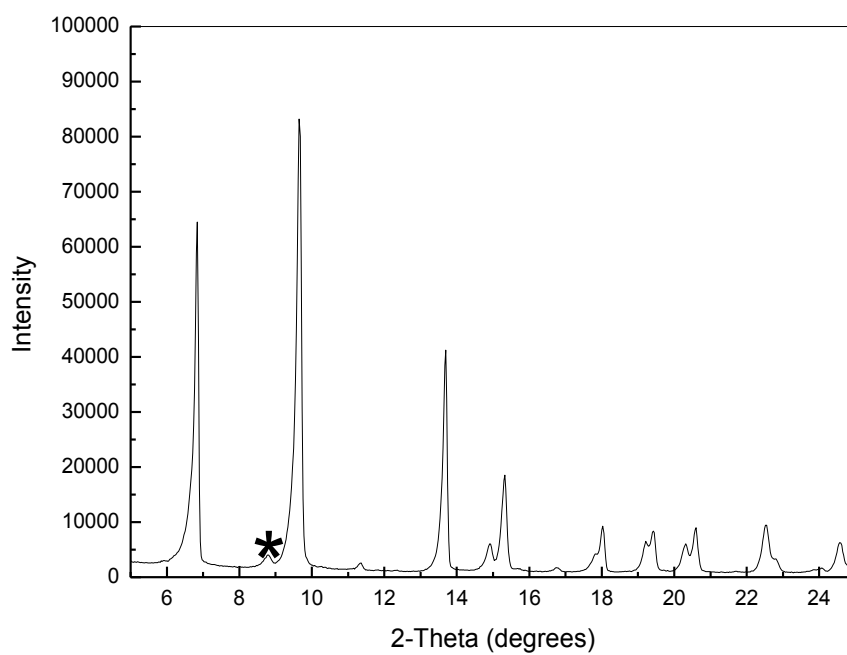


Figure 15: PXRD patterns of MOF-5 synthesised in DMF

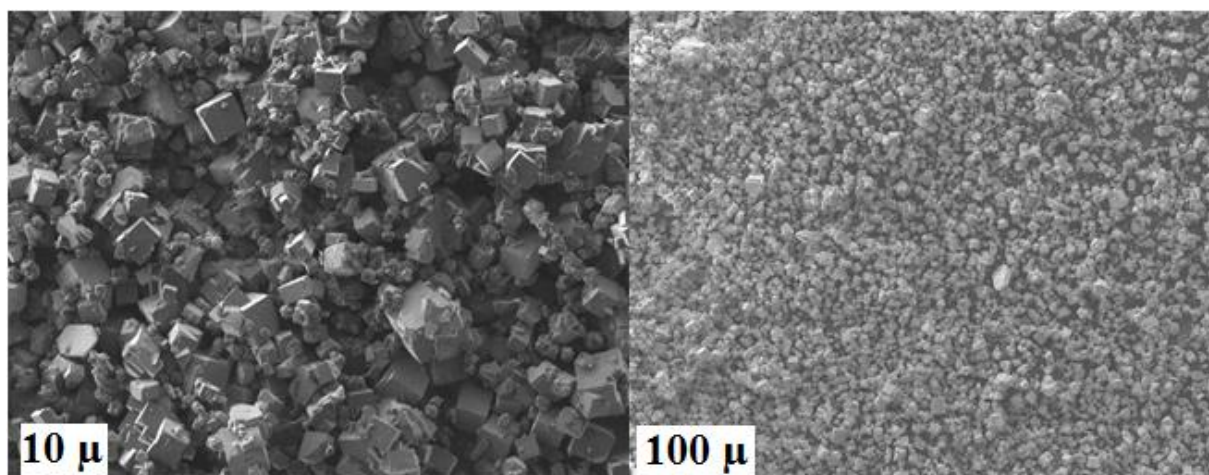


Figure 16: SEM images of MOF-5 synthesised in DMF

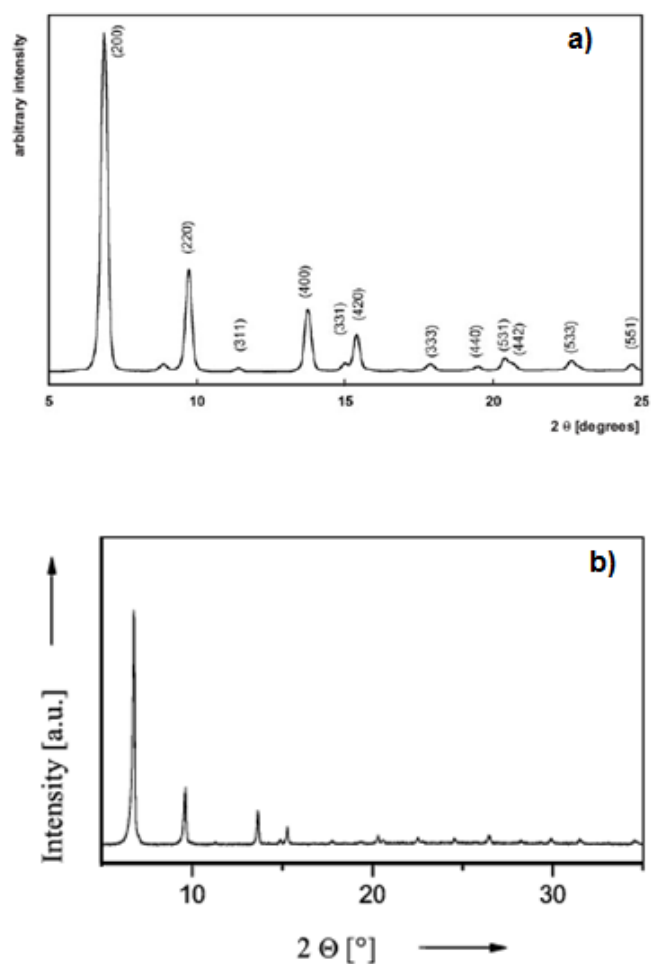


Figure 17: PXRD of MOF-5 obtained by a) Panella et al. using DEF (2006) and b) simulated PXRD obtained by Huang et al. (2003)

#### 4.2.1.2 Surface area, pore volume and pore size distribution

As earlier indicated in section 4.2.1.1, the MOF-5 samples synthesised in DEF showed better crystallinity than those synthesised in DMF. The nitrogen adsorption (Figures 18 and 19) isotherms used to determine the surface area and pore volumes also confirmed this with the DEF synthesised MOF-5 having a BET surface area of  $2662 \text{ m}^2\cdot\text{g}^{-1}$  and a Langmuir surface area of  $3861 \text{ m}^2\cdot\text{g}^{-1}$ , while the DMF synthesised MOF-5 had a BET surface area of  $657 \text{ m}^2\cdot\text{g}^{-1}$  and a Langmuir surface area of  $1036 \text{ m}^2\cdot\text{g}^{-1}$ . The calculated pore volumes were  $0.95 \text{ cm}^3\cdot\text{g}^{-1}$  for the DEF synthesised MOF-5 and  $0.27 \text{ cm}^3\cdot\text{g}^{-1}$  for the DMF synthesised MOF-5. This data corresponds well with the data obtained from the PXRD analysis in that the MOF-5 synthesised using DEF as the solvent offered better crystallinity and higher surface area and porosity.

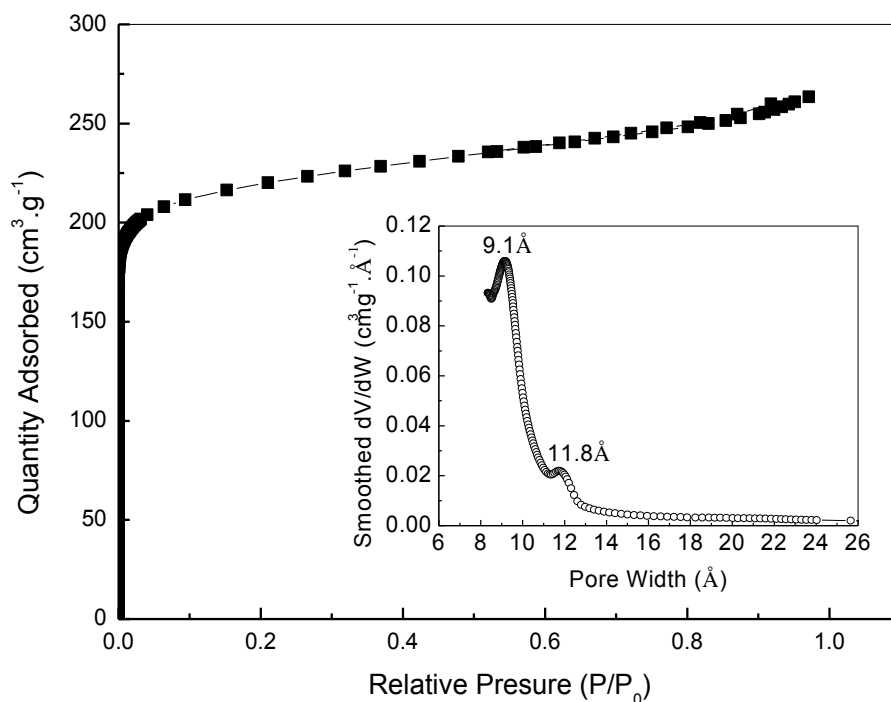


Figure 18: Nitrogen adsorption isotherm for MOF-5 synthesised using DMF at 77 K

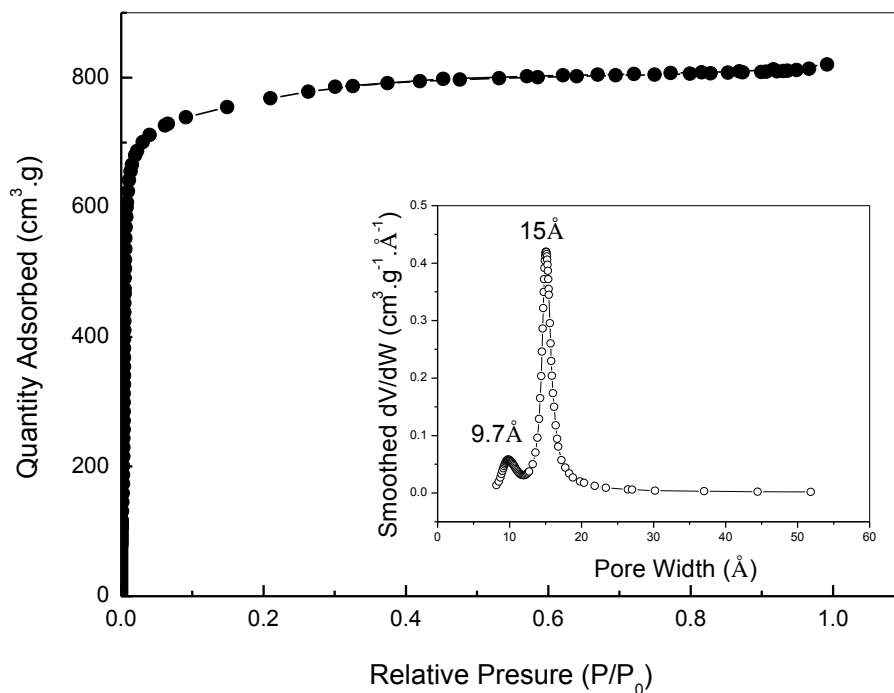


Figure 19 : Nitrogen adsorption isotherm for MOF-5 synthesised using DEF at 77 K

#### 4.2.2 Effect of stirring speed on the MOF-5 crystals

The investigations into the effect of stirring proved that stirring was essential for allowing the crystals to grow separately. In the synthesis with no stirring, the crystals were agglomerated, whereas when stirring was applied (250, 1000 and 1400 rpm), the crystals were able to grow independently as can be seen in the SEM images of the samples in Figure 20. In as much as interpenetration may improve hydrogen storage, in the case of MOF-5, it works in the opposite way. The crystals grow tightly together, restricting the pores from opening and lowering their hydrogen adsorption significantly. Therefore it was decided to stir all experiments involving MOF-5 at 1000 rpm.

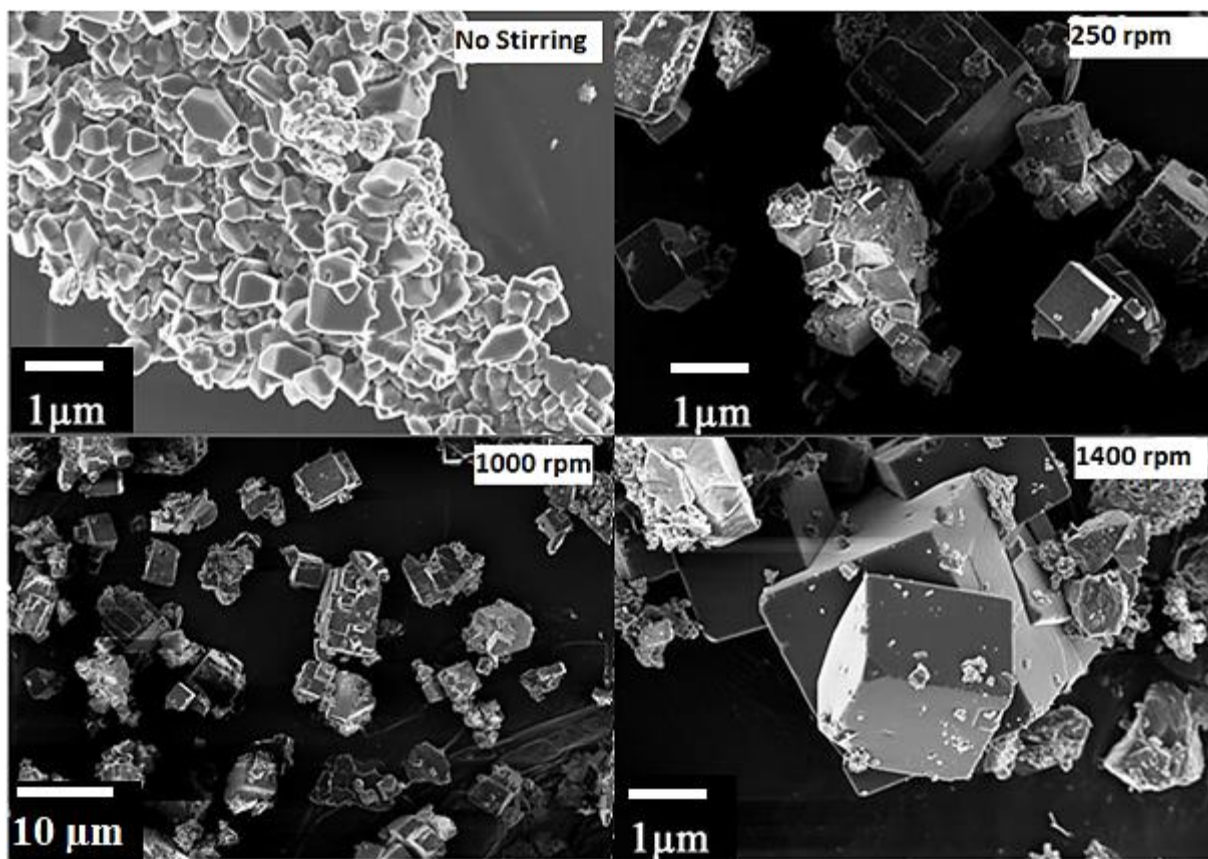


Figure 20: SEM images showing the effect of different stirring speeds

#### 4.2.3 Effect of reaction temperature on the MOF-5 crystals

Several experiments were conducted at different temperatures to determine the optimal temperature for the synthesis of MOF-5. The recovered MOF-5 crystals were characterised using PXRD and their hydrogen adsorption measurements were used to decide if the synthesised crystals were of sufficient quality. From this data, an optimum temperature for the MOF-5 synthesis was determined and that temperature was used in all subsequent MOF-5 synthesis. Finding the optimum temperature was crucial as it would assist in producing MOF-5 with good crystal structure in the most energy efficient way possible. The investigated temperatures were 100, 120, 130 and 140 °C. As mentioned before in section 3.2.2.1, the 100 °C reaction did not produce any crystals in the allowed reaction time of 4 h. The crystals obtained from the 120 °C reaction produced a few crystals (<0.1 g). This yield was too small to enable a full analysis as a sample size greater than 0.1 g was required for each of the available characterisation techniques. Therefore, it was concluded that the reactions at 100 and 120 °C had inadequate yields. The experiments that produced enough samples to perform a

full analysis, were from the 130 and 140 °C reactions. Figure 21 shows the SEM images of the crystals obtained from these two reactions. The crystals from the 130 °C reaction generally showed good quality crystals but it had a few crystals that were not fully developed. The reaction performed at 140 °C had crystals with good morphology and regular cubic shape. The 140 °C reaction crystals had a higher degree of crystallinity than those of the 130 °C reaction.

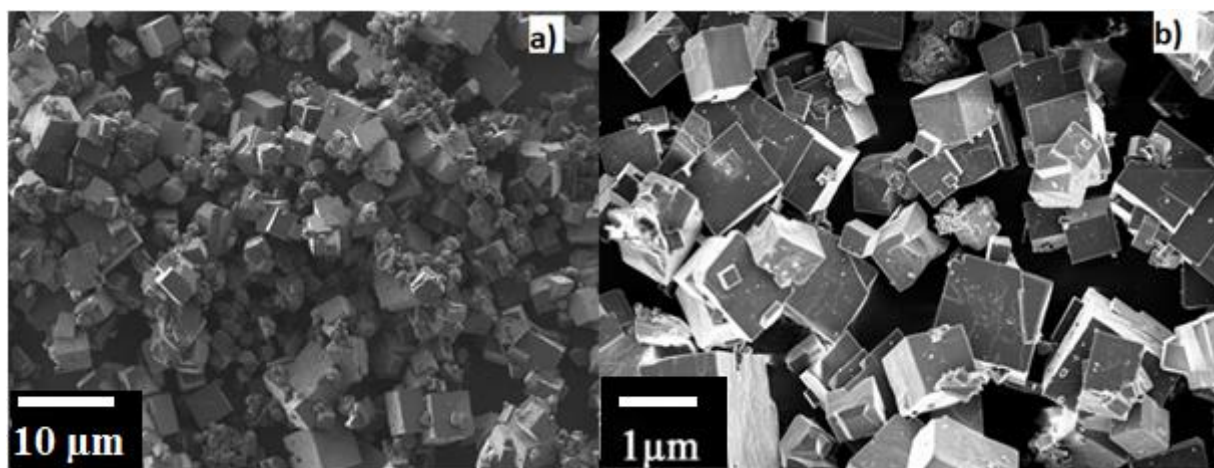


Figure 21: SEM images of MOF-5 samples synthesised at a) 130 °C and b) 140 °C

#### 4.2.4 Effect of reaction time on the MOF-5 crystals

The effect of reaction time on the MOF-5 crystals was investigated. The reaction times investigated were 1, 2, 3 and 4 h. In the case of the reaction time of 1 h, no crystals were recovered. In the 2 h reaction, only a very small amount of crystals was produced which was not enough for characterisation experiments. In the case of the 3 h reaction, there was enough sample produced but it was not pure and had poor crystal morphology as shown by the SEM image in Figure 22. The 4 h reaction had the best crystal structure which proved that 4 h was the minimum reaction time needed to produce a relatively good sample of MOF-5.

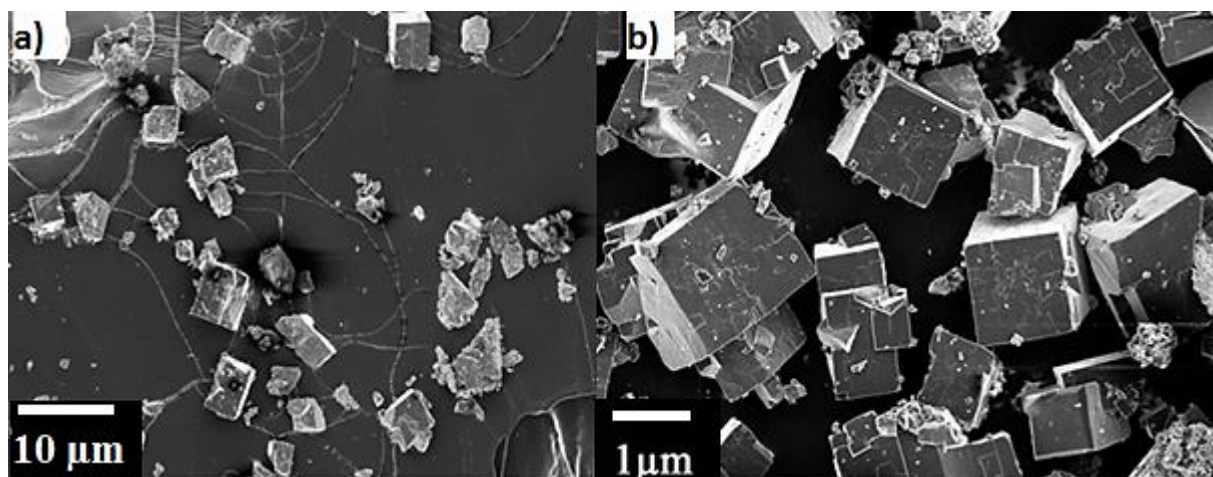


Figure 22: SEM images of MOF-5 synthesised in a) 3 h and b) 4 h

## 4.2.5 MOF-69c conversion to MOF-5

### 4.2.5.1 Morphology and phase crystallinity studies using SEM and PXRD

As mentioned in section 3.2.2.4, the reaction meant to produce MOF-5 produced MOF-69c in some instances. As indicated by several authors, the initial water content is a critical parameter for the synthesis of MOF-5 using zinc nitrate in DEF or DMF (Liao, Lee & Su 2006, Loiseau et al. 2005). Rosi and co-workers demonstrated that MOF-69c can reliably be generated by adding extra water to the MOF-5 procedure (Rosi et al. 2005). This further demonstrated the importance of the water content in the MOF-5 synthesis reaction. Considering the formulas of MOF-69c  $[\text{Zn}_3(\text{OH})_2(\text{BDC})_2]$  and MOF-5  $[\text{Zn}_4\text{O}(\text{BDC})_3]$ , Hausdorf et al. (Hausdorf et al. 2008) reported that the moisture-induced structural transition of MOF-5 to the hydroxide structure, MOF-69c can possibly be reversed by a thermal treatment to remove the hydroxide molecules. Several attempts to stop the formation of MOF-69c during the reaction have been reported in the literature. In the work of Hausdorf et al. an attempt to directly convert MOF-69c to MOF-5 by exposure to a DEF-water mixture in which MOF-5 is stable was unsuccessful. However, exposure of desolvated MOF-69c to either pure DEF or to solvent-water mixtures and temperatures where MOF-5 is stable led to the slow transition to MOF-5.

In this work, conversion of MOF-69c to MOF-5 without the need to add any other chemicals was conducted. The six samples in Table 3 (Sample A-F) that were prepared and given different treatments were analysed by SEM and PXRD. The as-prepared MOF-69c samples (samples A and B) were given different activation treatments and then analysed to determine

which of the two options, i.e. activation with anhydrous chloroform or anhydrous acetone, was more effective. In Figure 23, there were three distinct reflection peaks for sample A at  $2\theta = 8.9, 15.8$  and  $17.8^\circ$  which corresponded well to MOF-69c (Rosi et al. 2005, Kaye et al. 2007, Li et al. 2013). The position of these peaks also agreed well with the reported MOF-69c PXRD patterns reported by Rosi and co-workers (Rosi et al. 2005). The same peaks, along with other peaks, were also observed in sample B (Figure 23). Cubic shaped crystals with crystal sizes in the range 5–100  $\mu\text{m}$  were observed from the SEM images of sample A whereas the crystals from sample B, which was activated in anhydrous chloroform, lacked the cubic regular structures. This result suggested that activation in anhydrous chloroform was detrimental to the structural integrity of the samples.

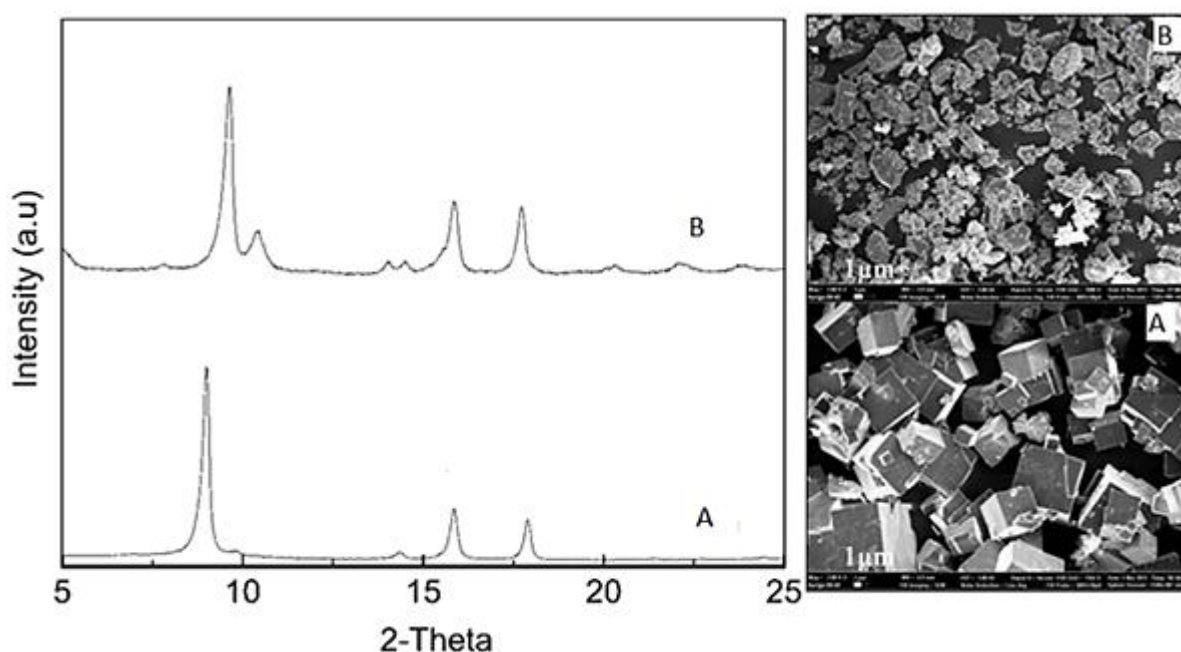


Figure 23: (a) PXRD patterns and (b) SEM images of MOF-69c samples A and sample B after activation.

The structural transition of MOF-69c to MOF-5 is shown in Figure 24 by the PXRD. The nine signals typical of MOF-5 appeared with increasing intensities for all the samples that received thermal treatment with the overall increasing intensities of the peaks indicating better crystallinities. The signals appeared at  $2\theta = 6.9, 9.8, 13.8, 15, 15.4, 19.5, 20.4, 20.7$  and  $22.6^\circ$ . The intensities of the MOF-69c peaks at  $2\theta = 15.8$  and  $17.8^\circ$  decreased significantly with the applied thermal treatment (Figure 24 I–V). The changes in the PXRD patterns prove that the

thermal treatment conducted in open air resulted in the structural transition from MOF-69c to MOF-5. The transition was shown to have been completed after 48 h. The PXRD pattern (IV in Figure 24) also matches the MOF-5 pattern derived from single-crystal structure data (Yaghi et al. 2002, Kaye et al. 2007). Structural transition from MOF-69c to MOF-5 was also achieved for sample F (V in Figure 24), which was contacted with a solution of anhydrous DMF and H<sub>2</sub>BDC before receiving thermal treatment. As explained in section 4.2.1.1, the residual peak at  $2\theta = 8.9^\circ$  (indicated by the arrow) is attributed to the exposure of the sample to moisture from the atmosphere during XRD measurement.

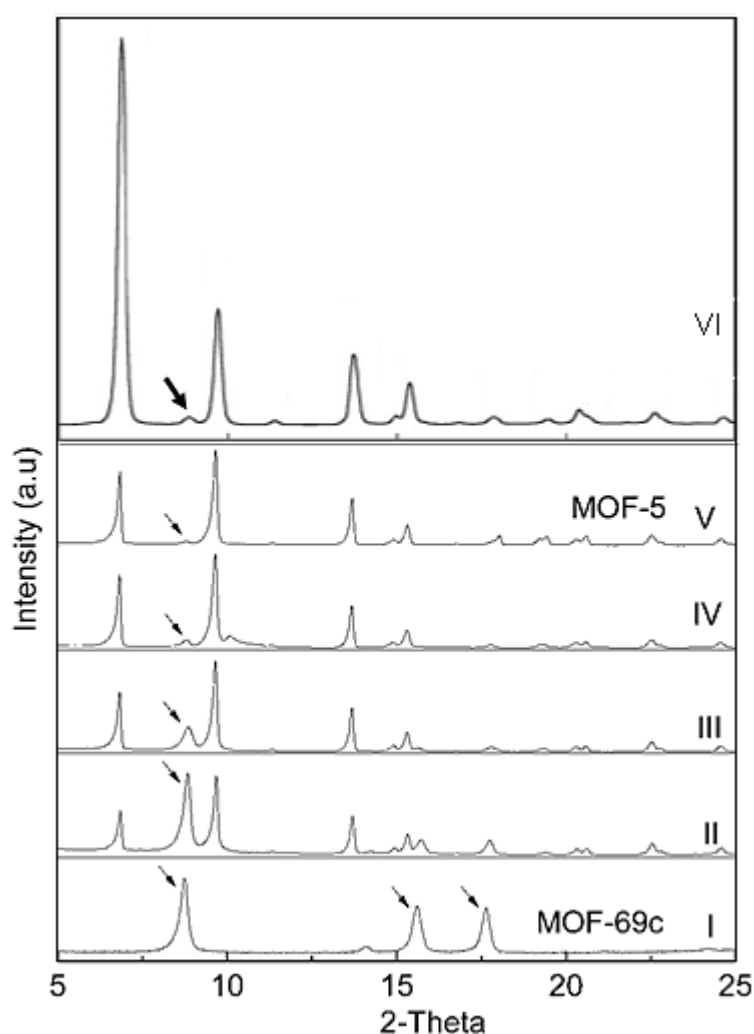


Figure 24: Thermal treatment induced transition from MOF-69c to MOF-5 structure (I) Sample A; (II) Sample C; (III) Sample D; (IV) Sample E; (V) Sample F; (VI) XRD pattern of MOF-5 taken from Panella et al. (Panella et al. 2006).

The surface area and pore volumes of the MOF-69c samples that were deemed to have successfully transitioned to MOF-5 (sample C and F) were measured and are presented together with the as-prepared MOF-69c (sample A) in Figure 25. The isotherms were Type I in nature which was an indication that the structure contained micropores (pores  $< 20 \text{ \AA}$ ). The inserted Horvath-Kawazoe differential pore volume plots exhibit two regions of pore size distribution for each sample with slightly different diameters which is due to the tilted BDC linkers connecting adjacent  $[\text{Zn}_4\text{O}]$  oxoclusters (Ren et al. 2014a).

#### 4.2.5.2 Surface area: BET, Langmuir and pore size distribution

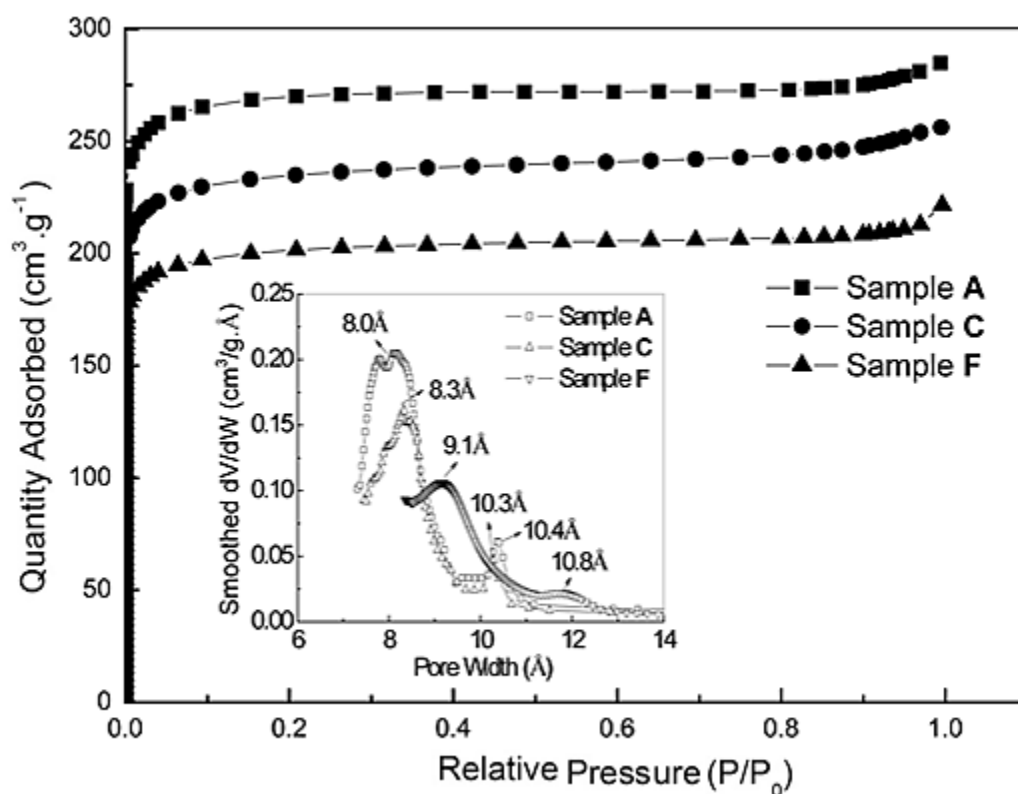


Figure 25: Nitrogen adsorption isotherms (insert, Horvath-Kawazoe differential pore volume plot) of the obtained MOF samples

The as-prepared MOF-69c (sample A) had a surface area of  $1011 \text{ m}^2 \cdot \text{g}^{-1}$  with a mean pore size of  $8.4 \text{ \AA}$ . The pore volume was found to be  $0.44 \text{ cm}^3 \cdot \text{g}^{-1}$ , and the micropore volume  $0.38 \text{ cm}^3 \cdot \text{g}^{-1}$ . After being heated to  $200 \text{ }^\circ\text{C}$  for 24 h under vacuum, the surface area decreased to  $850 \text{ m}^2 \cdot \text{g}^{-1}$ . A larger mean pore size of  $8.5 \text{ \AA}$  was observed. The micropore volume was  $0.32 \text{ cm}^3 \cdot \text{g}^{-1}$ . Thermal treatment of the obtained sample for a longer period resulted in decreasing surface area and micropore volume with an increased mean pore size of  $9.2 \text{ \AA}$ . The relative higher  $\text{N}_2$  adsorption capacity of as-prepared MOF-69c (sample A) can be attributed to the higher micropore volume compared to those of samples C and F. The Langmuir surface area of  $966 \text{ m}^2 \cdot \text{g}^{-1}$  for MOF-5 agreed well with the experimental surface area for MOF-5 using DMF as the solvent as reported in literature (Yaghi et al. 2003). The decreasing surface area from MOF-69c to MOF-5 can be attributed to the increasing pore diameters during the structural transition. Table 8 lists all the physical properties of the MOF-69c sample and the final MOF-5 samples.

**Table 8:** Pore characteristics of prepared MOF samples

| Sample | $\text{SSA}_{\text{BET}}$<br>( $\text{m}^2 \cdot \text{g}^{-1}$ ) <sup>a</sup> | $\text{SSA}_{\text{Lang}}$<br>( $\text{m}^2 \cdot \text{g}^{-1}$ ) <sup>b</sup> | Micropore<br>( $\text{m}^2 \cdot \text{g}^{-1}$ ) <sup>c</sup> | External<br>( $\text{m}^2 \cdot \text{g}^{-1}$ ) <sup>d</sup> | Pore<br>volume<br>( $\text{cm}^3 \cdot \text{g}^{-1}$ ) <sup>e</sup> | Micropore<br>volume<br>( $\text{cm}^3 \cdot \text{g}^{-1}$ ) <sup>f</sup> | Mean<br>diameter<br>( $\text{\AA}$ ) <sup>g</sup> | Pore |
|--------|--|---|--|---|--|---|---|------|
| A      | 1086   | 1186  | 1011   | 75  | 0.44   | 0.38  | 8.4   |      |
| C      | 937  | 1036  | 850  | 89  | 0.42   | 0.32  | 8.5   |      |
| F      | 860  | 966   | 704  | 156   | 0.41   | 0.27  | 9.2   |      |

<sup>a</sup> BET surface area. <sup>b</sup> Langmuir surface area. <sup>c</sup> From t-plot analysis. <sup>d</sup> From t-plot analysis. <sup>e</sup> From H-K analysis. <sup>f</sup> From H-K analysis. <sup>g</sup> Obtained by H-K analysis. <sup>h</sup> Absorbed at 77K and 1 bar.

#### 4.2.6 Optimised MOF-5 synthesis

An optimised synthesis for MOF-5 in DMF was achieved based on the data collected from the experiments with the results discussed above in section 4.2. The optimised synthesis is presented below in Table 9 in terms of the optimal condition of each variable investigated.

**Table 9:** Optimised variables for the synthesis of MOF-5

| Variables     | Condition | Zn(NO) <sub>3</sub><br>(mmol) | H <sub>2</sub> BDC<br>(mmol) | Zn(NO) <sub>3</sub> /H <sub>2</sub> BDC<br>(mol) |
|---------------|-----------|-------------------------------|------------------------------|--|
| Solvent       | DMF       | 10.52                         | 4                            | 2.63   |
| Stirring      | Yes       | 10.52                         | 4                            | 2.63   |
| Temperature   | 140 °C    | 10.52                         | 4                            | 2.63   |
| Reaction Time | 4 h       | 10.52                         | 4                            | 2.63   |

### 4.3 Characterisation of Zr-MOF crystals

#### 4.3.1 Solvothermal synthesis of Zr-MOF: effect of modulator ratio

##### 4.3.1.1 Morphology and phase crystallinity studies with SEM and PXRD

Zr-MOF crystals were synthesised using both the modulated and non-modulated solvothermal reactions. The reproducible synthesis of Zr-MOF without the use of a modulator was problematic and resulted in several failures in the initial synthesis efforts. It was also difficult to obtain good morphology without a modulator. As mentioned before in Chapter 3, the effect of the modulator ratio on the morphology of the Zr-MOF crystals was investigated.

PXRD patterns and their corresponding SEM images showing the Zr-MOF samples obtained using formic acid as a modulator in ratios of 0, 10, 50 and 100 eq and a synthesis time of 6 h are presented in Figure 26. The relative intensities of the reflection peaks in the PXRD patterns were used to gather qualitative information on the crystals. The patterns of the crystals obtained using 0 eq of formic acid has the intensity of the first reflection peak at  $2\theta = 7.4^\circ$  and is low in comparison to the second peak at  $2\theta = 8.5^\circ$ , and the peaks were also broader, indicating low crystallinity. This was confirmed by the corresponding SEM image which showed that the crystals were not well-defined and exhibited agglomeration.

When formic acid was added, the degree of crystallinity increased drastically. This increase was observed with the first addition of 10 eq formic acid to the synthesis. Reactions with increased additions of formic acid gave further evidence of enhanced crystallinity and

decreased agglomeration. When 50 eq of formic acid was used, the crystals began taking an octahedral shape with particle size around 100 nm. In the presence of 100 eq formic acid, the obtained Zr-MOF crystals showed clear octahedral shapes with sharp edges and clearly visible facets. The crystal sizes were in the range of 1 – 3  $\mu\text{m}$ . The PXRD patterns for the 10, 50 and 100 eq synthesis exhibited the full set of reflection peaks typical of a Zr-based MOF in the crystalline phase. The peaks were positioned at  $2\theta = 7.4, 8.5, 14.1, 14.7, 17, 18.6$  and  $19.1^\circ$ . The data collected confirmed a successful synthesis of Zr-MOF (Abid et al. 2012).

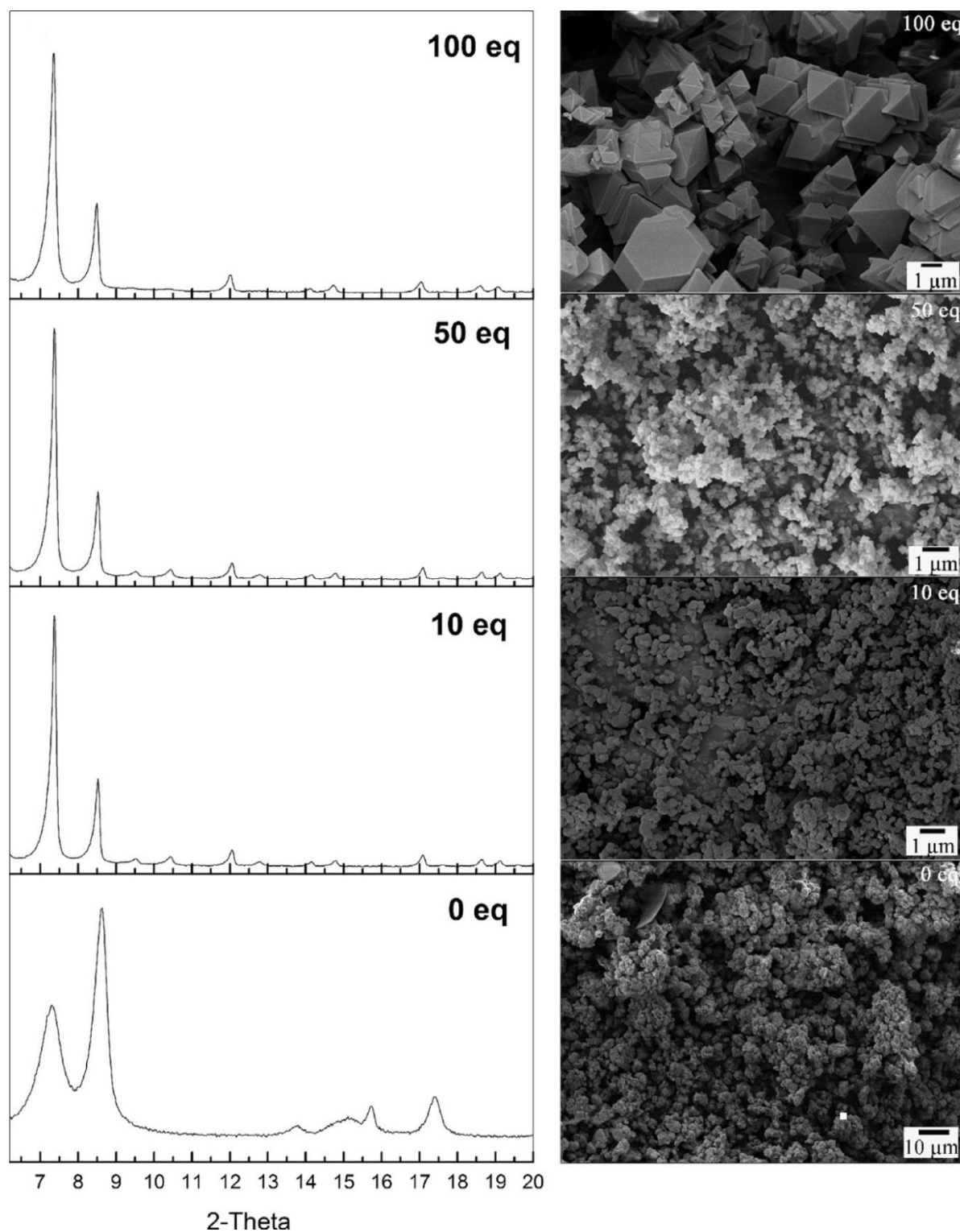
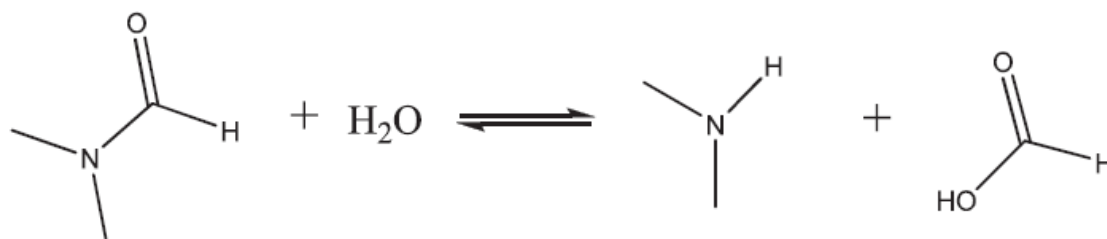


Figure 26: PXRD patterns of Zr-MOF from differing modulator ratios.

Formic acid acts as a modulator in two successive ways. The first can be described as follows: the presence of formic acid in the synthesis accelerated the formation of the Zr-MOF crystals, with the highest equivalent of formic acid giving the largest crystals. During the synthesis of Zr-MOF, water was identified as a necessity for the hydrolysis of the Zr precursor and oxygen

supply for the formation of  $Zr_6O_4(OH)_4(O_2C)_{12}$  SBUs. DMF, however, easily absorbs water and decomposes as presented in Reaction 2 (Schaate et al. 2011, Wißmann et al. 2012):



Reaction 2: Reaction of DMF with water

The presence of formic acid, added as a modulator, displaces the equilibrium to the left to make more water available for the hydrolysis reaction without decomposing the DMF solvent. This speeds up the formation of the SBUs.

The second step can be described as follows: with the first step speeding up the formation of the SBUs, the formation of the nuclei is accelerated. This, together with the excess SBUs available, allows the nuclei to grow into larger crystals.

#### 4.3.1.2 Surface area and pore volume

The surface areas and pore volumes of the Zr-MOFs synthesised using different equivalents of formic acid were analysed on the ASAP 2020 using nitrogen as the analysis gas at 77 K. The nitrogen adsorption isotherms of the desolvated Zr-MOFs using 0, 10 and 100 eq are presented below in Figure 27. The isotherms were Type I in nature which was an indication that the structure contained micropores (Walton, Snurr 2007, Bae, Snurr 2010). The surface area values were calculated from both BET and Langmuir equations. When comparing the synthesis of the non-modulated Zr-MOF to those that were modulated, the BET surface area and total pore volume increased from  $241 \text{ m}^2 \cdot \text{g}^{-1}$  and  $0.13 \text{ cm}^3 \cdot \text{g}^{-1}$  for the non-modulated Zr-MOF to a maximum of  $1367 \text{ m}^2 \cdot \text{g}^{-1}$  and  $0.56 \text{ cm}^3 \cdot \text{g}^{-1}$  for the modulated Zr-MOF synthesised using 100 eq formic acid. The Langmuir surface area also increased from  $273 \text{ m}^2 \cdot \text{g}^{-1}$  for the non-modulated Zr-MOF to a maximum of  $1581 \text{ m}^2 \cdot \text{g}^{-1}$  for the modulated Zr-MOF synthesised using 100 eq formic acid. The Langmuir values obtained with the 100 eq formic acid Zr-MOF are larger than the value of  $1187 \text{ m}^2 \cdot \text{g}^{-1}$  reported in the literature for Zr-MOF (Abid et al. 2012a). Table 10 lists the physical properties of the Zr-MOF samples obtained in this work against those reported in literature.

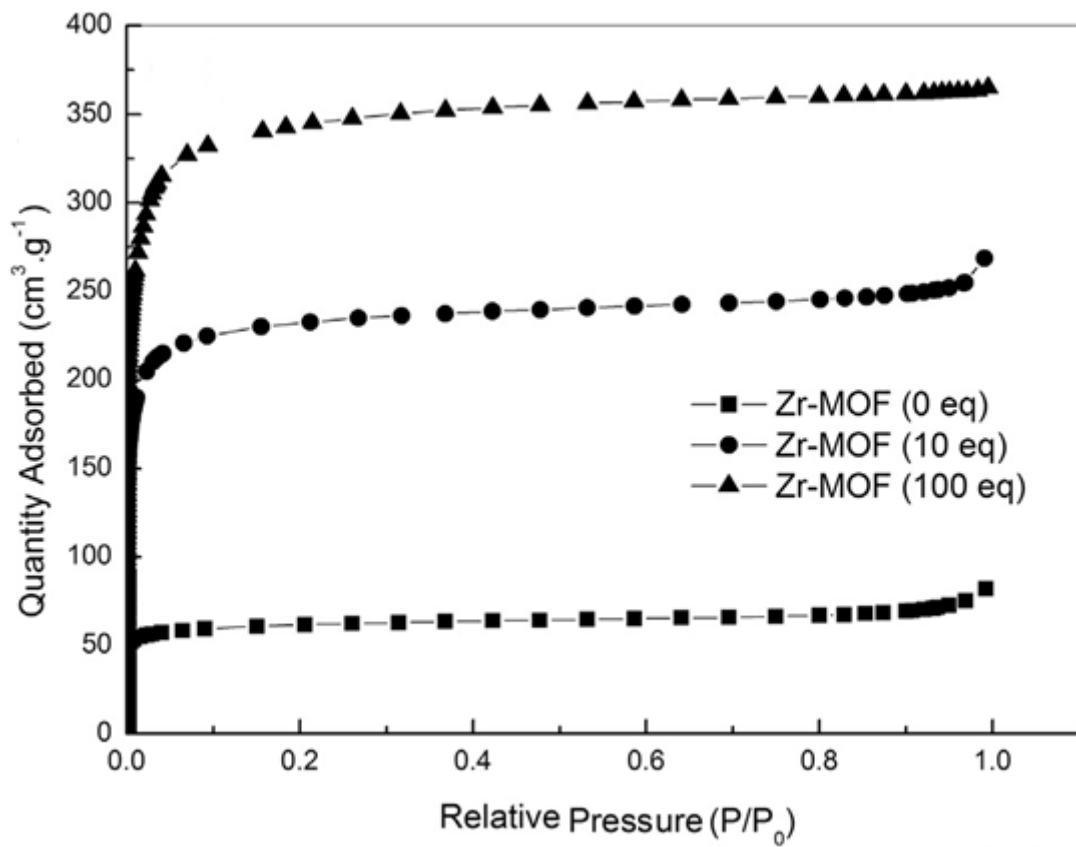


Figure 27: Nitrogen adsorption isotherms of the 0, 10 and 100 eq Zr-MOF samples.

**Table 10:** Comparison of physical properties of the Zr-MOF samples from this work with those reported in the literature

| Sample        | Size<br>(nm) <sup>a</sup> | SSA <sub>BET</sub><br>(m <sup>2</sup> ·g <sup>-1</sup> ) <sup>b</sup> | Pore vol.<br>(cm <sup>3</sup> ·g <sup>-1</sup> ) <sup>c</sup> | Micropore vol.<br>(cm <sup>3</sup> ·g <sup>-1</sup> ) <sup>d</sup> | Reference.              |
|---------------|---------------------------|---|---|--|-------------------------|
| UiO-66        | 200                       | 1080  | --  | --   | (Hafizovic et al. 2014) |
| UiO-66        | 100                       | 1434  | 0.65  | 0.43   | (Zhao et al. 2013)      |
| UiO-66        | 150-200                   | 1358  | --  | --   | (Abid et al. 2012a)     |
| Non-modulated |                           |   |   |  |                         |
| Zr-MOF        | 100–200                   | 918   | 0.42  | 0.30   | This work               |
| Modulated Zr- |                           |   |   |  |                         |
| MOF           | 1–3 μm                    | 1367  | 0.56  | 0.44   | This work               |
| MW-Zr-MOF     | 0.5–3 μm                  | 1087  | 0.44  | 0.38   | This work               |

<sup>a</sup> SEM images. <sup>b</sup> BET surface area. <sup>c</sup> From H-K analysis. <sup>d</sup> From H-K analysis.

### 4.3.2 Effect of synthesis time on the crystallisation of Zr-MOF

In the efforts to better understand and optimise variables of the Zr-MOF synthesis, experiments were conducted to investigate the effect of synthesis time on the formation of Zr-MOF crystals. The PXRD patterns of 1, 2, 4, 8, 16 and 24 h reactions (Figure 28) were analysed to understand which reaction time led to the proper formation of MOF crystals when using 100 eq of formic acid. The results showed that high quality Zr-MOF crystals with high intensity peaks indicating good crystal structure could be obtained in as short a reaction time as 2 h. The patterns matched that of the 100 eq synthesis which was earlier presented in Figure 26 and served as an indication that the Zr-MOF obtained had well-defined octahedral shapes. The increased reaction times did not have a detrimental effect on the crystals obtained such as phase change of the Zr-MOFs. The patterns indicated that Zr-MOF was obtained with the only change being the increased intensity of the reflection peaks.

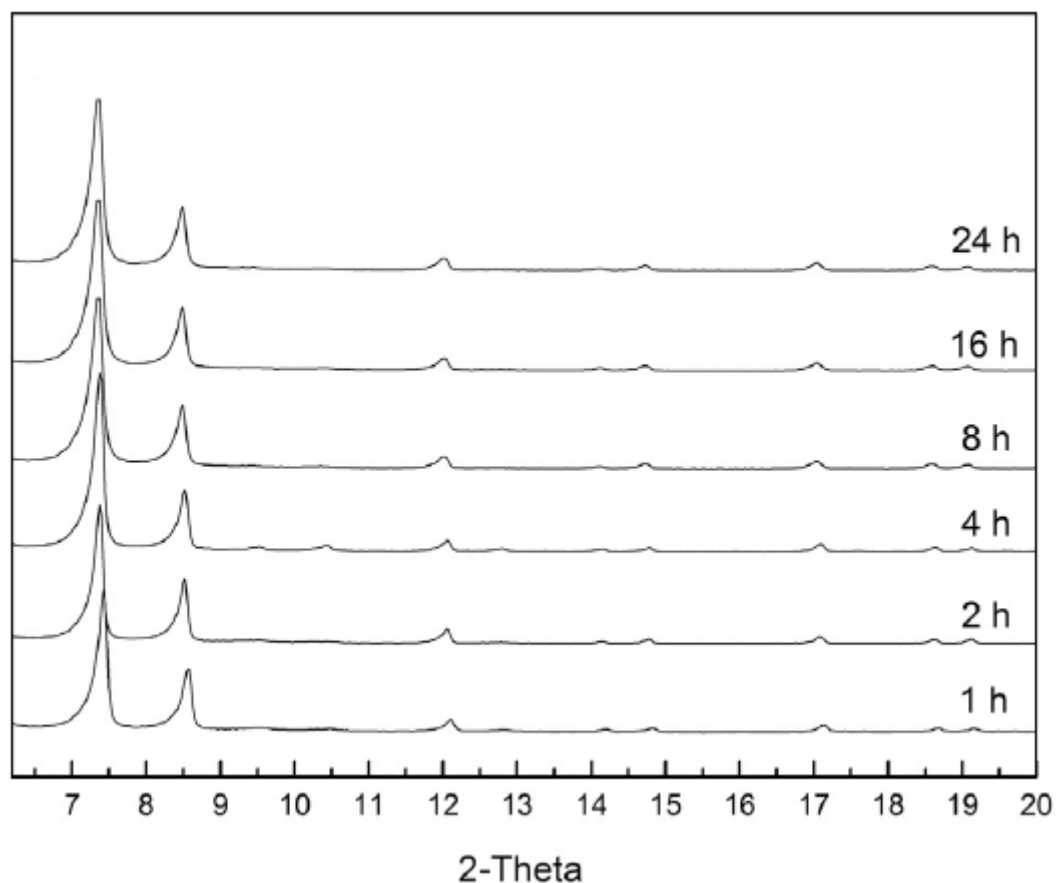


Figure 28: PXRD patterns of Zr-MOF from differing reaction times.

### 4.3.3 TGA analysis

Thermal analysis of the modulated Zr-MOF (100 eq) and the non-modulated Zr-MOF were carried out by thermo gravimetric analysis (TGA). The analysis showed that the mass loss profiles of both MOFs could be divided into three regions (Figure 29). The first region, from room temperature to about 350 °C, showed a continuous mass loss which is attributed to the removal of all organic materials, evaporation of guest molecules from the pores such as solvent DMF and the activation solvent, acetone and the modulator, formic acid (in the modulated synthesis). The total mass loss was 25% for the modulated Zr-MOF and 34% for the non-modulated Zr-MOF in the first region. The second region was between 350 and 500 °C, the weight loss was almost linear indicating the high thermal stability of the Zr-MOFs. The material found in the second region was desolvated and contained only the pure Zr-MOF with a chemical formula of  $Zr_6O(CO_2)_2(C_6H_4)$  (Valenzano et al. 2011). This also corresponds to a purity of about 75% of the starting material for the modulated Zr-MOF and 66% for the non-modulated Zr-MOF. The third and last region showed a sudden weight loss, which was

attributed to decomposition of the Zr-MOFs to  $ZrO_2$ . The total mass loss of the modulated Zr-MOF sample was 60% and that of the non-modulated Zr-MOF sample was 65%. The mass loss of the pure Zr-MOF from the start of the second region to the start of the third region was 15% for the modulated Zr-MOF and 35% for the non-modulated Zr-MOF. This difference in mass loss indicated the modulated Zr-MOF was more thermally stable than the non-modulated sample. Valenzano and co-workers, using TGA hyphenated with a mass spectrometer, found that Zr-MOF loses water and solvents in the first region, and benzene in the last region as the organic linker decomposes (Valenzano et al. 2011) (benzene from the organic linker  $H_2BDC$ ). The TGA profile of the modulated Zr-MOF sample (100 eq) agreed very well with that of UiO-66 originally reported by Cavka et al. and by Valenzano et al. (Bárcia et al. 2011, Valenzano et al. 2011) which showed the same stability up to 500 °C followed by a sudden structural collapse. The results suggest that the modulated synthesis produced highly crystalline Zr-MOFs with high thermal stability.

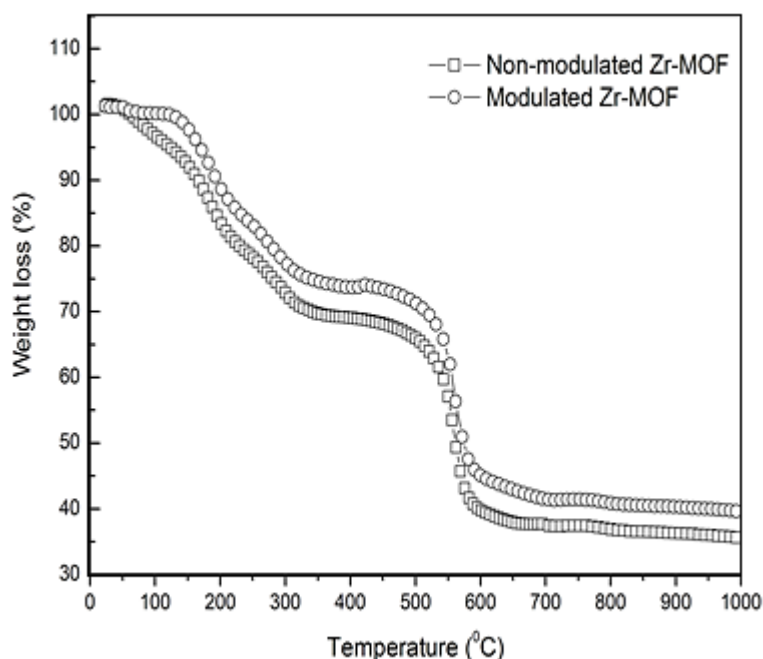


Figure 29: TGA curves of modulated and non-modulated Zr-MOF

#### 4.3.4 Microwave-assisted synthesis of Zr-MOF

##### 4.3.4.1 Morphology and phase crystallinity studies using SEM and PXRD

Powder XRD patterns and the corresponding SEM images of the Zr-MOF-Oil bath and Zr-MOF-MW materials are shown in Figure 30. Zr-MOF-Oil bath refers to the Zr-MOF sample synthesised using an oil bath to provide constant reaction temperature and Zr-MOF-MW refers to the Zr-MOF sample synthesised using a microwave. The PXRD patterns of both samples showed the full set of sharp diffraction peaks belonging to Zr-MOF (Zhao et al. 2013). Similarly to other MOF materials, the relative intensities of the reflection peaks normally give qualitative information of the crystals. The Zr-MOFs showed a high degree of crystallinity. It can be seen from the SEM image that the Zr-MOF crystals obtained from 24 h oil bath reaction undoubtedly were octahedral shaped with sharp edges and well-defined facets. The crystal sizes were in the range of 1–3  $\mu\text{m}$ . For the microwave reaction, not only was the same degree of crystallinity achieved within a much shorter reaction time of 5 min, but also clearly defined octahedral shaped crystals of sizes 0.5–3  $\mu\text{m}$  were obtained as shown in the SEM image. These results illustrate that the use of microwave significantly reduces the synthesis time of Zr-MOF without compromising the crystallinity of the material.

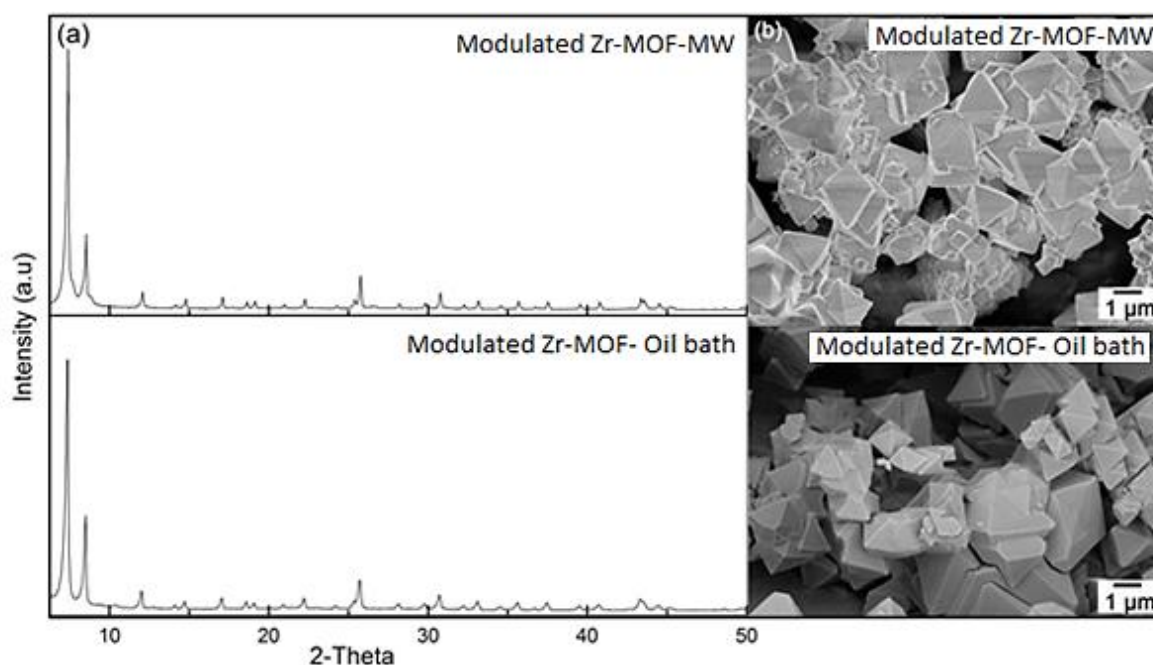


Figure 30: SEM and PXRD patterns of Zr-MOF, respectively obtained using an oil bath after 24 h for temperature control, and microwave heating after 5 min

#### 4.3.4.2 Surface area, pore volume and pore size distribution

Figure 32 shows the nitrogen adsorption isotherms at 77 K of desolvated Zr-MOF-Oil bath and Zr-MOF-MW powder samples were Type I in nature, characteristic of a structure with micropores. The surface area and pore volume data of the desolvated Zr-MOF-Oil bath and Zr-MOF-MW samples are given in Table 10, and are compared to values that have been reported in the literature. The Langmuir surface area (not shown in the Table) determined from the sorption isotherms were 1581 and 1186  $\text{m}^2 \cdot \text{g}^{-1}$  for Zr-MOF-Oil bath and Zr-MOF-MW, respectively. The latter value is very similar to the reported value of 1187  $\text{m}^2 \cdot \text{g}^{-1}$  for UiO-66 (Hafizovic et al. 2014). The BET surface area and total pore volume were 1367  $\text{m}^2 \cdot \text{g}^{-1}$  and 0.56  $\text{cm}^3 \cdot \text{g}^{-1}$  respectively for Zr-MOF-Oil bath, and 1087  $\text{m}^2 \cdot \text{g}^{-1}$  and 0.44  $\text{cm}^3 \cdot \text{g}^{-1}$  respectively for Zr-MOF-MW. The difference in surface areas between the Zr-MOF-Oil bath and Zr-MOF-MW samples also complements the observed differences in weight loss curves shown in Figure 33. The BET surface areas obtained here are within range of those reported for various UiO-66 samples shown in Table 10. The inserted Horvath–Kawazoe differential pore volume plots in Figure 32 exhibited two main regions of pores at 7.8 and 11.3 Å alongside others for Zr-MOF-Oil bath sample. While for Zr-MOF-MW sample, only one region of pores at 11.0 Å was observed. The absence of pores around 8 Å for the Zr-MOF-MW sample may, at least in part, be responsible for the lower surface area and pore volume when compared to the Zr-MOF-Oil bath sample.

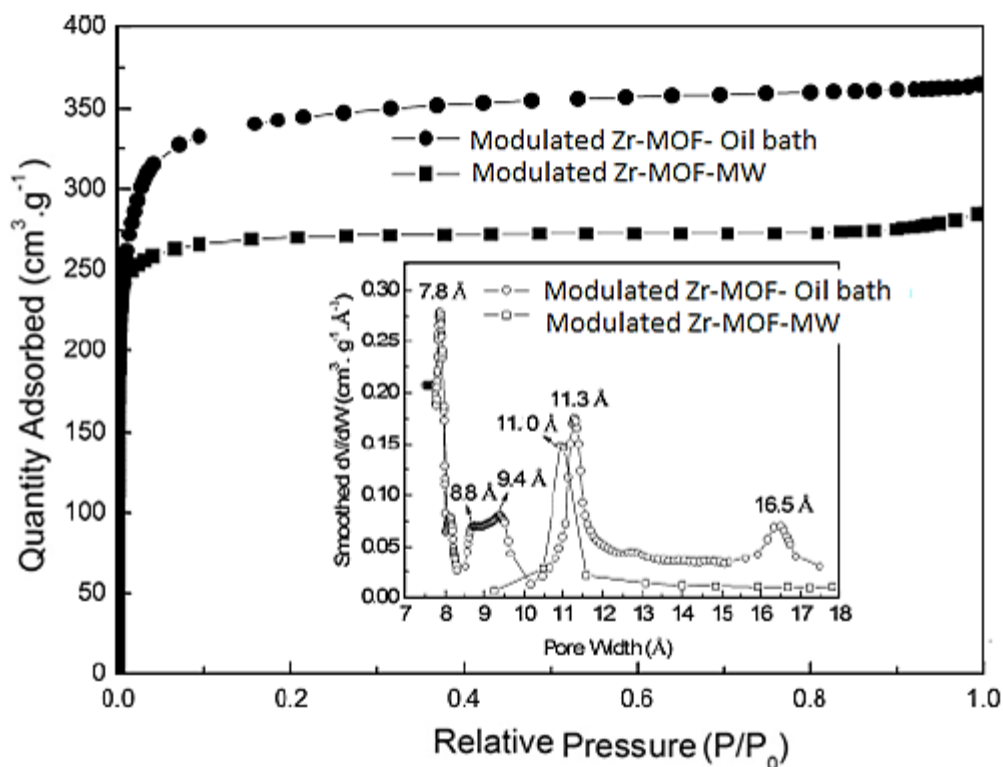


Figure 31: Nitrogen adsorption isotherms of the Zr-MOF obtained using an oil bath for temperature control and microwave conditions.

#### 4.3.4.3 TGA analysis

Thermo gravimetric analyses of the microwave-assisted synthesised Zr-MOF (100 eq) and solvothermal modulated Zr-MOF which was synthesised using an oil bath are shown in Figure 32. The analysis showed that the mass loss profiles of the microwave assisted Zr-MOF was very similar to that of the Zr-MOF synthesised in an oil bath. The TGA curve could be divided into three regions. The first region was from room temperature to about 350 °C. This region showed a continuous mass loss which is attributed to the removal of all organic materials. The total mass loss was 15% for the microwave synthesised Zr-MOF and 25% for the oil bath synthesised Zr-MOF. The second region was between 350 and 500 °C. Here the weight loss was almost linear indicating the high thermal stability of the Zr-MOFs. The material found in the second region was desolvated and contained only the pure Zr-MOF as stated in section 4.3.3 with the chemical formula of  $Zr_6O(CO_2)_2(C_6H_4)$  (Valenzano et al. 2011). This corresponded to a purity of about 85% of the starting material for the microwave synthesised Zr-MOF and 75 % for the oil bath Zr-MOF. The third and last region showed a

sudden weight loss, attributed to the decomposition of the Zr-MOFs to  $ZrO_2$ . The total mass loss of the microwave synthesised Zr-MOF sample was 45 % and that of the oil bath synthesised Zr-MOF 58 %. The mass loss of the pure Zr-MOF from the start of the second region to the start of the third region was 30% for the microwave synthesised Zr-MOF and 33% for the oil bath synthesised Zr-MOF. This difference in the mass loss curves indicated the microwave synthesised Zr-MOF sample had a higher purity than the oil bath synthesised Zr-MOF but because the mass loss of the Zr-MOF samples was very similar (30 % and 33 %), the stability of the two MOFs was similar. The TGA profile of the microwave synthesised Zr-MOF sample also agreed very well with that of UiO-66 (Zr-MOF) originally reported by Cavka et al. (Hafizovic et al. 2014), showing the same stability up to 500 °C followed by a sudden structural collapse. The results suggest that the microwave assisted synthesis produces highly crystalline Zr-MOFs with high thermal stability.

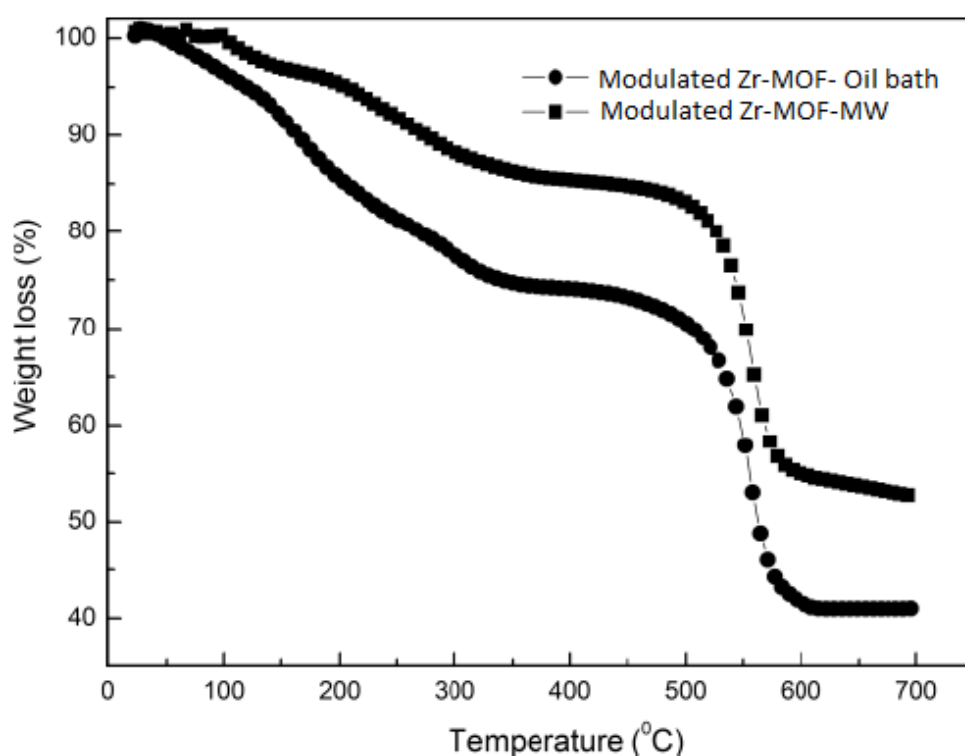


Figure 32: TGA curves of the oil bath and microwave Zr-MOF samples

#### 4.3.5 Optimised Zr-MOF synthesis

An optimised synthesis for the modulated Zr-MOF was achieved based on the data collected from the experiments with the results discussed above in section 4.3. The optimised synthesis is presented below in Table 11 in terms of the optimal condition of the variables which were investigated. The sample with 100 eq of modulator and with a synthesis time of 6 h was found

to have the optimum properties, both in terms of the morphology and gas adsorption. Therefore, this synthesis was deemed to be the optimum synthesis.

**Table 11:** Optimised variables for the synthesis of Zr-MOF

| Variables       | Condition | ZrCl <sub>4</sub><br>(mmol) | H <sub>2</sub> BDC<br>(mmol) | ZrCl <sub>4</sub> /H <sub>2</sub> BDC<br>(mol) |
|-----------------|-----------|-----------------------------|------------------------------|--|
| Solvent         | DMF       | 0.22                        | 0.22                         | 1  |
| Stirring        | Yes       | 0.22                        | 0.22                         | 1  |
| Temperature     | 120 °C    | 0.22                        | 0.22                         | 1  |
| Reaction Time   | 6 h       | 0.22                        | 0.22                         | 1  |
| Modulator ratio | 100 eq    | 0.22                        | 0.22                         | 1  |

#### 4.4 Characterisation of Cr-MOF crystals

##### 4.4.1 Solvothermal synthesis of Cr-MOF: Effect of modulator ratio

###### 4.4.1.1 Morphology and phase crystallinity studies using SEM and PXRD

Cr-MOF crystals were synthesised using both modulated and non-modulated solvothermal reactions. The crystals obtained from the non-modulated synthesis of Cr-MOF had poor crystallinity as shown by the PXRD pattern (0 eq plot in Figure 34). The peaks were broad which indicated that the sample had low crystallinity. The SEM image in Figure 35 showed that the crystals were not well-defined and exhibited a high degree of agglomeration. It has been noted in literature (Ren et al. 2014a) that the degree of crystallinity can be enhanced by the use of a modulator. In this work, formic acid was chosen as the modulator. When formic acid was added, an increase in the degree of crystallinity was observed from the first addition of 10 eq of formic acid (Figures 34 and 35). The effect of the modulator was investigated by using different ratios of the modulator and studying the influence on the crystallinity and morphology of the Cr-MOFs.

To study the effect that the different modulator ratios had on the crystallinity and morphology of the Cr-MOF, 10, 20, 50, 80 and 100 eq of formic acid were added to the reaction system. Ten characteristic peaks in the PXRD patterns of Cr-MOF were observed for both the modulated and non-modulated samples. However, the peaks of the sample from modulated

synthesis were much sharper than those of the sample from non-modulated synthesis. The peaks mentioned, are positioned at  $2\theta = 2.78, 3.26, 3.94, 4.3, 4.85, 5.59, 5.84, 8.43, 9.04$  and  $10.3^\circ$  (Figure 34). The presence of these peaks confirmed the successful synthesis of the Cr-MOF, MIL-101(Cr) as the pattern was identical to the patterns obtained from simulation (Oh et al. 2014). The relative crystallinity of the samples was determined by comparing the sum of the integrated intensities of two main diffraction peaks (at  $2\theta 2.78$  and  $3.26^\circ$ ) in relation to that of the most highly crystalline sample. It was found that both the relative crystallinity and autogenous pressure increased with increasing ratio of formic acid. This suggested that the formic acid modulator contributed to the autogenous pressure which in turn, helped to increase the degree of crystallinity of the Cr-MOF. The corresponding SEM images in Figure 35 showed that the Cr-MOF synthesised from modulated synthesis had some multifaceted shapes compared to those synthesised from the non-modulated synthesis. With the addition of 50 eq of formic acid to the synthesis mixture, the crystals began to take an octahedral shape. The best shaped crystals were obtained when maximum amounts of formic acid were added with particle size of 50-100 nm observed from the SEM analysis. The role of formic acid could be explained as follows: in order to increase the crystal growth and the rate of nucleation, competitive crystal growth had to be introduced. This competitive crystal growth will slow the reaction down and hence result in bigger MOF crystals. Formic acid, having the same functional group as terephthalic acid will compete for the metal ions. Therefore, the addition of formic acid had two overall advantages; the first was to speed up the formation of the SBUs and then accelerate the formation of the nuclei, and secondly, the excess SBUs available around allowed the nuclei to grow into larger crystals.

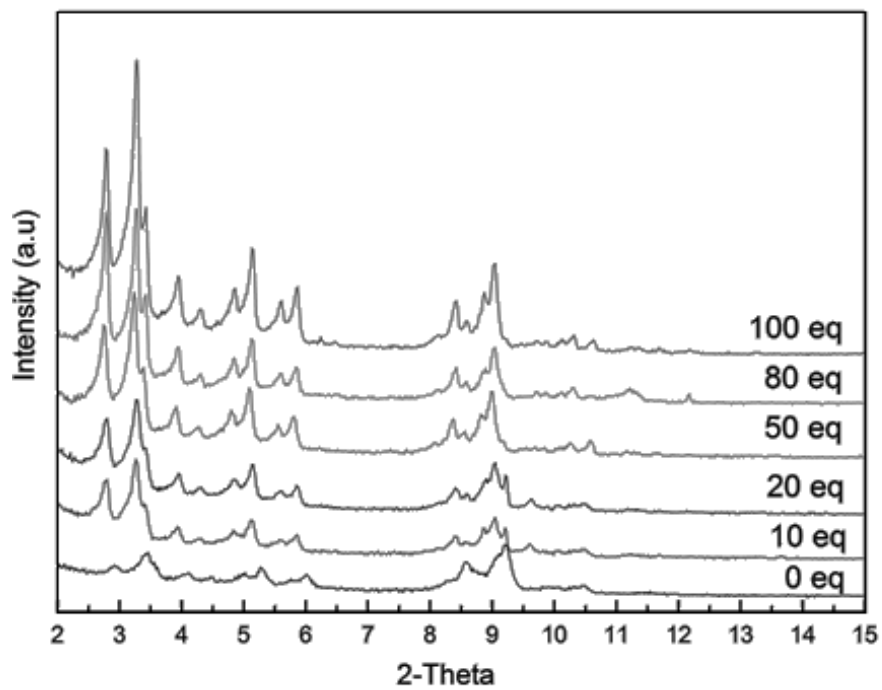


Figure 33: PXRD patterns of Cr-MOF from differing modulator ratios.

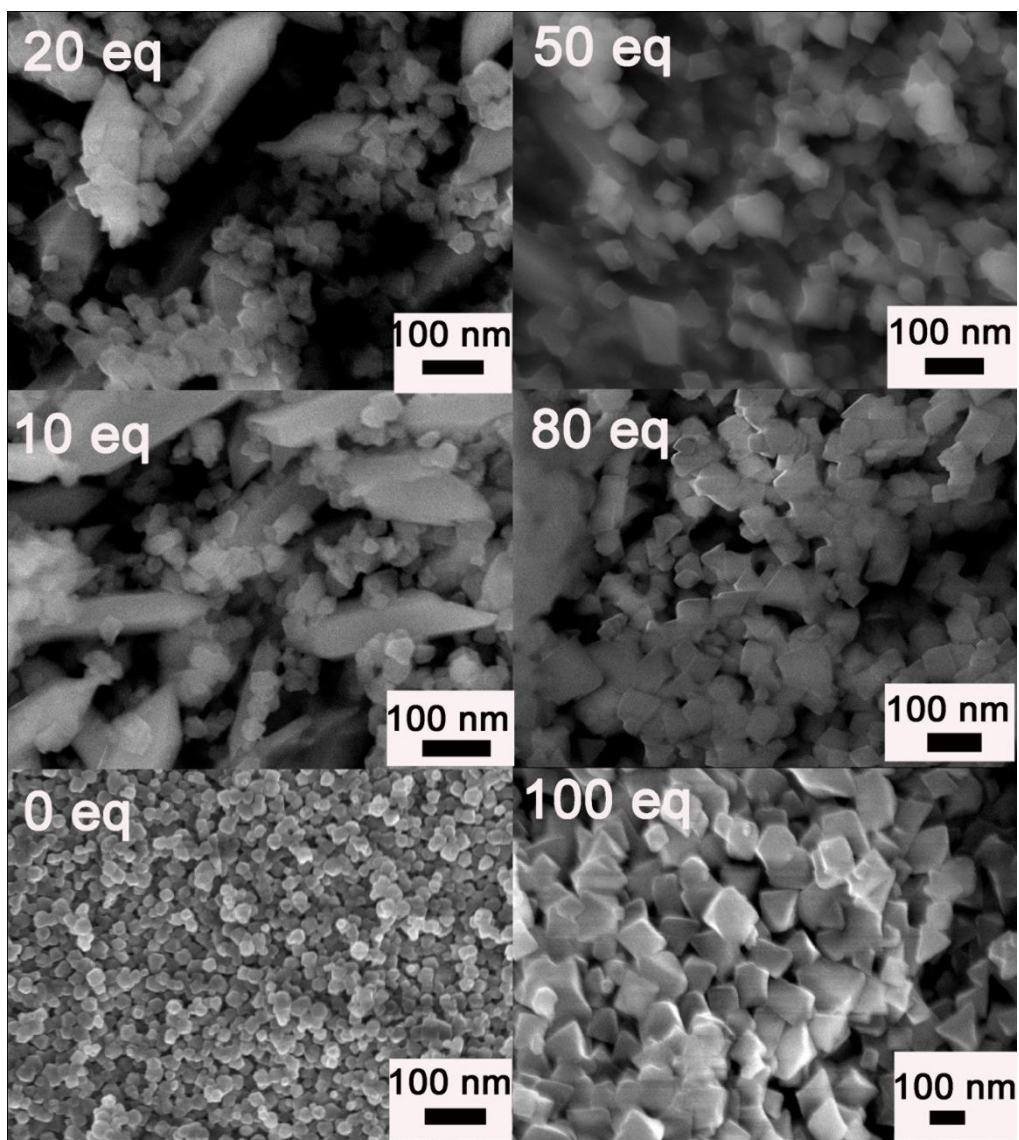


Figure 34: SEM images of Cr-MOF obtained using different modulator equivalents

#### 4.4.1.2 Surface area and pore volume

The nitrogen adsorption isotherm at 77 K for desolvated MIL-101(Cr) powder samples obtained from 0, 50 and 100 eq syntheses were analysed and presented in Figure 36. The observed isotherms were found to be Type IV in nature, which was indicative of a mesoporous structure (Latroche et al. 2006, Férey et al. 2005). Table 12 summarises the physical properties of the desolvated MIL-101(Cr) samples obtained from 0, 50 and 100 eq syntheses. The BET surface area and the pore volumes of the MIL-1010 (Cr) MOF increased as the amount of modulator increased. The measured surface area of  $2618 \text{ m}^2 \cdot \text{g}^{-1}$  for the sample from 100 eq synthesis compared well with those reported in literature of 2691 and  $2454 \text{ m}^2 \cdot \text{g}^{-1}$  and

(Latroche et al. 2006, Férey et al. 2005). Table 12 further shows that the relative crystallinity and skeletal density of Cr-MOF increased with increasing molar ratio of formic acid.

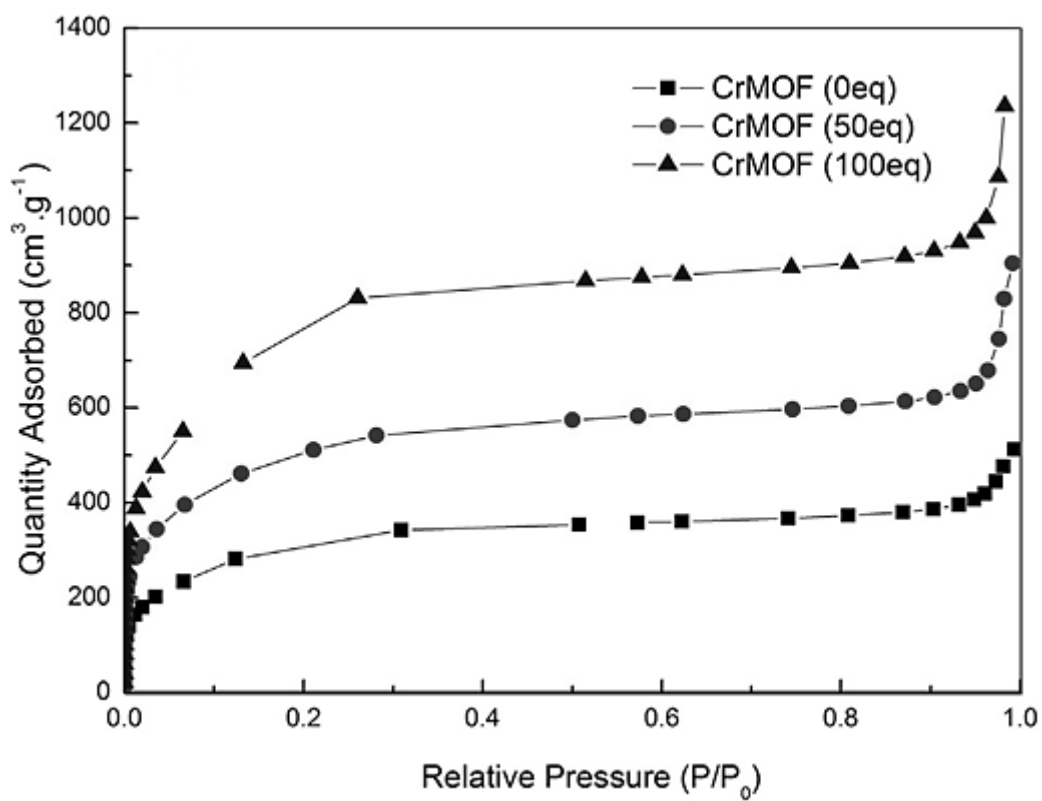


Figure 35: Nitrogen sorption isotherms of 0, 50 and 100 eq Cr-MOF

**Table 12:** Physical properties of the desolvated Cr-MOF (MIL-101) samples

| Sample          | Relative Crystallinity (%) <sup>a</sup> | Density (g·cm <sup>-3</sup> ) <sup>b</sup> | SSA <sub>BET</sub> (m <sup>2</sup> ·g <sup>-1</sup> ) <sup>c</sup> | Pore vol. (cm <sup>3</sup> ·g <sup>-1</sup> ) <sup>d</sup> | Micropore vol. (cm <sup>3</sup> ·g <sup>-1</sup> ) <sup>e</sup> |
|-----------------|---|--|--|--|---|
| MIL-101(0 eq)   | 21                                      | 1.55                                       | 1133.7   | 0.51   | 0.43  |
| MIL-101(50 eq)  | 55                                      | 1.58                                       | 1715.7   | 0.91   | 0.78  |
| MIL-101(100 eq) | 100                                     | 1.6  | 2618.5   | 1.36   | 1.22  |

<sup>a</sup> Calculated relative crystallinity. <sup>b</sup> Determined by pycnometer. <sup>c</sup> BET surface area. <sup>d</sup> From H-K analysis. <sup>e</sup> From H-K analysis.

#### 4.4.2 Effect of synthesis time on the crystallisation of Cr-MOF

Experiments were conducted to investigate the effect of synthesis time in order to find the optimum synthesis time to obtain the best Cr-MOF (MIL-101) crystals without the formation of MIL-53 (another Cr-MOF phase with the formula  $\text{CrO}_8\text{C}_{14}\text{H}_{11}$ ). The synthesis times investigated were 2, 4, 6, 8, 14, 16 and 24 h. In the case of the 2 h reaction, no products were produced. The Cr-MOF crystals were produced only from a minimum synthesis time of 4 h. The Cr-MOF crystals continued to form as the reaction time increased and the best quality crystals were obtained with the reaction time of 8 h as shown by the PXRD patterns and SEM images in Figures 37 and 38.

Beyond a synthesis time of 8 h, the quality of the crystals began to deteriorate. This was attributed to the formation of the more thermodynamically favoured MIL-53 phase. MIL-53 began forming from the 14 h long synthesis and continued to form as more of the Cr-MOF (MIL-101) continued to decompose and was reconstituted as MIL-53. The presence of MIL-53 was confirmed by the disappearance of the peaks at  $2\theta < 8^\circ$ , the increasing intensities of the peak at  $2\theta = 10^\circ$  and the appearance of the peaks at  $2\theta = 14.5^\circ$  and  $14.8^\circ$  in the PXRD patterns of the recovered samples in the 14, 16 and 24 h long reactions. These peaks were also observed by Hong et al. (Zhao, Li & Li 2011). As can be seen from the SEM images in Figure 35 with differing amounts of modulator added, the crystallinity increased and the crystal shape improved as the amount of modulator was increased. The big particles with sizes ranging from 300 to 500 nm in the SEM images shown in Figure 38 are MIL-53 crystals. However, the phase transition from MIL-101 to MIL-53 did not occur by a sudden direct conversion, but rather, it was a successive phase change which occurred with an increase in reaction time. This successive phase change was found to be in accordance with Ostwald's rule of successive phase transformation (Barrer 1982).

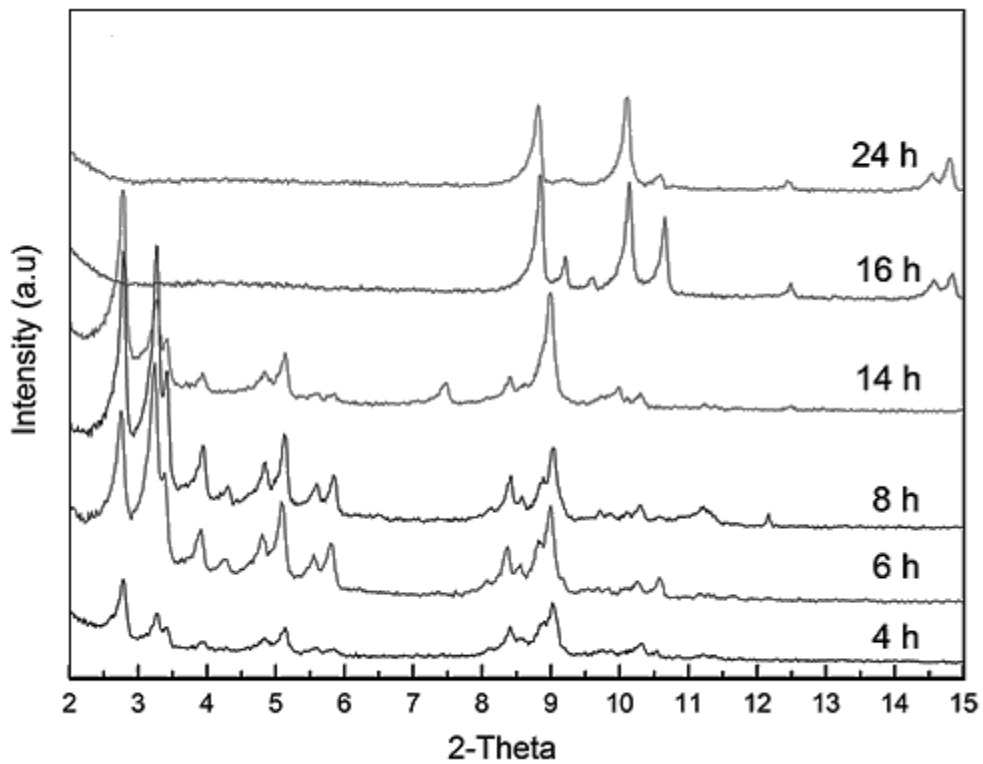


Figure 36: PXRD patterns of Cr-MOF samples obtained in different synthesis times using 100 eq of formic acid

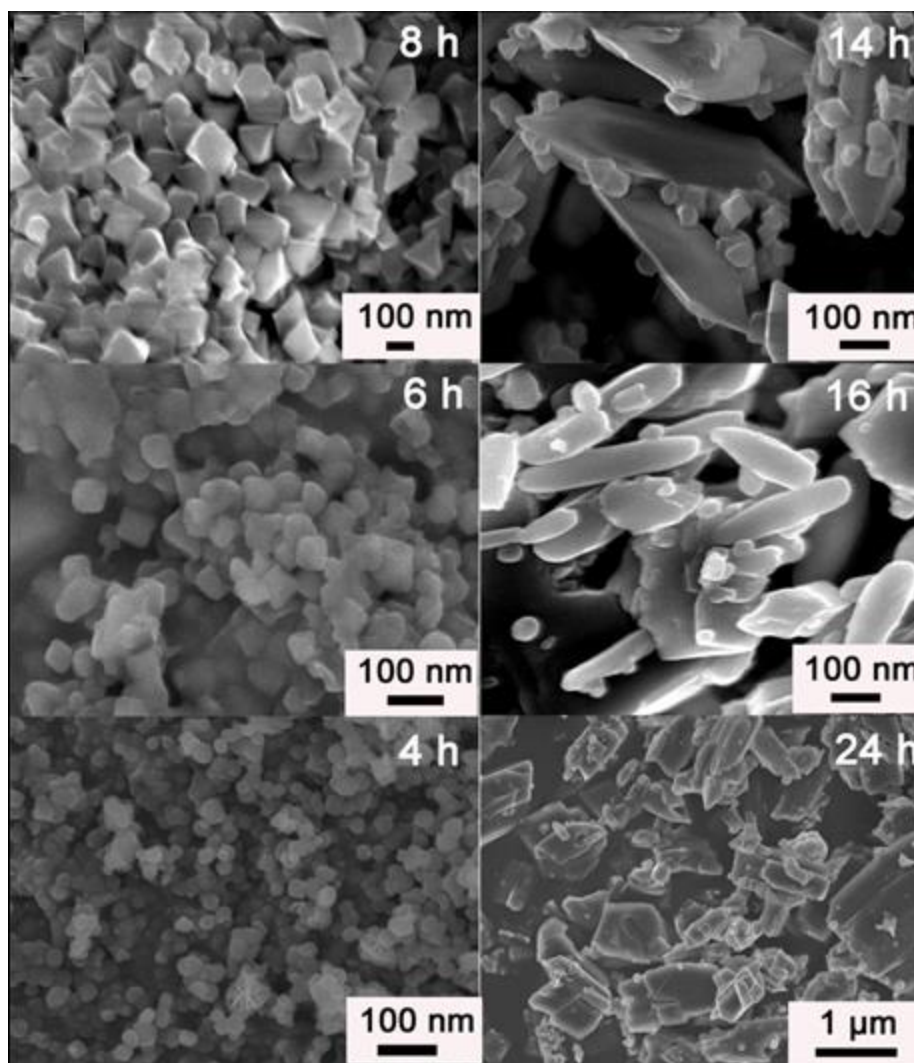


Figure 37: SEM images of Cr-MOF samples obtained in different synthesis times using 100 eq of formic acid

#### 4.4.3 TGA analysis

Figure 39 shows the thermo gravimetric analysis of the modulated Cr-MOF (50 eq and 100 eq) and the non-modulated Cr-MOF. The analysis showed that the mass loss profiles of all the MOFs could be divided into four regions. The first region was from room temperature to around 200 °C. This region showed a continuous mass loss attributed to the removal of all of guest molecules from the pores such as the water solvent and the activation solvent, DMF. The total mass loss for this region was 35%. The second region was between 200 and 350 °C, with a weight loss less continuous than the first stage and was attributed to the removal of residual terephthalic acid after washing with hot DMF. Although the pure Cr-MOF is not clearly

visible due to the residual terephthalic acid, the pure Cr-MOF can be estimated from the onset point of the third region. The third region starts at about 350 °C, with the mass loss about 45%. This indicated that the pure Cr-MOF was 55% of the starting material. The third region was a sharp mass loss which was ascribed to the collapse of the Cr-MOF structure. The total mass loss was about 80%. This region was between 350 and 600 °C and the structural collapse of the MOF was accompanied by the removal of the OH/Cl groups and the benzene from the decomposition of the organic terephthalic linkers (Hong et al. 2009, Valenzano et al. 2011). The fourth and last region was from 600 °C onwards, representing the residual after collapse of the Cr-MOF structure. In subsequent studies on the carbonisation of the Cr-MOF, it was found that the residual consisted of CrO and Cr<sub>3</sub>C<sub>2</sub> (Segakweng et al. 2015 submitted). The total mass loss of the sample was about 85%. The mass loss of the pure Cr-MOF from the start of the second region to the start of the third region was 25% for all the samples. The TGA profiles of all the Cr-MOFs were very similar and agreed very well with that reported by Yang et al. (Yang et al. 2010) for MIL-101. This data showed that the synthesised Cr-MOF was stable up to 350 °C. The sample with 100 eq of modulator and with a synthesis time of 8 h was found to have the best characteristics in terms of the morphology, crystallinity and gas adsorption. This synthesis was therefore deemed to be the optimum.

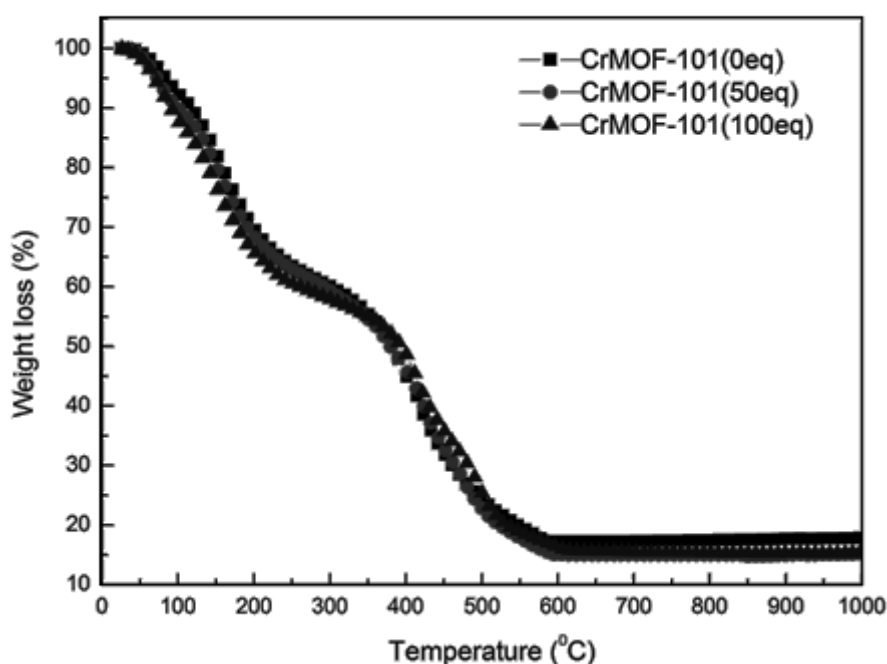


Figure 38 : TGA mass loss analysis of 0, 50, and 100 eq Cr-MOF

#### 4.4.4 Optimised Cr-MOF synthesis

An optimised synthesis for Cr-MOF samples was achieved based on the data collected from the experiments with the results discussed above in section 4.4. The optimised synthesis is presented below in Table 13 in terms of the optimal condition of each variable which was investigated.

**Table13:** Optimised variables for the synthesis of Cr-MOF

| Variables       | Condition        | CrCl <sub>3</sub> .6H <sub>2</sub> O<br>(mmol) | H <sub>2</sub> BDC<br>(mmol) | ZrCl <sub>4</sub> /H <sub>2</sub> BDC<br>(mol) |
|-----------------|------------------|--|------------------------------|--|
| Solvent         | H <sub>2</sub> O | 5  | 5                            | 1  |
| Stirring        | No               | 5  | 5                            | 1  |
| Temperature     | 210 °C           | 5  | 5                            | 1  |
| Reaction Time   | 8 h              | 5  | 5                            | 1  |
| Modulator ratio | 100 eq           | 5  | 5                            | 1  |

#### 4.5 Hydrogen storage studies

This section reports the hydrogen adsorption results of the synthesised MOF materials. All measurements were performed at 77 K and pressures up to 1 bar due to the pressure limitation of the instrument available that was used in this study. At pressures below 1 bar, several factors affect the hydrogen adsorption of MOF materials. At these pressures, hydrogen adsorbs by binding on sites that have a high affinity for hydrogen and factors such as open metal sites, pore size, catenation and surface area influence the hydrogen capacity of the MOFs. At 77 K and 1 bar, hydrogen uptake occurs by physisorption and is completely reversible although for this work, only the adsorption curve is shown..

##### 4.5.1 Hydrogen adsorption isotherms of MOF-5

The hydrogen adsorption isotherms for the desolvated MOF-5 sample that was synthesised in DEF and that which was synthesised in DMF were recorded at 77 K and a pressure up to 1 bar

and are presented in Figures 39 and 40. The MOF-5 sample obtained using DEF as the solvent showed a maximum hydrogen storage capacity of 1.6 wt%, and the sample obtained using DMF as the solvent had a capacity of 1.4 wt%. These values are comparable to values reported by Yaghi et al (Rosi et al. 2003, Rowsell & Yaghi 2005) for MOF-5 that was synthesised using DEF and DMF as solvents, respectively. The increased hydrogen storage capacity of the sample obtained from DEF is due to the higher crystallinity and larger surface area ( $2662 \text{ m}^2 \cdot \text{g}^{-1}$ ) of the sample (section 4.2.1.2). In addition, the DEF synthesised MOF-5 had a higher proportion of micropores than the DMF synthesised MOF-5, this favored hydrogen adsorption.

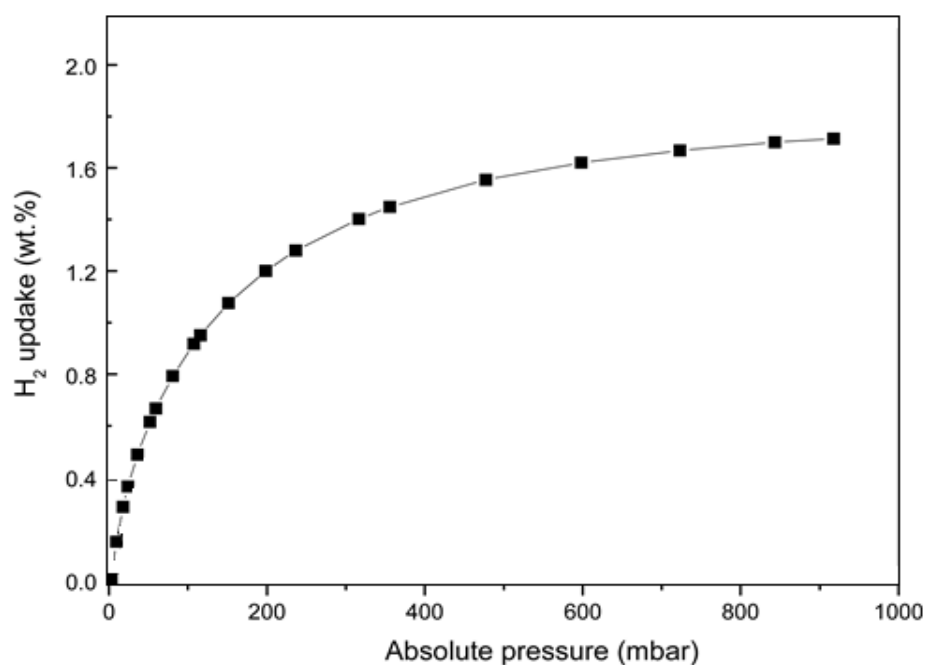


Figure 39: Hydrogen adsorption of MOF-5 synthesised in DEF obtained at 77 K and up to 1 bar

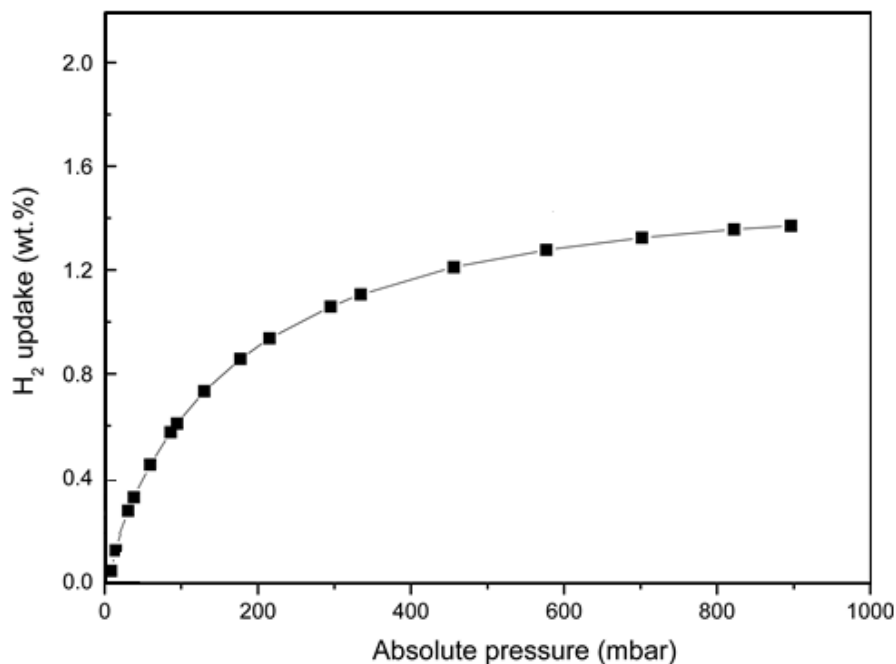


Figure 40: Hydrogen adsorption of MOF-5 synthesised in DMF obtained at 77 K and up to 1 bar

#### 4.5.2 Hydrogen adsorption isotherms of MOF-69c and transitioned MOF-5

The hydrogen adsorption isotherms for the obtained products measured at 77 K and pressure up to 1 bar are shown in Figure 41. The obtained samples A, C, F showed hydrogen storage capacities of 1.9, 1.6 and 1.4 wt%, respectively. The results correspond well with a successful transition from MOF-69c to MOF-5. The decrease in hydrogen storage capacity also corresponds with the change in pore size and pore volume from MOF-69c to MOF-5 (Table 8 in section 4.2.5.2). An increase in pore diameter and a decrease in pore volume during the transition from MOF-69c to MOF-5 resulted in a reduced hydrogen uptake. The prepared sample of MOF-69c (sample A) had the largest pore volume ( $0.44 \text{ cm}^3 \cdot \text{g}^{-1}$ ) and specific surface area ( $1186 \text{ m}^2 \cdot \text{g}^{-1}$ ) and thus highest storage capacity. The hydrogen storage capacity of 1.4 wt% obtained for MOF-5 (sample F) was the same as that recorded in the direct MOF-5 synthesis and is comparable to the value reported by Yaghi et al. (Rowell & Yaghi 2005). The amount of hydrogen stored in all three samples increased as the surface area increased.

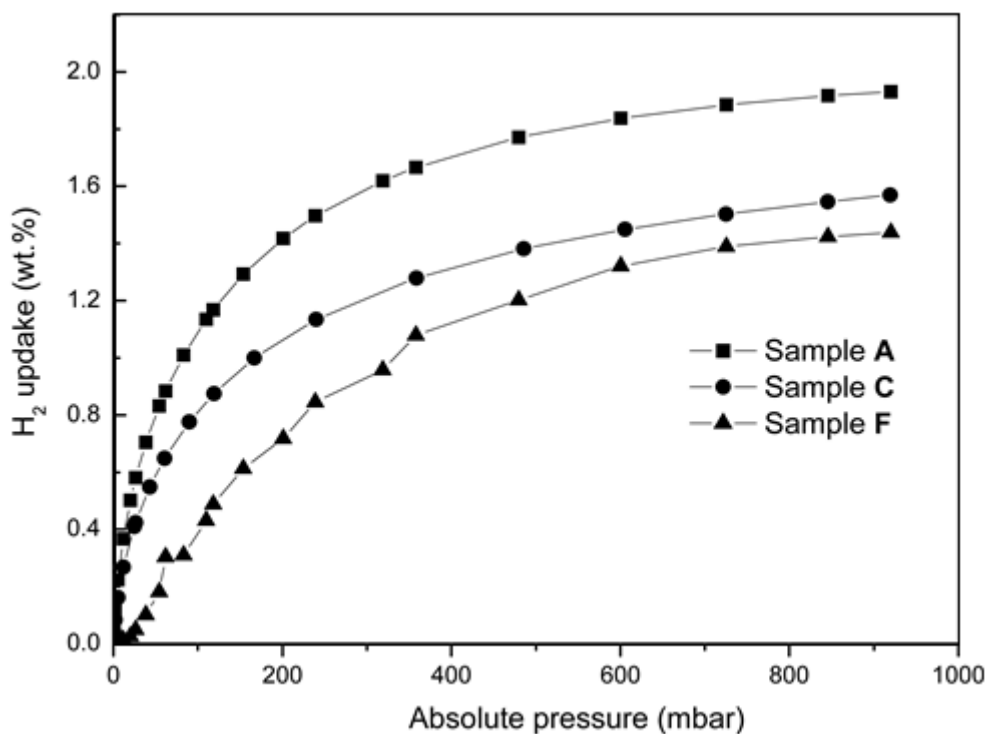


Figure 41: Hydrogen uptake isotherms for MOF-5 and MOF-69c samples

### 4.5.3 Hydrogen adsorption isotherms of Zr-MOF

The hydrogen adsorption isotherms measured at 77 K and up to 1 bar for the desolvated Zr-MOF samples from 0, 10 and 100 eq syntheses are presented in Figure 42. The hydrogen storage capacity of the non-modulated Zr-MOF was found to be 0.3 wt% which is quite low when compared to the hydrogen storage capacity recorded for the Zr-MOFs from modulated synthesis (1.1 and 1.5 wt%). The non-modulated Zr-MOF also reached saturation below 1 bar whilst the modulated Zr-MOF sample steep increase up to a pressure of 1 bar but did not reach saturation, this serves as an indication that at higher pressures, the samples would adsorb more hydrogen. The hydrogen storage capacity of 1.1 wt% for Zr-MOF (10 eq) sample compares quite well with the value in a patent reported by Hafizovic et al. (Hafizovic et al. 2014), measured in the same manner. Due to the direct relationship between hydrogen capacity and the specific surface area of materials under cryogenic conditions and ambient pressure, the modulated Zr-MOF using 100 eq modulator was found to have the highest hydrogen storage capacity of 1.5 wt%, which results from its better crystallinity and higher surface area. As shown in Table 10 in section 4.3.1., the specific surface area and pore volumes of the modulated Zr-MOF increased as the amount of modulator added was increased.

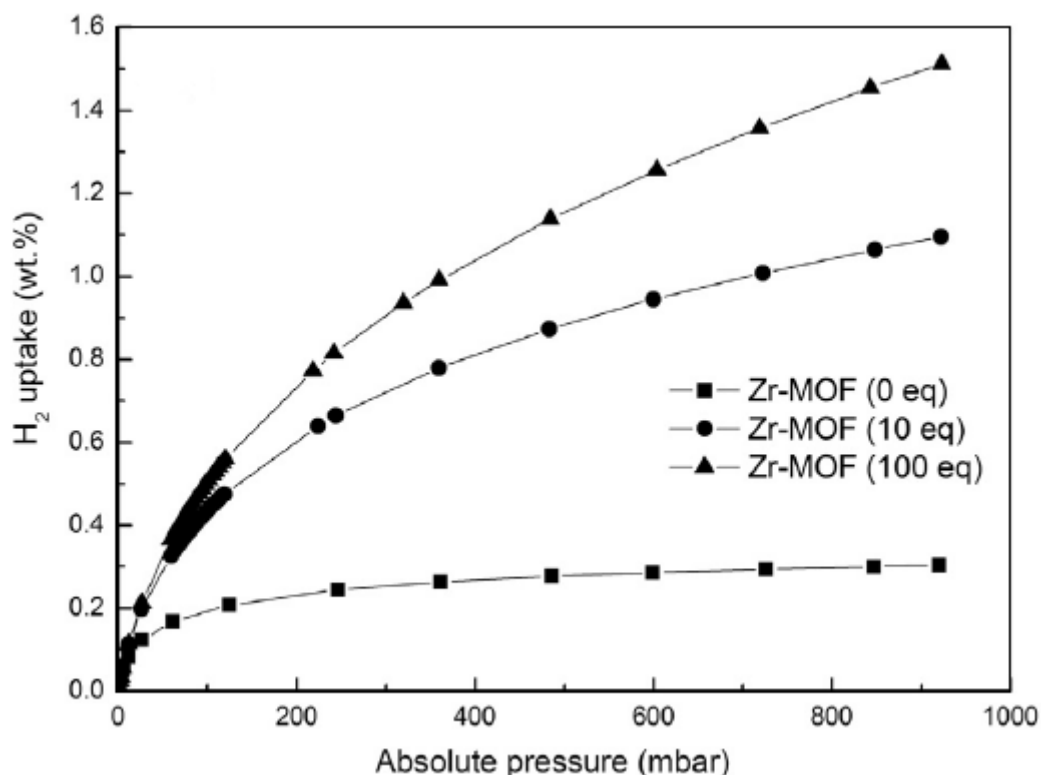


Figure 42: Hydrogen uptake isotherms for Zr-MOF (UiO-66) obtained at 77 K and up to 1 bar

#### 4.5.4 Hydrogen adsorption isotherms of microwave-assisted Zr-MOF

The hydrogen adsorption isotherms for the desolvated Zr-MOF from both the oil bath and the microwave-assisted synthesis are presented in Figure 43. The hydrogen storage capacity of the sample synthesised using the oil bath was found to be 1.5 wt%, which is among the highest values reported in the literature papers listed in Table 10. Under the same conditions, the microwave-assisted Zr-MOF was found to have a hydrogen storage capacity of 1.26 wt% which is in agreement with the lower values reported in the literature. The higher hydrogen storage capacity for the oil bath synthesised Zr-MOF sample was as a result of its higher specific surface area and multiple pore sizes in the microporous range (see section 4.3.4.2 and Figure 32). Both samples showed a steep increase up to a pressure of 1 bar but did not reach saturation. These results demonstrated that although the microwave-assisted modulated synthesis method generated Zr-MOFs with good morphology within a relatively short reaction time of 5 min, it had a smaller surface area than the sample that was synthesised using the oil bath. This ultimately resulted in it having a lower hydrogen storage capacity. This supports the

direct relationship between hydrogen storage capacity and the specific surface area that was found to exist at 77 K and approximately 1 bar for these MOF materials. The hydrogen storage capacities obtained in this work correlated very well with the BET surface areas of the Zr-MOFs.

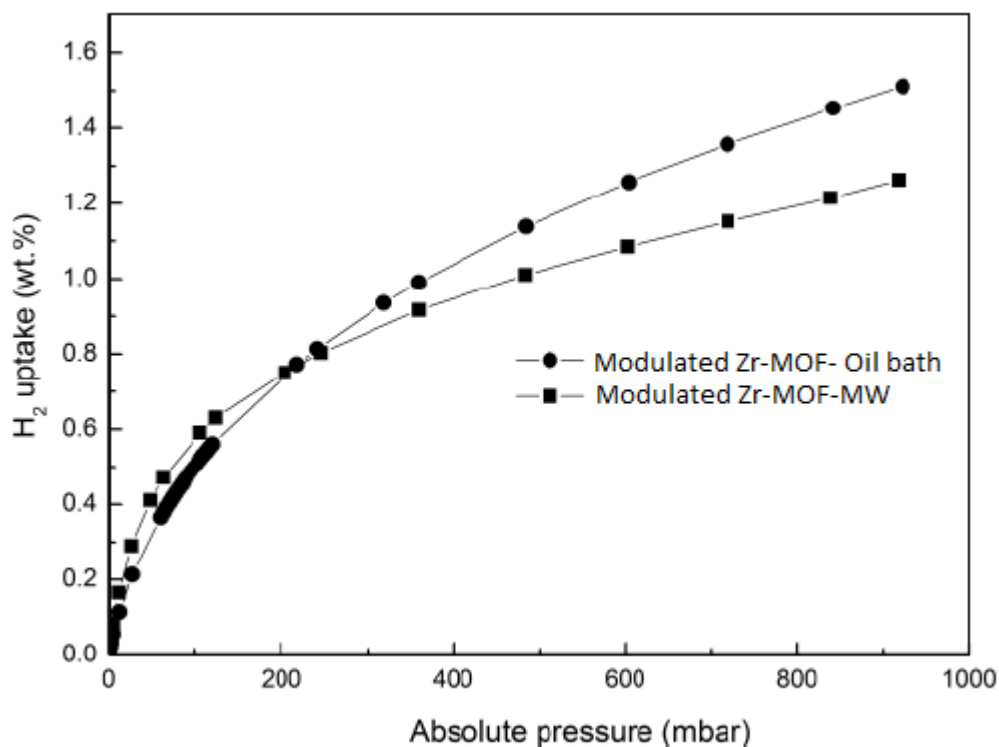


Figure 43: Hydrogen uptake isotherms for Zr-MOF from the microwave and oil bath synthesis.

#### 4.5.5 Hydrogen adsorption isotherms of solvothermal Cr-MOF

The hydrogen adsorption isotherms for the desolvated Cr-MOF (MIL-101) samples from 0, 50 and 100 eq syntheses are presented in Figure 44. The hydrogen adsorption isotherms for all the Cr-MOF samples showed a steep increase up to a pressure of 1 bar but did not reach saturation. This indicated that the Cr-MOFs had the potential to store more hydrogen at higher pressures. The non-modulated Cr-MOF had a hydrogen storage capacity of 0.99 wt%. Upon addition of 50 eq of the modulator (formic acid), this value was nearly doubled to a value of 1.65 wt%. With further additions of formic acid, the hydrogen uptake increased to a final value of 1.9 wt% for the addition of 100 eq of formic acid. This increase in hydrogen uptake corresponded well with the increasing surface area values found for the increased additions of formic acid (see section 4.4.1.2 and Table 12), confirming the direct relationship

between specific surface area and hydrogen uptake as discussed earlier. The value of 1.9 wt% for hydrogen storage capacity from this study fits well in the sorption curve plotted by Yang et al. (Yang et al. 2010) at 77 K and pressure of up to 10 bar.

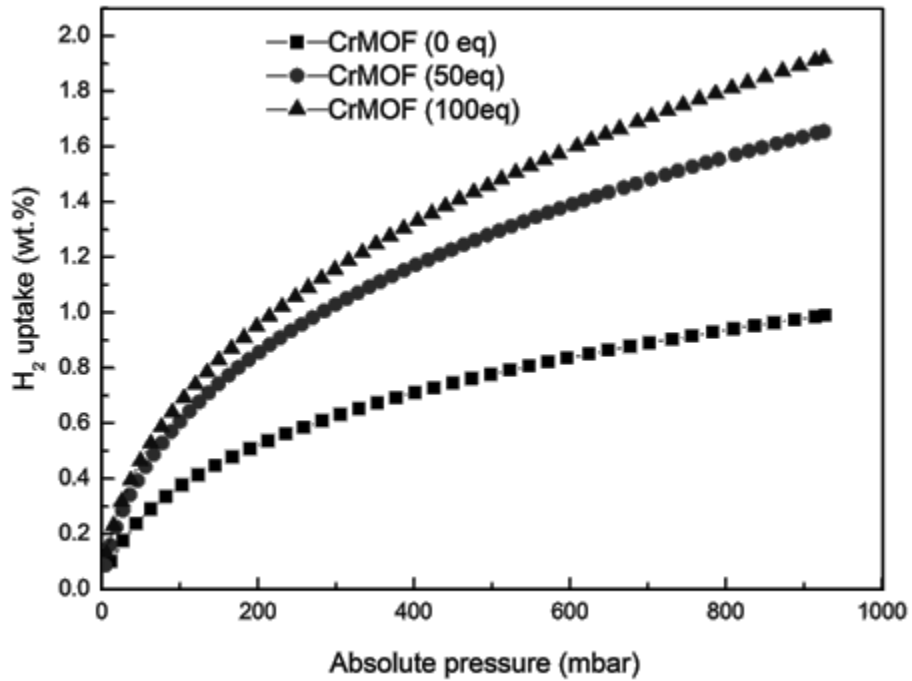


Figure 44: Hydrogen uptake isotherms for Cr-MOF (MIL-101) samples.

## Chapter 5

### Conclusions

The study has shown that MOFs do indeed store substantial amounts of hydrogen at cryogenic temperatures and possess the potential to store hydrogen at conditions that could possibly approach the US DOE 2017 targets. This is due to their highly porous nature and their ability to be modified. Not only can the storage targets, but also cost and environmental safety targets, possibly be met. The synthesis of the MOFs investigated was optimised and as a result, a small yet significant step was made towards achieving the 2017 targets. The use of solvents and modulators, that are more environmentally friendly, can help make the synthesis more cost effective. Furthermore, the use of a modulator shortens the reaction time, which also saves cost.

This study showed that a simple variation in the synthesis of the MOFs was able to have a significant effect on the storage properties of the MOFs, and enable a fast and reproducible synthesis method.

The optimum synthesis conditions for preparing MOF-5 using DMF as a solvent was found to be when the temperature was raised from 130 °C, as done by BASF, to 140 °C with a reaction time of 4 h, yielding significantly pure products with good morphology, high crystallinity and good hydrogen storage capacity. The required molar ratio of the terephthalic acid to zinc nitrate was found to be 1:2.63 with no other reagents needed. This optimised synthesis resulted in a maximum hydrogen adsorption of the DMF synthesised MOF-5, which was comparable and sometimes higher the reported literature values. A maximum hydrogen uptake of 1.4 wt% was achieved for the DMF synthesised MOF-5 at 77 K and pressure up to 1 bar.

The accidental stumble upon MOF-69c during the synthesis of MOF-5 was beneficial in that it helped in getting crystals with good morphology. It was found that MOF-69c could be transformed to MOF-5 via a simple thermal treatment without the addition of any chemicals.

The moisture sensitivity of MOF-5, as a result of the Zn-O bonds being attacked by atmospheric water, was encountered. Hence there was a need to find a MOF with a metal centre that formed a stronger bond with an oxygen atom within the framework. The solution was found in the form of another MOF, Zr-MOF (UiO-66). This MOF was successfully

synthesised using a modulated solvothermal approach and microwave-assisted synthesis. UiO-66 was synthesised using equimolar reagents and it was found that the best characterisation and adsorption results were obtained when using 100 equivalents of the formic acid modulator. A maximum hydrogen uptake of 1.5 wt% at 77 K and pressure up to 1 bar was achieved for the Zr- MOF, synthesised using the modulated solvothermal approach.

A main drawback of Zr-based MOFs is that they require DMF as a solvent in the synthesis, this solvent presents an environmental concern. It was through investigating possible MOFs that utilize more environmentally safe solvents that decided to work with Cr-MOF and measure its hydrogen adsorption. Using water as a solvent is also a cost saving measure. Although this MOF was not studied extensively for hydrogen storage, it possesses desirable characteristics for hydrogen storage. Cr-MOF, otherwise known as MIL-101, was successfully synthesised via a modulated hydrothermal synthesis with formic acid as the modulator. MIL-101 had relatively high surface area and hydrogen uptake. MIL-101 was synthesised using equimolar reagents and it was found that the best characterisation and adsorption results were obtained using 100 equivalents of formic acid as modulator. A maximum hydrogen uptake of 1.9 wt% was achieved for MIL-101 at 77 K and pressure up to 1 bar.

Although a considerable amount of work has been done so far on the MOFs synthesised, there is still a lot more to do before the goal of successful hydrogen storage in MOFs for practical applications can be realised. Amongst these is the evaluation of the hydrogen uptake of these MOFs at higher pressures and at room temperature.

Furthermore, post-synthetic modification of the synthesised MOFs needs to be investigated to optimise the hydrogen uptake of these MOFs at both cryogenic and elevated temperatures.

Another key step to investigating the hydrogen storage properties of the MOFs is to gain a better understanding of the interaction between hydrogen and MOFs themselves. This will require synthesising single crystals of these MOFs and using neutron diffraction to study the position of the hydrogen within the pores.

## References

- Abid, H.R., Tian, H., Ang, H., Tade, M.O., Buckley, C.E. and Wang, S. (2012) "Nanosize Zr-metal organic framework (UiO-66) for hydrogen and carbon dioxide storage" *Chemical Engineering Journal*, 187: 415-420.
- Bae, Y. and Snurr, R.Q. (2010), "Optimal isosteric heat of adsorption for hydrogen storage and delivery using metal-organic frameworks", *Microporous and Mesoporous Materials*, 132(1), 300-303.
- Bárcia, P.S., Guimarães, D., Mendes, P.A.P., Silva, J.A.C., Guillerm, V., Chevreau, H., Serre, C. and Rodrigues, A.E. (2011) "Reverse shape selectivity in the adsorption of hexane and xylene isomers in MOF UiO-66" *Microporous and Mesoporous Materials*, 139(1-3), 67-73.
- Barrer, R.M. (1982), *Hydrothermal chemistry of zeolites*, Academic Press, London.
- Canivet, J., Fateeva, A., Guo, Y., Coasne, B. and Farrusseng, D. (2014), "Water adsorption in MOFs: fundamentals and applications", *Chemical Society Reviews*, 43(16), 5594-5617.
- Chae, H.K., Siberio-Pérez, D.Y., Kim, J., Go, Y., Eddaoudi, M., Matzger, A.J., O'Keeffe, M. and Yaghi, O.M. (2004) "A route to high surface area, porosity and inclusion of large molecules in crystals" *Nature*, 427 (6974), 523-527.
- Chen, B., Eddaoudi, M., Hyde, S.T., O'Keeffe, M. and Yaghi, O.M. (2001) "Interwoven metal-organic framework on a periodic minimal surface with extra-large pores" *Science*, 291(5506), 1021-1023.
- Cheon, Y.E. and Suh, M.P. (2009) "Enhanced Hydrogen Storage by Palladium Nanoparticles Fabricated in a Redox-Active Metal-Organic Framework" *Angewandte Chemie International Edition*, 48(16), 2899-2903.
- Czaja, A., Trukhanb, N. and Ulrich, M. (2009) "Industrial applications of metal-organic frameworks" *Chemical Society reviews*, 38(5), 1284-1293.

- Dey, C., Kundu, T., Biswal, B.P., Mallick, A. and Banerjee, R. (2013) "Crystalline metal-organic frameworks (MOFs): synthesis, structure and function" *Acta Crystallographica Section B: Structural Science, Crystal Engineering and Materials*, 70(1), 3-10.
- Dharmarathna, S., King'onde, C.K., Pedrick, W., Pahalagedara, L. and Suib, S.L. (2012) "Direct sonochemical synthesis of manganese octahedral molecular sieve (OMS-2) nanomaterials using cosolvent systems, their characterization, and catalytic applications", *Chemistry of Materials*, 24(4), 705-712.
- Dinca, M. and Long, J.R. (2005) "Strong H<sub>2</sub> binding and selective gas adsorption within the microporous coordination solid Mg<sub>3</sub>(O<sub>2</sub>C-C<sub>10</sub>H<sub>6</sub>-CO<sub>2</sub>)<sub>3</sub>" *Journal of the American Chemical Society*, 127(26), 9376-9377.
- Dueren, T., Millange, F., Férey, G., Walton, K.S. and Snurr, R.Q. (2007) "Calculating Geometric Surface Areas as a Characterization Tool for Metal-Organic Frameworks" *Journal of Physical Chemistry*, 111(42), 15350-15356
- Férey, G., Latroche, M., Serre, C., Millange, F., Loiseau, T. and Percheron-Guégan, A. (2003) "Hydrogen adsorption in the nanoporous metal-benzenedicarboxylate M(OH)(O<sub>2</sub>C-C<sub>6</sub>H<sub>4</sub>-CO<sub>2</sub>)(M= Al<sub>3</sub>, Cr<sub>3</sub>), MIL-53" *Chemical communications*, 24, 2976-2977.
- Férey, G., Mellot-Draznieks, C., Serre, C., Millange, F., Dutour, J., Surblé, S. and Margiolaki, I. (2005) "A Chromium Terephthalate-Based Solid with Unusually Large Pore Volumes and Surface Area" *Science*, 309(5743), 2040-2042.
- Furukawa, H., Cordova, K.E., O'Keeffe, M. and Yaghi, O.M. (2013) "The chemistry and applications of metal-organic frameworks" *Science (New York, N.Y.)*, 341(6149), 1230444.
- Furukawa, H., Ko, N., Go, Y.B., Aratani, N., Choi, S.B., Choi, E., Yazaydin, A.Ö., Snurr, R.Q., O'Keeffe, M., Kim, J. and Yaghi, O.M. (2010) "Ultrahigh Porosity in Metal-Organic Frameworks" *Science*, 329(5990), 424-428.
- Gedrich, K., Senkowska, I., Klein, N., Stoeck, U., Henschel, A., Lohe, M.R., Baburin, I.A., Mueller, U. and Kaskel, S. (2010) "A highly porous metal-organic framework with open nickel sites" *Angewandte Chemie - International Edition*, 49(45), 8489-8492.

- Grochala, W. and Edwards, P.P. (2004) "Thermal decomposition of the non-interstitial hydrides for the storage and production of hydrogen" *Chemical reviews*, 104(3), 1283-1316.
- Hafizovic, J., Olsbye, U., Lillerud, K.P., Jakobsen, S. and Guillou, N. (2013) "*Metal organic framework compounds.*" *U.S. Patent 20140322123 assigned to University of Oslo, NOR.*
- Halder, G.J., Kepert, C.J., Moubaraki, B., Murray, K.S. and Cashion, J.D. (2002) "Guest-dependent spin crossover in a nanoporous molecular framework material" *Science (New York, N.Y.)*, 298(5599), 1762-1765.
- Hausdorf, S., Wagler, J., Moßig, R. and Mertens, F.O. (2008) "Proton and water activity-controlled structure formation in zinc carboxylate-based metal organic frameworks" *The Journal of Physical Chemistry A*, 112(33), 7567-7576.
- Henschel, A., Gedrich, K., Kraehnert, R. and Kaskel, S. (2008) "Catalytic properties of MIL-101" *Chemical Communications*, (35), 4192-4194.
- Hong, D., Hwang, Y.K., Serre, C., Férey, G. and Chang, J. (2009) "Porous Chromium Terephthalate MIL-101 with Coordinatively Unsaturated Sites: Surface Functionalization, Encapsulation, Sorption and Catalysis" *Advanced Functional Materials*, 19(10), 1537-1552.
- Huang, L., Wang, H., Chen, J., Wang, Z., Sun, J., Zhao, D. and Yan, Y. (2003) "Synthesis, morphology control, and properties of porous metal–organic coordination polymers" *Microporous and mesoporous materials*, 58(2), 105-114.
- Jhung, S.H., Lee, J., Yoon, J.W., Serre, C., Férey, G. and Chang, J. (2007) "Microwave Synthesis of Chromium Terephthalate MIL-101 and Its Benzene Sorption Ability" *Advanced Materials*, 19(1), 121-124.
- Kaye, S.S., Dailly, A., Yaghi, O.M. and Long, J.R. (2007) "Impact of preparation and handling on the hydrogen storage properties of Zn<sub>4</sub>O(1,4-benzenedicarboxylate)<sub>3</sub> (MOF-5)" *Journal of the American Chemical Society*, 129(46), 14176-14177.

- Khan, A., Kuek, C., Chaudhry, T., Khoo, C. and Hayes, W. (2000) "Role of plants, mycorrhizae and phytochelators in heavy metal contaminated land remediation" *Chemosphere*, 41(1), 197-207.
- Kondo, M., Yoshitomi, T., Matsuzaka, H., Kitagawa, S. and Seki, K. (1997) "Three-Dimensional Framework with Channeling Cavities for Small Molecules:  $\{[M_2(4,4'\text{-bpy})_3(\text{NO}_3)_4] \cdot x\text{H}_2\text{O}\}_n$  (M= Co, Ni, Zn)" *Angewandte Chemie International Edition in English*, 36(16), 1725-1727.
- Kubota, Y., Takata, M., Matsuda, R., Kitaura, R., Kitagawa, S., Kato, K., Sakata, M. and Kobayashi, T.C. (2005) "Direct observation of hydrogen molecules adsorbed onto a microporous coordination polymer", *Angewandte Chemie International Edition*, 44(6), 920-923.
- Langmi, H.W., Ren, J., North, B., Mathe, M. and Bessarabov, D. (2014) "Hydrogen Storage in Metal-Organic Frameworks: A Review" *Electrochimica Acta*, 128, 368-392.
- Latroche, M., Surblé, S., Serre, C., Mellot-Draznieks, C., Llewellyn, P.L., Lee, J.H., Chang, J.S., Sung, H.J. and Férey, G. (2006) "Hydrogen storage in the giant-pore metal-organic frameworks MIL-100 and MIL-101" *Angewandte Chemie - International Edition*, 45(48), 8227-8231.
- Lebedev, O., Millange, F., Serre, C., Van Tendeloo, G. and Férey, G. (2005) "First direct imaging of giant pores of the metal-organic framework MIL-101", *Chemistry of materials*, 17(26), 6525-6527.
- Li, Z., Zhang, M., Liu, B., Guo, C. and Zhou, M. (2013) "Rapid fabrication of metal-organic framework thin films using in situ microwave irradiation and its photocatalytic property", *Inorganic Chemistry Communications*, 36, 241-244.
- Li, H., Eddaoudi, M., O'Keeffe, M. and Yaghi, O.M. (1999) "Design and synthesis of an exceptionally stable and highly porous metal-organic framework" *Nature*, 402(6759), 276-279.

- Liao, J., Lee, T. and Su, C. (2006) "Synthesis and characterization of a porous coordination polymer,  $Zn_5(OH)_4(BDC)_3 \cdot 2DMF$  (DMF= N, N-dimethylformamide)" *Inorganic Chemistry Communications*, 9(2), 201-204.
- Lin, X., Telepeni, I., Blake, A.J., Dailly, A., Brown, C.M., Simmons, J.M., Zoppi, M., Walker, G.S., Thomas, K.M., Mays, T.J., Hubberstey, P., Champness, N.R. and Schröder, M. (2009) "High capacity hydrogen adsorption in Cu(II) tetracarboxylate framework materials: The role of pore size, ligand functionalization, and exposed metal sites" *Journal of the American Chemical Society*, 131(6), 2159-2171.
- Liu, Y., Eubank, J.F., Cairns, A.J., Eckert, J., Kravtsov, V.C., Luebke, R. and Eddaoudi, M. (2007) "Assembly of Metal-Organic Frameworks (MOFs) based on indium-trimer building blocks: A porous MOF with soc topology and high hydrogen storage" *Angewandte Chemie - International Edition*, 46(18), 3278-3283.
- Loiseau, T., Muguerra, H., Férey, G., Haouas, M. and Taulelle, F. (2005) "Synthesis and structural characterization of a new open-framework zinc terephthalate  $Zn_3(OH)_2(bdc)_2 \cdot 2DEF$ , with infinite Zn-( $\mu_3$ -OH)-Zn chains" *Journal of solid state chemistry*, 178(3), 621-628.
- Lowell, S., Shields, J.E., Thomas, M.A. and Thommes, M. (2010) "*Characterization of Porous Solids and Powders Surface Area, Pore Size and Density*".
- M. Schubert, U. Müller and H. Mattenheimer, (2007) *M. Schubert, U. Müller and H. Mattenheimer, Patent, WO 2007090864 A1, 2007.*
- Ma, L., Abney, C. and Lin, W. (2009) "Enantioselective catalysis with homochiral metal-organic frameworks", *Chemical Society Reviews*, 38(5), 1248-1256.
- Ma, S. and Zhou, H. (2010) "Gas storage in porous metal-organic frameworks for clean energy applications" *Chemical Communications*, 46(1), 44-53.
- Maksimchuk, N.V., Zalomaeva, O.V., Skobelev, I.Y., Kovalenko, K.A., Fedin, V.P. and Kholdeeva, O.A. (2012) "Metal-organic frameworks of the MIL-101 family as heterogeneous single-site catalysts" *Proceedings of the Royal Society A: Mathematical, Physical and Engineering Science*, , pp. rspa20120072.

- Marsh, H. (1987), "Adsorption methods to study microporosity in coals and carbons - a critique" *Carbon*, 25(1), 49-58.
- Mines, G.A., Tzeng, B., Stevenson, K.J., Li, J. and Hupp, J.T. (2002) "Microporous supramolecular coordination compounds as chemosensory photonic lattices" *Angewandte Chemie*, 114(1), 162-165.
- Mondloch, J.E., Karagiari, O., Farha, O.K. and Hupp, J.T. (2013) "Activation of metal-organic framework materials" *Cryst Eng Comm*, 15(45), 9258-9264.
- Mueller, U., Schubert, M., Teich, F., Puetter, H., Schierle-Arndt, K. and Pastre, J. (2006) "Metal-organic frameworks—prospective industrial applications" *Journal of Materials Chemistry*, 16(7), 626-636.
- Mulfort, K.L. and Hupp, J.T. (2008) "Alkali metal cation effects on hydrogen uptake and binding in metal-organic frameworks" *Inorganic chemistry*, 47(18), 7936-7938.
- Murray, L.J., Dincă, M. and Long, J.R. (2009) "Hydrogen storage in metal-organic frameworks" *Chemical Society Reviews*, 38(5), 1294-1314.
- Nelson, A.P., Farha, O.K., Mulfort, K.L. and Hupp, J.T. (2008) "Supercritical processing as a route to high internal surface areas and permanent microporosity in metal-organic framework materials" *Journal of the American Chemical Society*, 131(2), 458-460.
- Nouar, F., Eckert, J., Eubank, J.F., Forster, P. and Eddaoudi, M. (2009) "Zeolite-like metal-organic frameworks (ZMOFs) as hydrogen storage platform: Lithium and magnesium ion-exchange and H-(rho-ZMOF) interaction studies" *Journal of the American Chemical Society*, 131(8), 2864-2870.
- Oh, H., Lupu, D., Blanita, G. and Hirscher, M. (2014) "Experimental assessment of physical upper limit for hydrogen storage capacity at 20 K in densified MIL-101 monoliths", *RSC Advances*, 4(6), 2648-2651.
- Panella, B., Hirscher, M., Pütter, H. and Müller, U. (2006) "Hydrogen Adsorption in Metal-Organic Frameworks: Cu-MOFs and Zn-MOFs Compared" *Advanced Functional Materials*, 16(4), 520-524.

- Perles, J., Iglesias, M., Martín-Luengo, M., Monge, M.A., Ruiz-Valero, C. and Snejko, N. (2005) "Metal-organic scandium framework: Useful material for hydrogen storage and catalysis" *Chemistry of Materials*, 17(23), 5837-5842.
- Pichon, A., Lazuen-Garay, A. and James, S.L. (2006) "Solvent-free synthesis of a microporous metal-organic framework" *CrystEngComm*, 8(3), 211-214.
- Ren, J., Musyoka, N.M., Langmi, H.W., Segakweng, T., North, B.C., Mathe, M. and Kang, X. (2014a) "Modulated synthesis of chromium-based metal-organic framework (MIL-101) with enhanced hydrogen uptake" *International Journal of Hydrogen Energy*, 39(23), 12018-12023.
- Ren, J., Rogers, D.E., Segakweng, T., Langmi, H.W., North, B.C., Mathe, M. and Bessarabov, D. (2014b) "Thermal treatment induced transition from  $Zn_3(OH)_2(BDC)_2$  (MOF-69c) to  $Zn_4O(BDC)_3$  (MOF-5)", *International Journal of Materials Research*, 105(1), 89-93.
- Ren, J., Segakweng, T., Langmi, H.W., North, B.C. and Mathe, M. (2015), "Ni foam-immobilized MIL-101 (Cr) nanocrystals toward system integration for hydrogen storage", *Journal of Alloys and Compounds*, 645(1), 170-173.
- Rosi, N.L., Kim, J., Eddaoudi, M., Chen, B., O'Keeffe, M. and Yaghi, O.M. (2005) "Rod packings and metal-organic frameworks constructed from rod-shaped secondary building units" *Journal of the American Chemical Society*, 127(5), 1504-1518.
- Rosi, N.L., Eckert, J., Eddaoudi, M., Vodak, D.T., Kim, J., O'Keeffe, M. and Yaghi, O.M. (2003) "Hydrogen storage in microporous metal-organic frameworks", *Science (New York, N.Y.)*, 300(622), 1127-1129.
- Rowsell, J.L. and Yaghi, O.M. (2005) "Strategies for hydrogen storage in metal-organic frameworks" *Angewandte Chemie International Edition*, 44(30), 4670-4679.
- Sabo, M., Henschel, A., Fröde, H., Klemm, E. and Kaskel, S. (2007) "Solution infiltration of palladium into MOF-5: Synthesis, physisorption and catalytic properties" *Journal of Materials Chemistry*, 17(36), 3827-3832.

- Saha, D. and Deng, S. (2010) "Hydrogen Adsorption on Metal-Organic Framework MOF-177" *Tsinghua Science & Technology*, 15(4), 363-376.
- Sandrock, G. (1999) "A panoramic overview of hydrogen storage alloys from a gas reaction point of view" *Journal of Alloys and Compounds*, Vol. 293–295, 877-888.
- Schaate, A., Roy, P., Godt, A., Lippke, J., Waltz, F., Wiebcke, M. and Behrens, P. (2011) "Modulated Synthesis of Zr-Based Metal-Organic Frameworks: From Nano to Single Crystals" *Chemistry- A European Journal*, 17(24), 6643-6651.
- Schlapbach, L. (2009) "Technology: Hydrogen-fuelled vehicles" *Nature*, 460(7257), 809-811.
- Son, W., Kim, J., Kim, J. and Ahn, W. (2008) "Sonochemical synthesis of MOF-5", *Chemical Communications*, (47), 6336-6338.
- Song, P., Li, Y., He, B., Yang, J., Zheng, J. and Li, X. (2011) "Hydrogen storage properties of two pillared-layer Ni(II) metal-organic frameworks" *Microporous and Mesoporous Materials*, 142(1), 208-213.
- Suh, M.P., Park, H.J., Prasad, T.K. and Lim, D. (2011) "Hydrogen storage in metal–organic frameworks" *Chemical reviews*, 112(2), 782-835.
- Tan, C., Yang, S., Champness, N.R., Lin, X., Blake, A.J., Lewis, W. and Schröder, M. (2011) "High capacity gas storage by a 4,8-connected metal-organic polyhedral framework" *Chemical Communications*, 47(15), 4487-4489.
- United States Department of Energy (2009) "Targets for on board hydrogen storage systems for light-duty vehicles",  
[http://www1.eere.energy.gov/hydrogenandfuelcells/storage/pdfs/targets\\_onboard\\_hydro\\_storage.pdf](http://www1.eere.energy.gov/hydrogenandfuelcells/storage/pdfs/targets_onboard_hydro_storage.pdf) [2013, February 12].
- Valenzano, L., Civalleri, B., Chavan, S., Bordiga, S., Nilsen, M.H., Jakobsen, S., Lillerud, K.P. and Lamberti, C. (2011) "Disclosing the complex structure of UiO-66 metal organic framework: A synergic combination of experiment and theory" *Chemistry of Materials*, 23(7), 1700-1718.

- Walton, K.S. and Snurr, R.Q. (2007) "Applicability of the BET Method for Determining Surface Areas of Microporous Metal-Organic Frameworks", *129(27)*, 8552-8556.
- Wang, X.-., Ma, S., Forster, P.M., Yuan, D., Eckert, J., López, J.J., Murphy, B.J., Parise, J.B. and Zhou, H.-. (2008) "Enhancing H<sub>2</sub> uptake by "close-packing" alignment of open copper sites in metal-organic frameworks" *Angewandte Chemie - International Edition*, *47(38)*, 7263-7266.
- Wißmann, G., Schaate, A., Lilienthal, S., Bremer, I., Schneider, A.M. and Behrens, P. (2012) "Modulated synthesis of Zr-fumarate MOF", *Microporous and Mesoporous Materials*, *152*, 64-70.
- Wu, C., Rathi, M., Ahrenkiel, S.P., Koodali, R.T. and Wang, Z. (2013) "Facile synthesis of MOF-5 confined in SBA-15 hybrid material with enhanced hydrostability" *Chemical Communications*, *49(12)*, 1223-1225.
- Wu, T., Shen, L., Luebbbers, M., Hu, C., Chen, Q., Ni, Z. and Masel, R.I. (2010) "Enhancing the stability of metal-organic frameworks in humid air by incorporating water repellent functional groups" *Chemical communications*, *46(33)*, 6120-6122.
- Yaghi, O.M., O'Keeffe, M., Ockwig, N.W., Chae, H.K., Eddaoudi, M. and Kim, J. (2003) "Reticular synthesis and the design of new materials" *Nature*, *423(6941)*, 705-714.
- Yang, H., Orefuwa, S. and Goudy, A. (2011) "Study of mechanochemical synthesis in the formation of the metal-organic framework Cu<sub>3</sub>(BTC)<sub>2</sub> for hydrogen storage" *Microporous and Mesoporous Materials*, *143(1)*, 37-45.
- Yang, J., Zhao, Q., Li, J. and Dong, J. (2010) "Synthesis of metal-organic framework MIL-101 in TMAOH-Cr(NO<sub>3</sub>)<sub>3</sub>-H<sub>2</sub>BDC-H<sub>2</sub>O and its hydrogen-storage behavior", *Microporous and Mesoporous Materials*, *130(1-3)*, 174-179.
- Yildirim, T. and Hartman, M. (2005) "Direct observation of hydrogen adsorption sites and nanocage formation in metal-organic frameworks" *Physical Review Letters*, *95(21)*, 215504.

- Zhao, Z., Li, X. and Li, Z. (2011), "Adsorption equilibrium and kinetics of p-xylene on chromium-based metal organic framework MIL-101" *Chemical Engineering Journal*, 173(1), 150-157.
- Zhao, D., Yuan, D., Yakovenko, A. and Zhou, H (2010) "A NbO-type metal-organic framework derived from a polyyne-coupled di-isophthalate linker formed in situ" *Chemical Communications*, 46(23), 4196-4198.
- Zhao, Q., Yuan, W., Liang, J. and Li, J. (2013) "Synthesis and hydrogen storage studies of metal-organic framework UiO-66" *International Journal of Hydrogen Energy*, 38(29), 13104-13109.
- Zhao, X., Xiao, B., Fletcher, A.J., Thomas, K.M., Bradshaw, D. and Rosseinsky, M.J. (2004) "Hysteretic Adsorption and Desorption of Hydrogen by Nanoporous Metal-Organic Frameworks" *Science*, 306(5698), 1012-1015.